



# Diffusivity of CO<sub>2</sub> in H<sub>2</sub>O: A Review of Experimental Studies and Molecular Simulations in the Bulk and in Confinement

H. Mert Polat,<sup>II</sup> Felipe M. Coelho,<sup>II</sup> Thijs J. H. Vlugt, Luís Fernando Mercier Franco,\*  
Ioannis N. Tsimpanogiannis,\* and Othonas A. Moulton\*



Cite This: *J. Chem. Eng. Data* 2024, 69, 3296–3329



Read Online

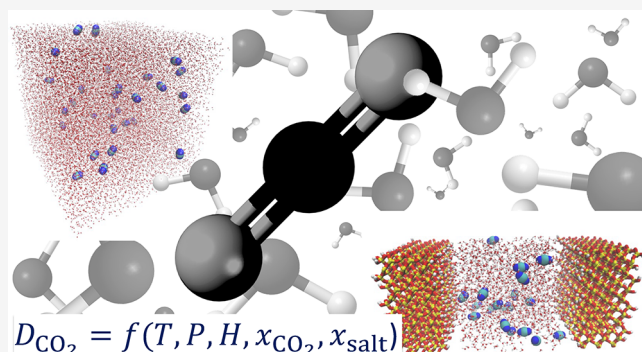
ACCESS |

Metrics & More

Article Recommendations

Supporting Information

**ABSTRACT:** An in-depth review of the available experimental and molecular simulation studies of CO<sub>2</sub> diffusion in H<sub>2</sub>O, which is a central property in important industrial and environmental processes, such as carbon capture and storage, enhanced oil recovery, and in the food industry is presented. The cases of both bulk and confined systems are covered. The experimental and molecular simulation data gathered are analyzed, and simple and computationally efficient correlations are devised. These correlations are applicable to conditions from 273 K and 0.1 MPa up to 473 K and 45 MPa. The available experimental data for diffusion coefficients of CO<sub>2</sub> in brines are also collected, and their dependency on temperature, pressure, and salinity is examined in detail. Other engineering models and correlations reported in literature are also presented. The review of the simulation studies focuses on the force field combinations, the data for diffusivities at low and high pressures, finite-size effects, and the correlations developed based on the Molecular Dynamics data. Regarding the confined systems, we review the main methods to measure and compute the diffusivity of confined CO<sub>2</sub> and discuss the main natural and artificial confining media (i.e., smectites, calcites, silica, MOFs, and carbon materials). Detailed discussion is provided regarding the driving force for diffusion of CO<sub>2</sub> and H<sub>2</sub>O under confinement, and on the role of effects such as H<sub>2</sub>O adsorption on hydrophilic confining media on the diffusivity of CO<sub>2</sub>. Finally, an outlook of future research paths for advancing the field of CO<sub>2</sub> diffusivity in H<sub>2</sub>O at the bulk phase and in confinement is laid out.



## 1. INTRODUCTION

The accurate knowledge of the intradiffusivity of CO<sub>2</sub> in liquid H<sub>2</sub>O over a wide range of temperatures and pressures is crucial for the design and optimization of numerous industrial and environmental processes and applications. The most prominent applications are the following:

- Carbon Capture & Sequestration (CCS).** CO<sub>2</sub> is a greenhouse gas, produced from virtually every industrial process, and emitted into the atmosphere.<sup>1–3</sup> In an effort to reduce the emissions of “man-made” CO<sub>2</sub>, and thus, partially mitigate the effects on the global climate change, CCS has been explored as a promising technology.<sup>4</sup> CCS involves three major steps. At first, CO<sub>2</sub> is captured from stationary CO<sub>2</sub>-intensive sources (i.e., fossil-fuel-burning power plants, cement, steel, hydrogen, ammonia, and other chemical industries).<sup>5</sup> During the second step, the captured gas is transported through a network of pipelines to a permanent gas-storage site.<sup>6,7</sup> During the third step, the captured gas is stored into subsurface, geological formations,<sup>8–10</sup> such as active or depleted gas/oil reservoirs,<sup>11–14</sup> saline aquifers,<sup>15–22</sup> and methane-gas-producing coal deposits or unminable coal seams.<sup>23–26</sup>

The diffusivity of CO<sub>2</sub> in aqueous solutions is an important transport property mainly encountered in steps one and three.

- CO<sub>2</sub>-based Enhanced Geothermal Systems (EGS).** Conventional geothermal systems that use H<sub>2</sub>O for the transmission of heat suffer from the drawback of fluid loss that has a significant negative economic effect. Dense-phase CO<sub>2</sub> has thermal characteristics that allow it to transfer large quantities of heat, while at the same time having better physical characteristics (e.g., lower viscosity, higher compressibility, and expansibility).<sup>27,28</sup> Therefore, CO<sub>2</sub> has been considered for utilization in the process of geothermal energy by extracting heat from the ground.<sup>29–31</sup> Such a process combines heat recovery from the subsurface, while the working fluid (e.g., CO<sub>2</sub>)

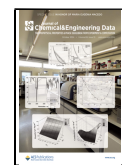
**Special Issue:** In Honor of Maria Eugenia Macedo

**Received:** December 27, 2023

**Revised:** February 25, 2024

**Accepted:** February 29, 2024

**Published:** March 20, 2024



losses can be considered as a part of CCS. In this way, value is added to the heat recovery process instead of considering it a financial loss, as occurs when using H<sub>2</sub>O as the working fluid. Depending on the depth from which heat is extracted, CO<sub>2</sub> may encounter aqueous solutions, therefore CO<sub>2</sub> dissolution, and subsequent diffusion in the aqueous phase, need to be studied to accurately describe the evolution of the CO<sub>2</sub> plume. The flow of CO<sub>2</sub> over aqueous brines is accompanied by a series of phenomena such as H<sub>2</sub>O evaporation<sup>32,33</sup> and salt precipitation,<sup>34,35</sup> thus affecting the porosity and permeability of the geologic formation.

- (iii) *Enhanced Oil Recovery (EOR)*. The injection of CO<sub>2</sub> into an oil-producing reservoir has been considered as an alternative approach to increase oil production during tertiary oil recovery<sup>36</sup> and is known as an EOR process. Usually EOR follows the secondary (i.e., waterflooding) oil recovery. Therefore, during the design of such a process, it is essential to account for the dissolution and diffusion of CO<sub>2</sub> in the aqueous phase (e.g., either the formation water or the residual water after the waterflooding process).
- (iv) *CO<sub>2</sub> ocean uptake*. Oceanic waters have absorbed approximately 40% of CO<sub>2</sub> emissions since the beginning of the industrial era<sup>37,38</sup> making the oceans the largest sink for anthropogenic CO<sub>2</sub>.<sup>39</sup> Therefore, it is essential to accurately know the dissolution and diffusion mechanisms/parameters to delineate the amount of CO<sub>2</sub> stored in the oceanic waters and its fate.
- (v) *CO<sub>2</sub> in the food industry*. The diffusivity of CO<sub>2</sub> in carbonated hydroalcoholic drinks, particularly in champagne, plays a pivotal role in influencing bubble dynamics and gas discharge kinetics, ultimately shaping the taste and mouthfeel of these beverages.<sup>40</sup> Thus, the accurate knowledge of various thermophysical properties (with transport mechanisms being central) of CO<sub>2</sub> in aqueous solutions relevant to this industry is essential for the production and quality control phases.

Therefore, it becomes apparent that during the preliminary study, and the design and optimization of the processes described above, the accurate knowledge of the diffusivity of CO<sub>2</sub> in liquid H<sub>2</sub>O under bulk conditions (applications (iv) and (v)) and in confined media (applications (i), (ii), and (iii)) is crucial. As shown in the schematic of Figure 1, the three major routes that are usually followed for the measurement/estimation of diffusion coefficients are experimental measurements, theoretical/semiempirical models, and molecular simulations, with the most common method used being molecular dynamics (MD).

At relatively low pressures (e.g., below 1 MPa), the solubilities of CO<sub>2</sub> in H<sub>2</sub>O are rather low.<sup>41</sup> For example, the solubility of CO<sub>2</sub> in H<sub>2</sub>O at atmospheric pressure and temperatures in the range 303.15–363.15 K ranges from  $5.03 \times 10^{-3}$  to  $6.50 \times 10^{-5}$  (in mole fractions).<sup>41</sup> At pressures up to 10 MPa and temperatures up to 423 K, the solubilities can increase by 2 orders of magnitude. For high pressures (i.e., 100 MPa), the solubilities can increase to a maximum of approximately  $4.3 \times 10^{-2}$ . An extensive discussion on the effect of pressure on the solubility of CO<sub>2</sub> in H<sub>2</sub>O can be found in a number of studies.<sup>41–44</sup> Therefore, the intradiffusivity of CO<sub>2</sub> in H<sub>2</sub>O essentially corresponds to the infinite dilution limit,<sup>45</sup> since for

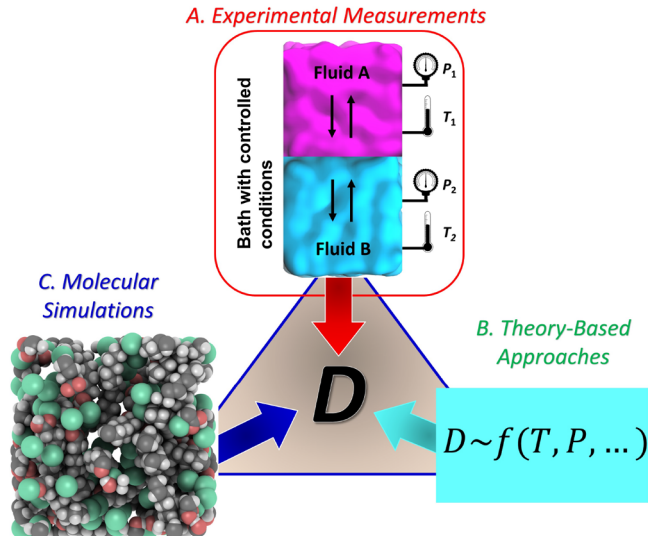


**Figure 1.** Schematic showing the common approaches considered for the estimation of diffusivities. A. Experiments, B. Theory-Based modeling, and C. Molecular Simulation.

most applications relatively low pressures and temperatures are concerned.

At higher pressures, at which the solubilities of CO<sub>2</sub> in H<sub>2</sub>O are significantly higher than in the infinite dilution limit, it is of practical interest to measure/compute the mutual diffusivities (Fick and Maxwell-Stefan<sup>46–49</sup>) since the mass transport occurs due to gradients in chemical potentials.<sup>46,50,51</sup> To this end, one can either use models that are based on the Darken equation<sup>46,52,53</sup> or can follow the well-established methodology of computing the Maxwell-Stefan diffusivities ( $D_{MS}$ ) from the Onsanger coefficients in MD simulations,<sup>47,49,54</sup> and the thermodynamic factor ( $\Gamma$ ), e.g., from Kirkwood-Buff integrals<sup>55–58</sup> or with Continuous Fractional Component Monte Carlo (CFCMC) simulations.<sup>59</sup> In binary systems, Fick diffusivities follow from  $D_{Fick} = \Gamma D_{MS}$ .<sup>46–49</sup> In this review paper, we limit our attention to the diffusivity of infinite diluted CO<sub>2</sub> in H<sub>2</sub>O. In this case, the intra-, Maxwell-Stefan, and Fick diffusivities are all equal  $D_{self} = D_{MS} = D_{Fick}$ .<sup>46</sup>

Experimentally measured diffusivities are often scarcely available, and in most cases at/or close to the atmospheric pressure.<sup>60,61</sup> A detailed discussion on how to overcome this lack of data through the use of semiempirical approaches is provided elsewhere.<sup>50,53</sup> Namely, semiempirical correlations have been extensively used for obtaining the self- and intradiffusivity values at conditions outside the range of experimental measurements.<sup>46,50,53,62,63</sup> The accuracy of such semiempirical methods depends on the extent and quality of the experimental measurements that have been used for their development and calibration. Although these methods are relatively easy to use and computationally fast, almost no insight into the physical mechanisms controlling the mass transport in the real system can be obtained.

Alternatively, approaches such as MD simulations can provide detailed physical insight;<sup>64,65</sup> the downside being that they are significantly more computationally demanding compared to engineering models. During the past three decades years, MD has become a reliable and widely used approach for obtaining diffusivities of pure components and mixtures.<sup>21,49,66–82</sup> This development is the direct result of a number of factors including: (i) the increase of available computational power, (ii) the

availability and wide use of optimized open-source software,<sup>83,84</sup> and (iii) the development of accurate force fields.<sup>85–88</sup> The data obtained from MD simulations can be further used to devise engineering models and validate the semiempirical approaches.<sup>72,89,90</sup> Macro-scale modeling approaches involving an equation-of-state such as PC-SAFT coupled with Stokes–Einstein equation or entropy scaling to compute self-diffusivities have been reported in literature, although, to the best of our knowledge, such methods have not been used to compute diffusivity of CO<sub>2</sub> in H<sub>2</sub>O.<sup>91–96</sup>

This review paper focuses on: (a) reporting diffusivity data (experimental or from MD) of CO<sub>2</sub> in pure H<sub>2</sub>O or brines, in bulk or under confinement, (b) providing engineering-type correlations of the collected data when possible, (c) critically discussing the insights from the literature, and (d) providing a few opinions to guide future developments. The remainder of this review paper is organized as follows: in **Section 2**, we examine the CO<sub>2</sub> diffusion in bulk H<sub>2</sub>O, considering both experimental and MD studies. In **Section 3** the corresponding cases under confinement are discussed. Finally, in **Section 4** the future outlook and the conclusions are presented, respectively.

## 2. AQUEOUS CO<sub>2</sub> DIFFUSION IN THE BULK

**2.1. Experimental Studies.** **2.1.1. Experimental Measurement Techniques.** Many different methods have been reported in the literature for the experimental measurement of the diffusion coefficients of gases in liquids, and have been extensively reviewed in a number of studies.<sup>50,60,97–99</sup> Providing a detailed description of all these methods is beyond the scope of the current study. Instead, we provide a brief description of the experimental methods that have been used for the measurement of gas diffusivity in liquids, focusing primarily on those used for CO<sub>2</sub> diffusing in H<sub>2</sub>O or brines. Such experimental methodologies include the following: (1) diaphragm cells,<sup>100–102</sup> (2) wetted surface absorbers,<sup>103,104</sup> (3) laminar jets,<sup>105–108</sup> (4) capillary cells,<sup>109,110</sup> (5) Taylor dispersion,<sup>111–113</sup> (6) laser-induced fluorescence,<sup>114</sup> (7) dynamic light scattering (DLS),<sup>115</sup> (8) in situ Raman spectroscopy,<sup>116,117</sup> (9) nuclear magnetic resonance (NMR) spectroscopy using pulsed field gradients (PFG),<sup>118–120</sup> (10) pH-based methods,<sup>121</sup> (11) pressure decay methods,<sup>122–124</sup> and (12) dynamic interfacial tension method.<sup>125</sup> Additional methodologies used for measuring gas diffusion in other liquids (e.g., CO<sub>2</sub> in heavy oil or bitumen) include, but are not limited to, the following: (1) the dynamic pendant drop volume analysis (DPDVA),<sup>126</sup> (2) the dynamic pendant drop surface analysis (DPDSA),<sup>127</sup> (3) X-ray computer-assisted tomography (CAT) scanning,<sup>128,129</sup> and (4) magnetic resonance imaging (MRI).<sup>130</sup>

The experimental methods mentioned above can be divided into conventional (direct) and nonconventional (indirect),<sup>99</sup> as shown in **Figure 2**. For the direct methods (e.g., diaphragm cells, wetted surface absorbers, laminar jets, capillary cells), it is essential to perform compositional measurements of fluid mixtures collected during the diffusion experiment to determine the gas diffusion coefficients. Therefore, direct methods are intrusive, can disturb the experiment if the removed samples are not minimal, can be time-consuming and labor intensive, are often expensive, and complex. These drawbacks are more pronounced when diffusion coefficients at higher temperatures/pressures are required.<sup>122</sup> On the contrary, the indirect methods (e.g., laser-induced fluorescence, dynamic light scattering, Raman spectroscopy, nuclear magnetic resonance, pH-based methods, pressure decay methods) require less time compared

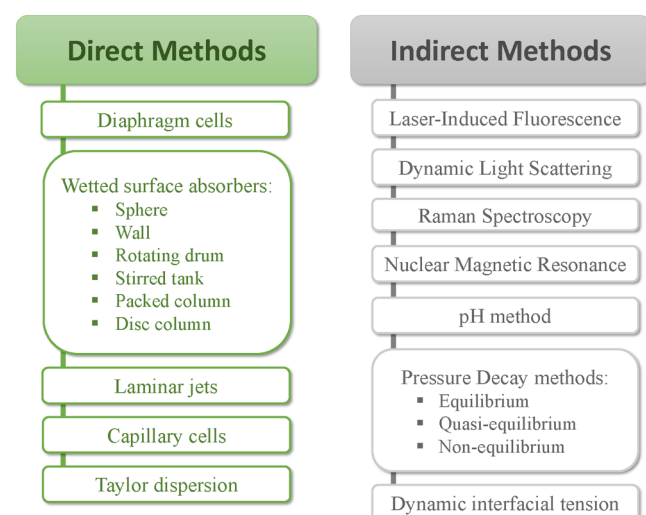


**Figure 2.** Direct and indirect experimental methods that have been used for the measurement of gas diffusivity in liquids.

to the conventional methods, and thus, are preferable in engineering applications.<sup>123</sup> In these methods, the diffusion coefficients are indirectly determined by measuring a different property (e.g., interfacial tension, pH, gas pressure, gas volume, gas/liquid interface position) of the gas/liquid system that is known to be directly affected by the diffusion process. Diffusivity measurement methods, such as DLS, Raman spectroscopy, and NMR, that were mentioned earlier, or similar ones such as magnetic resonance imaging (MRI) and X-ray computer-assisted tomography (CAT) scanning (reported for the study of gas diffusion in hydrocarbon systems), require very expensive and highly sophisticated equipment, whose operation is limited to highly specialized technicians.<sup>126</sup>

In a diaphragm cell, two solutions of different composition are brought into contact by a diaphragm. The cell usually has to be calibrated with a mixture of known diffusion coefficient. The method has a significant drawback, since it requires a large amount of time (i.e., 2–3 days) for each measurement.

In the wetted surface absorber technique, absorption takes place in a thin laminar film flowing over a surface of defined geometry, such as a sphere<sup>104</sup> or a wall/plate.<sup>131,132</sup> This method has the following two limitations that are important only at high degrees of liquid saturation: (i) the finite thickness of the liquid film, which absorbs finite amount of gas, and (ii) nonuniform velocity profile. Olbrich and Wild<sup>133</sup> extended the earlier mathematical analysis of Davidson<sup>134</sup> for absorption on a sphere to any flow geometry exhibiting a certain degree of symmetry. In a similar manner, the laminar jet method is based on the gas absorption taking place in a free-flowing laminar jet. Both these methods require knowledge of the fluid dynamics for the analysis and calculation of the diffusion coefficients. Tang and Himmelblau<sup>131</sup> reviewed other gas–liquid contacting devices that have been used in fundamental studies including the rotating drum,<sup>135</sup> the stirred tank,<sup>136</sup> the packed column, and the disk column,<sup>137</sup> and concluded that in such devices it is difficult to measure the hydrodynamic characteristics of the liquid phase, therefore making it difficult to interpret the obtained diffusivity results.

Single<sup>110</sup> or multiple<sup>109</sup> capillary cells (with the capillaries having size of approximately 1 mm) are used to restrict liquid convection within the capillaries. The liquid component is placed in the capillary and then brought into contact with the

second diffusing component. If diffusion is allowed to proceed until the steady-state is reached, then the rate of diffusion can be described by relatively simple mathematics. This method has, however, two disadvantages: (i) solubility data are required; therefore, the accuracy of diffusivity depends on the accuracy of the solubility data, and (ii) as a result of the gas absorption rate being measured volumetrically, accurate diffusivities are limited only to systems for which gas solubilities are at least moderate.

The measurement of the diffusion coefficient of a gas in a solvent with the Taylor dispersion technique requires the simultaneous injection of a sample of a solution containing the gas and the solvent into a stream of the pure solvent while the dispersion of the gas during the laminar flow through a capillary is monitored. In this approach, the parabolic flow profile results in spreading the solute pulse out longitudinally, while simultaneously radial diffusion acts to keep the pulse confined. Extracting the diffusion coefficient from the mathematical analysis of this problem is based on the seminal work of Taylor<sup>111</sup> and Aris.<sup>112</sup> An extensive discussion on the accuracy of this methodology has been presented by Alizadeh et al.<sup>138</sup> For experimental studies using the Taylor dispersion method for the diffusivity of CO<sub>2</sub> in H<sub>2</sub>O, the reader is referred to refs 113, 139–141.

By performing an analysis of the intensity of the quasielastically scattered light, a number of thermophysical properties (i.e., viscosity, surface tension, speed of sound, thermal diffusivity) can be determined in an absolute way by using dynamic light scattering (DLS).<sup>115</sup> Klein et al.<sup>142</sup> provided a comprehensive description of the techniques used, including the optical and electronic arrangement of the setup used for performing those measurements. Therefore, when applying DLS to the bulk of fluids which are at macroscopic thermodynamic equilibrium, the mean lifetimes of fluctuations in concentration, temperature or entropy, and pressure are analyzed by calculating the correlation function (CF) of the scattered light intensity. By such an analysis the thermophysical properties of interest can be extracted. Contrary, inelastically scattered light analyzed by Raman spectroscopy can provide insight into the molecular structure. In situ Raman spectroscopy in horizontal fused silica capillary has become a powerful technique utilized to determine CO<sub>2</sub> diffusion coefficients at high pressures and temperatures.<sup>116,117</sup> In an alternative approach, Hirai et al.<sup>114</sup> used laser-induced fluorescence (LIF) to measure CO<sub>2</sub> dissolution in water under high pressures.

The PFG-NMR methodology is a noninvasive means for measuring translational motion and is based on the use of magnetic gradient fields which imprint phase shifts on the nuclear spins of the diffusing species.<sup>120</sup> For cases in which an increase in gradient strength or the Brownian motion is present, a decrease in NMR signals is observed. As a result, the molecular motion can be quantified and the self-diffusion coefficient can be obtained. The PFG-NMR method does not require any calibration or additional information on the investigated systems, which constitutes an advantage of this method when compared to others discussed earlier. A detailed description of the theory behind this method, as well as the experimental aspects associated with the method, can be found in the review articles of Price.<sup>143,144</sup>

Sell et al.<sup>121</sup> utilized a microfluidic-based approach to measure the mutual diffusion coefficient of carbon dioxide in water and brine. With their approach the diffusion is quantified by imaging fluorescence quenching of a pH-dependent dye, and subsequent mathematical analysis. An important advantage of the method is

the efficacy and speed of the diffusivity measurements. The authors reported measurements completed in less than 90 s, which should be compared to hours or days required by other methods.

The pressure decay method is considered the most widely applied indirect method for the measurement of gas diffusivities in the liquid phase.<sup>99,123</sup> The method was established by Riazi<sup>145</sup> for the measurement of diffusion coefficients of gas in hydrocarbon systems. The method is based on the measurement of the decrease in the pressure of gas in direct contact with a liquid at a constant temperature PVT setup or diffusion cell. To obtain the gas diffusion coefficient, the pressure decay data as a function of time are matched with a mathematical model. Therefore, such an approach makes the calculation of the diffusion coefficient dependent on how detailed the mathematical model used for the analysis is.<sup>146</sup> This issue becomes more evident when the pressure decay method is used to measure the diffusivity of CO<sub>2</sub> in H<sub>2</sub>O where the density-driven convection needs to be considered.<sup>147,148</sup> A number of studies<sup>124,147,149–154</sup> used the pressure decay method for the measurement of the diffusivity of CO<sub>2</sub> in H<sub>2</sub>O.

Based on the boundary condition of the gas/liquid interface used in the modeling of the pressure decay method, Tharanivasan et al.<sup>155</sup> recommended the classification of the mathematical models under three categories as follows: (i) equilibrium, (ii) quasi-equilibrium, and (iii) nonequilibrium. The first category considers that the concentration on gas/liquid interface is constant and always equal to the equilibrium concentration. An important limitation of the models belonging to the first category is that the decay in pressure of the gas phase should be very small; otherwise, higher errors (originating from the assumption of constant equilibrium concentration at the interface) will occur when the model is used to analyze pressure-decay data. Models of the second category consider a nonconstant concentration, corresponding to the existing cell pressure at the gas/liquid interface, resolving thus, the deficiency of the equilibrium model. However, for quasi-equilibrium models an exact analytical solution has not been reported to date. Finally, the nonequilibrium models<sup>156,157</sup> assume that a mass transfer resistance is considered at the gas/liquid interface. Such an assumption, however, is still under scientific debate.<sup>123</sup>

The dynamic interfacial tension method<sup>125</sup> is capable of simultaneously determining the gas diffusion coefficient and the interface mass transfer coefficient in a liquid. Initially, the dynamic and equilibrium interfacial tensions of the gas–liquid system are measured by using the axisymmetric drop shape analysis (ADSA) technique for the pendant drop case. Next, a mathematical model is developed to study the mass transfer in the gas–liquid system. The gas diffusion coefficient in the liquid is used as an adjustable parameter and is the result of an optimization process to match the numerically calculated and experimentally measured dynamic interfacial tensions.

**2.1.2. Correlation of Experimental Data.** Mutoru et al.<sup>61</sup> presented a comprehensive collection of experimental data of CO<sub>2</sub> diffusion in bulk pure H<sub>2</sub>O that are available in the open literature. This database covers studies up to 2010, and includes 150 experimental data points (also incorporating the experimental data from the earlier review by Himmelblau<sup>60</sup>), the majority of which are at pressure equal to 0.1 MPa. Mutoru et al.<sup>61</sup> presented a detailed discussion of mean-field-theory models that consider the diffusion coefficient of CO<sub>2</sub> in H<sub>2</sub>O. They also reported a novel methodology for the calculation of the diffusion coefficient at infinite dilution of either of the two components.

**Table 1.** Percentage Average Absolute Deviation (%AAD) between Experimental Data and Correlations for the Diffusion Coefficient of CO<sub>2</sub> in H<sub>2</sub>O<sup>a</sup>

case	parameter fitting	data base used for %AAD calculations	ARR (%AAD)	VTF (%AAD)	SA (%AAD)	Mutoru et al. (%AAD)
1	original	original	4.9	5.0	5.7	4.9
2	original	new data	24.6	30.8	16.4	11.5
3	extended	extended	11.2	5.7	6.9	na
4	extended	new data	10.8	7.7	7.5	na
5	limited	limited	3.7	3.7	4.3	3.7
6	limited	original	5.1	5.2	5.2	na
7	limited	extended	7.4	7.4	5.9	na
8	limited	new data	17.2	17.2	8.7	na

<sup>a</sup>Notation for the experimental data: Original: database reported by Mutoru et al.<sup>61</sup> New data: Lu et al.,<sup>116</sup> Cadogan et al.;<sup>113</sup> Extended: Original + New data; Limited: database reported by Versteeg et al.,<sup>161</sup> na: not applicable. ARR stands for the Arrhenius equation (eq 1), VTF stands for the Vogel–Tamann–Fulcher equation (eq 2), and SA stands for the Speedy-Angell power-law equation (eq 3).

Magalhães et al.<sup>158</sup> examined the performance of a number of empirical correlations for the diffusion coefficients of CO<sub>2</sub> in H<sub>2</sub>O. The experimental data were correlated as a function of temperature and the viscosity or density of the solvent. For the particular system they limited their study to 111 experimental data points that are mainly at 0.1 MPa (all data were included in the database of Mutoru et al.<sup>61</sup>).

Since the methodology of Mutoru et al.<sup>61</sup> seems to be in principle accurate, and general in nature, it can be used for computing the diffusion coefficient of other gases in H<sub>2</sub>O as well, but requires significant computational effort to be applied. This section is motivated by the need to develop an equally accurate method for the calculation of the diffusion coefficient of CO<sub>2</sub> in H<sub>2</sub>O, yet simple enough to be used in reservoir simulators, where the repeated use of the diffusivity correlation is required. In reservoir simulators,<sup>159</sup> the domain of interest is discretized in a (usually) large number of grid-blocks, and the balance equations of momentum, mass, and energy need to be numerically solved in each one of them, while the solution process is repeated for all the time-steps considered.<sup>160</sup> To this purpose, two different groups of correlations are examined. The first considers two Arrhenius-type correlations,<sup>116,161</sup> while the second group considers the Speedy-Angel power-law type of correlation.<sup>162</sup>

Two are the major advantages of the correlations that were examined in the current study: (i) they are equally accurate at low pressures (0.1 MPa) and provide higher accuracy at pressures that are higher than atmospheric, and (ii) they are simple to use, and therefore, they are computationally efficient, and thus can be used during the process design and optimization. However, they are component-specific, therefore they are not general in nature. To examine different diffusion systems, the parameters of the equations need to be refitted to the corresponding, component-specific experimental diffusivity data.

Initially, we briefly present three correlations that have been reported in literature. Next, the three correlations are fitted to the experimental data used for the development of the Mutoru et al.<sup>61</sup> methodology to obtain the correlation parameters. Then, the three correlations, and the methodology of Mutoru et al.<sup>61</sup> are extrapolated to pressure and temperature conditions that are outside the range of development, and are compared to the experimental data of Lu et al.<sup>116</sup> and Cadogan et al.<sup>113</sup> Finally, an extended experimental database that includes the database of Mutoru et al.<sup>61</sup> and the experimental studies of Lu et al. and Cadogan et al. is used to re-evaluate the parameters for the three correlations. The new correlations are further tested against

experimental data at higher pressures that have not been included in the correlation development.

**2.1.3. Model Development for Diffusion in Pure H<sub>2</sub>O.** Here, we consider three literature-reported correlations presented in eqs 1–3 below to describe the experimental data of the diffusion coefficient of CO<sub>2</sub> in pure H<sub>2</sub>O collected by Mutoru et al.<sup>61</sup> This database is termed “original” in Table 1. The term “limited” in the same table corresponds to the experimental data used by Versteeg et al.,<sup>161</sup> which is a subset of the “original” database that contains only 30 experimental data points. “new data” correspond to the experimental values reported by Lu et al.,<sup>116</sup> and Cadogan et al.<sup>113</sup> that are at higher pressures. The three correlations examined have been previously reported in the literature, and have been used in a number of studies to correlate experimental data<sup>116,161</sup> or molecular simulation results.<sup>45,163</sup>

Versteeg et al.<sup>161</sup> used a limited number of experiments (i.e., 30 data points of diffusion coefficients of CO<sub>2</sub> in H<sub>2</sub>O at 0.1 MPa and for temperatures up to 348 K) and fitted the experimental data to an Arrhenius-type equation (denoted with superscript “ARR”) given as follows:

$$D_{\text{CO}_2}^{\text{ARR}} = D_0 \exp\left(\frac{\alpha}{T}\right) \quad (1)$$

where  $D_0$ , and  $\alpha$  are fitting parameters, and  $T$  is the temperature. The correlation has high accuracy within the range of development (i.e., for temperatures up to 348 K). Moulton et al.<sup>45</sup> showed that the extrapolation of the correlation by Versteeg et al.<sup>161</sup> to temperatures higher than 348 K deviates significantly from recent experimental data that were not included in the original development of the Arrhenius-type correlation.

This is clearly shown in Table 1 where the percentage average absolute deviation (%AAD), defined as %AAD = 100 ×  $\left| \frac{D_{\text{CO}_2}^{\text{calc}} - D_{\text{CO}_2}^{\text{exp}}}{D_{\text{CO}_2}^{\text{exp}}} \right|$ , is given for a number of different cases. The superscripts “calc” and “exp” denote the computed and experimental values respectively of the diffusion coefficients,  $D_{\text{CO}_2}$ , of CO<sub>2</sub> in H<sub>2</sub>O. When the correlation by Versteeg et al.<sup>161</sup> is used to compute the  $D_{\text{CO}_2}$  at the temperatures in the “limited” database, it produces a value for %AAD equal to 3.7% (i.e., case 5). Alternatively, %AAD rises to 17.2% when the experimental data of Lu et al.<sup>116</sup> and Cadogan et al.<sup>113</sup> are considered (i.e., case 8).

Lu and co-workers<sup>116</sup> used a modified Arrhenius-type of equation, known as the Vogel–Tamann–Fulcher (denoted with superscript “VTF”) to correlate the experimental data from a new set of experimental measurements that they performed in

**Table 2.** Parameters for the Diffusion Coefficient of CO<sub>2</sub> in H<sub>2</sub>O Calculated Using Different Correlations<sup>a</sup>

correlation	$D_0$ (m <sup>2</sup> s <sup>-1</sup> )	$m$	$\alpha$	$\beta$	$\gamma$
ARR-type	$3.657 \times 10^{-6}$	na	$2.2546 \times 10^3$	na	na
VTF-type	na	na	$4.3152 \times 10^3$	-123.2149	9.84018
SA-type	$19.798 \times 10^{-9}$	2.01489	na	na	na

<sup>a</sup>The case of using the “Original” database.

the pressure range 10–45 MPa and temperature range 268–473 K. The VTF equation is given as

$$D_{\text{CO}_2}^{\text{VTF}} = \exp \left[ \frac{-\alpha}{(T - \beta)} - \gamma \right] \quad (2)$$

where  $\alpha$ ,  $\beta$ , and  $\gamma$  are fitting parameters. Lu et al.<sup>116</sup> found better agreement, however, with their experimental data when they used a power-law-type of equation expressed as follows:

$$D_{\text{CO}_2}^{\text{SA}} = D_0 \left( \frac{T}{T_s} - 1 \right)^m \quad (3)$$

where  $D_0$ ,  $T_s$ , and  $m$  are fitting parameters. In most cases,  $T_s$  = 227 K. This type of correlation is known as the Speedy-Angell power-law equation<sup>162</sup> and is denoted with the superscript “SA”.

**2.1.4. Results for Experimental Data at Low Pressures.** Initially, we used the experimental data collected by Mutoru et al.<sup>61</sup> to perform comparisons between the methodology of Mutoru et al.<sup>61</sup> and the three correlations examined here. The computed values for the parameters of the three correlations are reported in Table 2.

The values for the %AAD in calculating the diffusion coefficients of CO<sub>2</sub> in H<sub>2</sub>O for the three correlations are given in Table 1. All correlations are in very good agreement with the methodology of Mutoru et al.<sup>61</sup> with the Arrhenius-type (ARR-type) correlation having the lowest %AAD. When the pressure is equal to 0.1 MPa, the temperature range of applicability of the three correlations, as well as the methodology of Mutoru et al., is limited to temperatures up to 373 K.

The good agreement between the experimental data and the methods considered is also demonstrated in Figure 3, where  $D_{\text{CO}_2}$  is shown as a function of temperature. In Figure 3, we show

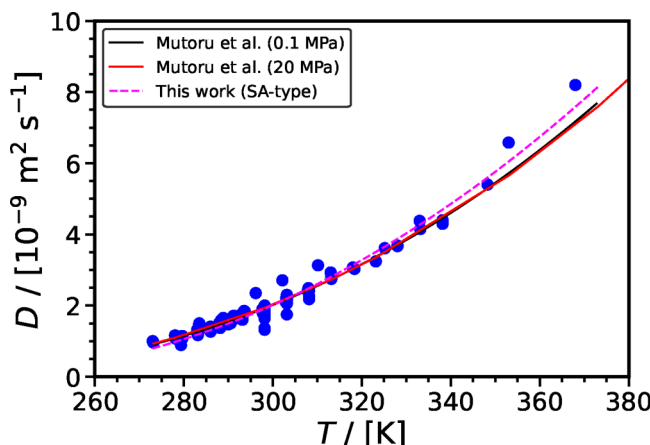


**Figure 3.** Diffusion coefficient of CO<sub>2</sub> in H<sub>2</sub>O as a function of temperature. Circles denote the experimental data collected by Mutoru et al.<sup>61</sup> The solid lines denote the calculations using the methodology by Mutoru et al. [calculations at: 0.1 MPa (black line), and 20 MPa (red line)]. The magenta dashed line denotes the correlation (SA-type) developed in this work.

only the SA-type correlation, which performs the least satisfactory among the three correlations considered. Yet we can observe that this correlation follows very closely the calculations using the methodology of Mutoru et al.<sup>61</sup>

The calculations discussed so far correspond to pressures that are equal to 0.1 MPa. Figure 3 also shows the calculations of  $D_{\text{CO}_2}$  using the methodology of Mutoru et al.,<sup>61</sup> however at pressure equal to 20 MPa. The resulting curve for the diffusion coefficient of CO<sub>2</sub> in H<sub>2</sub>O as a function of temperature is practically indistinguishable from the case of 0.1 MPa. Pressure effects on the diffusion coefficient of CO<sub>2</sub> in H<sub>2</sub>O is addressed further in the following section.

**2.1.5. Results for Experimental Data at High Pressures.** The extensive experimental studies by Lu et al.<sup>116</sup> and Cadogan et al.<sup>113</sup> have shown that pressure has a very limited effect on the diffusion coefficient of CO<sub>2</sub> in H<sub>2</sub>O, up to 45 MPa and temperatures up to 473 K. This is expected due to the low compressibility of liquid H<sub>2</sub>O at these conditions. For this pressure and temperature range, a similar conclusion was reached from the MD simulations reported by Moulton et al.<sup>45</sup> Interestingly, MD simulations show that pressure effects could become significant at higher temperatures and pressures.

Therefore, for all practical engineering applications at the conditions where pressure has a negligible effect on the diffusion coefficient of CO<sub>2</sub> in H<sub>2</sub>O, one could use the correlation that gives the diffusion coefficient of CO<sub>2</sub> in H<sub>2</sub>O only as a function of temperature (which is independent of pressure). Essentially, one could use the correlations developed in section 2.1.2 (i.e., for pressures equal to 0.1 MPa and temperatures up to 373 K) or the methodology developed by Mutoru et al.<sup>61</sup> In Figure 4(a), the diffusion coefficient of CO<sub>2</sub> in H<sub>2</sub>O is shown as a function of temperature for temperatures up to 473 K. Namely, we extrapolate the use of the methodology of Mutoru et al.<sup>61</sup> or the three correlations by 100 K. These calculations are compared with the experimental data by Lu et al.,<sup>116</sup> and Cadogan et al.,<sup>113</sup> which are at higher pressures. While very good agreement is observed for temperatures lower than 373 K, deviations increase significantly for higher temperatures as can be seen by the values of %AAD listed in Table 1. Among all cases considered in this section, the methodology of Mutoru et al.<sup>61</sup> performs better in predicting the diffusion coefficient of CO<sub>2</sub> in H<sub>2</sub>O under extrapolated conditions.

**2.1.6. Results for Combined Experimental Data.** Motivated by the observations in the previous section, we re-evaluate the parameters of the three correlations using the “extended” database that includes also the experimental data of Lu et al.<sup>116</sup> and Cadogan et al.<sup>113</sup> at higher pressures and temperatures in addition to the experimental data collected by Mutoru et al.<sup>61</sup> The new parameters that resulted from the fitting are reported in Table 3. %AAD in calculating  $D_{\text{CO}_2}$  for the three correlations are also given in Table 1. Significant improvements can be observed in the calculations of the diffusion coefficients of the experimental data of Lu et al.<sup>116</sup> and Cadogan et al.<sup>113</sup> In particular, for the case of the SA-type correlation, the %AAD

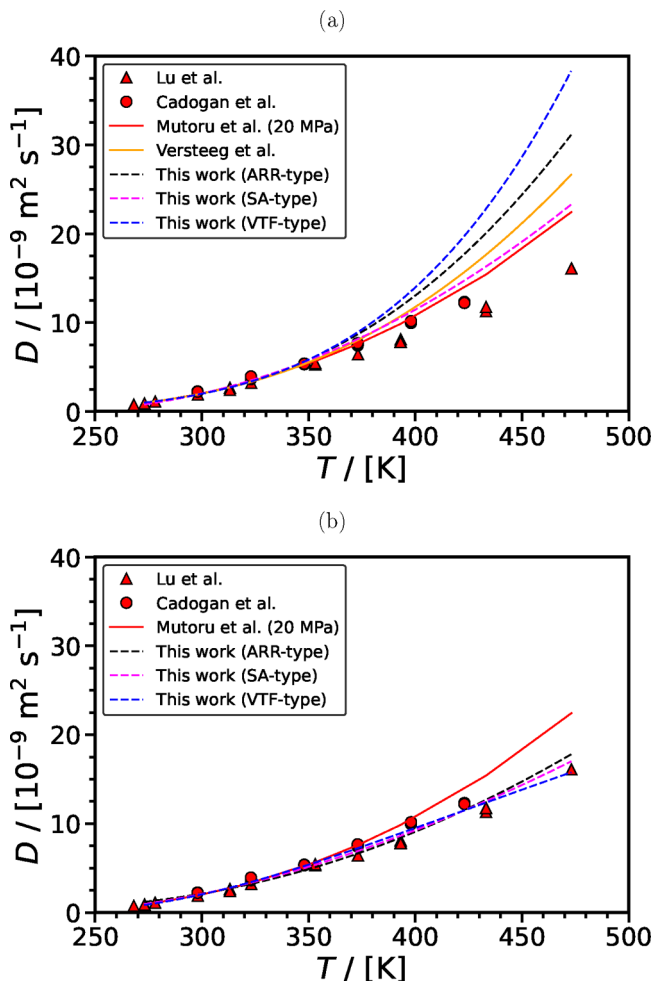


**Figure 4.** Diffusion coefficient of  $\text{CO}_2$  in  $\text{H}_2\text{O}$  as a function of temperature. Triangles denote the experimental data by Lu et al.,<sup>116</sup> and circles the experimental data by Cadogan et al.<sup>113</sup> The red solid line denotes the calculations of the diffusion coefficient of  $\text{CO}_2$  in  $\text{H}_2\text{O}$  at various temperatures and 20 MPa using the correlation of Mutoru et al.,<sup>61</sup> and the orange solid line denotes the calculation using the correlation of Versteeg et al.<sup>161</sup> The dashed lines denote the correlations examined in this work (SA-type: magenta; VTF-type: blue; ARR-type: black): (a) Extrapolation and comparison with recent experimental data at higher pressures. (b) The parameters for the three correlations are re-evaluated to include recent experimental data (Lu et al.,<sup>116</sup> Cadogan et al.<sup>113</sup>).

drops from 16.4% to 7.5% when the new parameters are used. The improvement is more pronounced for the case of the VTF-type correlation. The %AAD drops from 30.8% to 7.7% when the new parameters are used. An intermediate behavior is observed for the case of the ARR-type correlation (the %AAD drops from 24.6% to 10.8%).

Figure 4(b) shows the diffusion coefficient of  $\text{CO}_2$  in  $\text{H}_2\text{O}$  as a function of temperature. As can be seen, the reparameterized

correlations are in very good agreement with the experimental values at higher temperatures and pressures. All three correlations examined here perform better than the methodology of Mutoru et al.<sup>61</sup>

The proposed correlations are further tested with some additional experimental data at higher pressures which are indicated in Figure 5. These experimental studies have not been

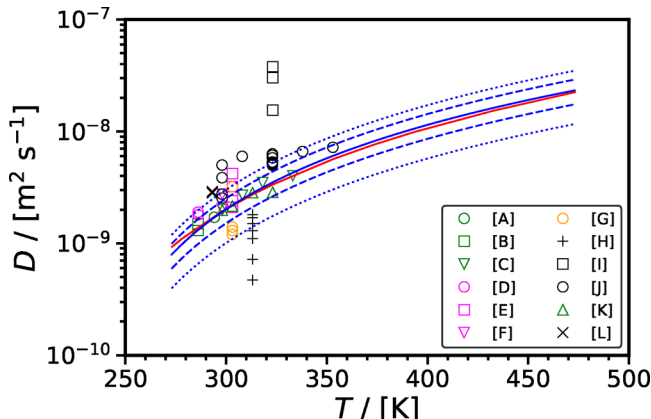


**Figure 5.** Diffusion coefficient of  $\text{CO}_2$  in  $\text{H}_2\text{O}$  as a function of temperature. The solid red line denotes the calculations using the methodology by Mutoru et al. at 20 MPa. The solid blue line denotes the correlation (SA-type) developed in this work, while the dashed and dotted blue lines indicate the boundaries of  $\pm 25\%$  and  $\pm 50\%$  of the diffusion coefficient computed with the SA correlation, respectively. Symbols denote the experimental data. Legend: [A] Belgodere et al.,<sup>117</sup> [B] Hirai et al.,<sup>114</sup> [C] Bellaire et al.,<sup>120</sup> [D] Shimizu et al.,<sup>164</sup> [E] Tomita et al.,<sup>165</sup> [F] Farajzadeh et al.,<sup>147</sup> [G] Chiquet,<sup>166</sup> [H] Tewes and Boury,<sup>167</sup> [I] Li et al.,<sup>168</sup> [J] Ahmad et al.,<sup>169</sup> [K] Lee et al.,<sup>132</sup> and [L] Basilio et al.<sup>124</sup>

included in any of the databases<sup>61,158,161</sup> discussed in the previous sections. The figure shows the comparison of the experimental diffusion coefficient of  $\text{CO}_2$  in  $\text{H}_2\text{O}$  as a function of temperature against calculations using (i) the Mutoru et al. methodology (at 20 MPa) and (ii) the SA correlation developed in the current study. The dotted lines indicate the boundaries of  $\pm 25\%$  and  $\pm 50\%$  of the diffusion coefficient calculated with the SA correlation. There are four different groups of experimental data which are indicated by a different color in the figure. The experimental data (green symbols) of Belgodere et al.,<sup>117</sup> Hirai et al.,<sup>114</sup> Bellaire et al.,<sup>120</sup> and Lee et al.<sup>132</sup> are in good agreement with the SA correlation. Most of the experimental data (magenda symbols) of Shimizu et al.,<sup>164</sup> Tomita et al.,<sup>165</sup> and Farajzadeh et al.,<sup>147</sup> fall in the zone of  $\pm 25\%$  from the SA correlation (with a limited number of experimental data falling outside). The experimental data (orange symbols) of Chiquet<sup>166</sup> fall in the range  $\pm (25-50)\%$  from the SA correlation. Finally, the experimental data (black symbols) of Tewes and Boury,<sup>167</sup> Li et al.,<sup>168</sup> Basilio et al.,<sup>124</sup> and Ahmad et al.

**Table 3. Parameters for the Diffusion Coefficient of  $\text{CO}_2$  in  $\text{H}_2\text{O}$  Calculated Using Different Correlations<sup>a</sup>**

correlation	$D_0 (\text{m}^2 \text{ s}^{-1})$	$m$	$\alpha$	$\beta$	$\gamma$
ARR-type	$0.7056 \times 10^{-6}$	na	$1.7407 \times 10^3$	na	na
VTF-type	na	na	$0.52369 \times 10^3$	159.003	16.2975
SA-type	$14.802 \times 10^{-9}$	1.72362	na	na	na

<sup>a</sup>The case of using the “extended” database.

**Table 4.** List of Experimental Studies for the Diffusion Coefficient of CO<sub>2</sub> in Aqueous Brines

year	authors	T range (K)	P range (MPa)	$D$ range ( $10^{-9} \text{ m}^2 \text{s}^{-1}$ )	salinity	variable	brine solution
1959	Nijssing et al. <sup>173</sup>	298.15	0.1	1.06–1.95	0–1.28 mol L <sup>-1</sup>	S	Na <sub>2</sub> SO <sub>4</sub> ; MgSO <sub>4</sub>
1963	Ratcliff & Holdcroft <sup>170</sup>	298.15	0.1	1.28–1.84	0.32–3.78 mol L <sup>-1</sup>	S	NaCl; NaNO <sub>3</sub> ; Na <sub>2</sub> SO <sub>4</sub> ; MgCl <sub>2</sub> ; Mg(NO <sub>3</sub> ) <sub>2</sub> ; MgSO <sub>4</sub>
1996	Wang et al. <sup>174</sup>	311.15	1.524–5.178	2.925–4.827	0.25 N	P	NaCl
2006	Yang & Gu <sup>149</sup>	300.15, 331.15	2.6–7.54	170.7–269.8	4310 mg L <sup>-1</sup>	P	reservoir (Instow) brine
2006	Yang et al. <sup>125</sup>	300.15	0.1–6	0.31–1.34	64 160 mg L <sup>-1</sup>	P	reservoir (Weyburn) brine
2008	Bahar & Liu <sup>175</sup>	356.15	na	na	2 wt %	na	NaCl
2013	Azin et al. <sup>151</sup>	305.15–323.15	5.9–6.9	3.52–6.16	182 513 mg L <sup>-1</sup>	T, P	Aquifer brine
2013	Wang et al. <sup>176</sup>	318.15	3.43–8.02	233.6–251.34	6778 mg L <sup>-1</sup>	P	reservoir brine
2015	Cadogan et al. <sup>119</sup>	298.15	0.1	1.25–2.13	0–5 mol kg <sup>-1</sup>	S	NaCl; CaCl <sub>2</sub> ; Na <sub>2</sub> SO <sub>4</sub>
2015	Belgodere et al. <sup>117</sup>	294.15	4	0.93–1.71	0–6 mol kg <sup>-1</sup>	S	NaCl
2015	Zhang et al. <sup>153</sup>	298.15	1.17	1.5–1.91	0–100 000 ppm	T, P, S	NaCl; Na <sub>2</sub> SO <sub>4</sub> ; NaHCO <sub>3</sub> ; MgCl <sub>2</sub> ; CaCl <sub>2</sub>
2015	Jafari et al. <sup>152</sup>	303.15, 313.15	5.459–6.10	0.678–23.3	0–200 000 mg L <sup>-1</sup>	P, S	NaCl; KCl; CaCl <sub>2</sub> ; MgCl <sub>2</sub> ; reservoir brine
2017	Zarghami et al. <sup>177</sup>	341.15	1.745	6.5–8.2	0–80 ppt	T, S	NaCl
2017	Shu et al. <sup>178</sup>	293.15	1.7–2.2	18.08–22.42	3 wt %	P	NaCl
2017	Shu et al. <sup>179</sup>	293.15, 303.15	1.77–2.22	1.0–3.5	3 wt %	P	NaCl
2018	Shi et al. <sup>154</sup>	323.15	4.25–5.786	1.25–293	248 991 mg L <sup>-1</sup>	na	reservoir (Mt. Simon) brine
2018	Perera et al. <sup>172</sup>	323.15	9	1.72–3.08	0–4 M	S	NaCl
2018	Li et al. <sup>180</sup>	313	2–8	1.92–2.1	1 M	P	NaCl + KI
2019	Tang et al. <sup>181</sup>	355.65	14–24	4.98–9.04	243 143 mg L <sup>-1</sup>	P	reservoir brine
2019	Tang et al. <sup>181</sup>	293–393	20.2	3.09–8.46	243 143 mg L <sup>-1</sup>	T	reservoir brine
2023	Zhang et al. <sup>182</sup>	286.15–303.15	0.1–5	0.126–0.73	3 wt %	T, P	NaCl
2024	Basilio et al. <sup>124</sup>	293.15	1.5	1.28–2.91	0–5 mol L <sup>-1</sup>	S	NaCl

al.<sup>169</sup> exhibit deviations which can be significantly higher than 50%.

**2.1.7. Diffusion in Brines.** Only a limited number of experimental measurements has been reported for the case of CO<sub>2</sub> diffusing in brines of various compositions. Table 4 shows a number of experimental studies that were identified in this review. The table also shows the range of parameters examined and the different brines considered.

Figure 6 shows the effect of salinity [in units of mol NaCl/(kg H<sub>2</sub>O)] on the diffusion coefficient of CO<sub>2</sub> in various aqueous solutions of NaCl. Each set of experiments is performed at constant temperature and pressure. We observe that for a constant temperature and pressure the diffusivity of CO<sub>2</sub> in the brine decreases as the salinity increases. This observation is

confirmed by all five experimental studies considered in Figure 6. As expected, higher temperatures result in higher diffusivities.

The experimental data of Ratcliff and Holdcroft<sup>170</sup> and Cadogan et al.<sup>119</sup> exhibit an increasing deviation at lower salinity values, even though both studies are performed at the same *P* and *T* conditions. In particular, for the case of salinity equal to 1 mol L<sup>-1</sup>, the CO<sub>2</sub> diffusivity reported by Cadogan et al. (using the Taylor dispersion method) is higher than the value reported by Ratcliff and Holdcroft (using the wetted sphere absorber technique) by approximately 16%. For the limiting case of pure H<sub>2</sub>O, Cadogan et al. reported a diffusivity equal to  $(2.130 \pm 0.028) \times 10^{-9} \text{ m}^2 \text{s}^{-1}$ , while the calculation with the method of Mutorou et al.<sup>171</sup> resulted in a value equal to  $(1.927 \pm 0.001) \times 10^{-9} \text{ m}^2 \text{s}^{-1}$ , while the calculation with the SA-type correlation of this study resulted in a value equal to  $(1.917 \pm 0.001) \times 10^{-9} \text{ m}^2 \text{s}^{-1}$ . Both calculations indicate that the experimental measurements of Cadogan et al. seem to be overestimated.

Finally, the experimental data of Basilio et al.<sup>124</sup> performed at 293 K and 1.5 MPa have higher values than the data from Belgodere et al.<sup>117</sup> performed at 294 K and 4 MPa. A similar analysis indicates that the data of Basilio et al. are higher than expected when compared to calculations with the method of Mutorou et al. and the SA-type correlation. For example, the SA-type correlation estimates the diffusivity to be  $(1.664 \pm 0.001) \times 10^{-9} \text{ m}^2 \text{s}^{-1}$  and  $(1.715 \pm 0.001) \times 10^{-9} \text{ m}^2 \text{s}^{-1}$  for 293 and 294 K, respectively. However, Basilio et al. (at 293 K) reported an experimental value equal to  $2.91 \times 10^{-9} \text{ m}^2 \text{s}^{-1}$ , while Belgodere et al. (at 294 K) reported an experimental value equal to  $1.71 \times 10^{-9} \text{ m}^2 \text{s}^{-1}$ .

Figure 7 shows the effect of pressure on the diffusion coefficient of CO<sub>2</sub> in various brines. A mixed picture is obtained regarding the effect of pressure. While the data of Tang et al.<sup>181</sup> indicate that the CO<sub>2</sub> diffusivity decreases as the pressure increases (at constant temperature and salinity), the opposite conclusion is reached when examining the data of Yang et al.,<sup>125</sup> Shu et al.,<sup>178,179</sup> Zhang et al.,<sup>182</sup> and Wang et al.<sup>174</sup> This

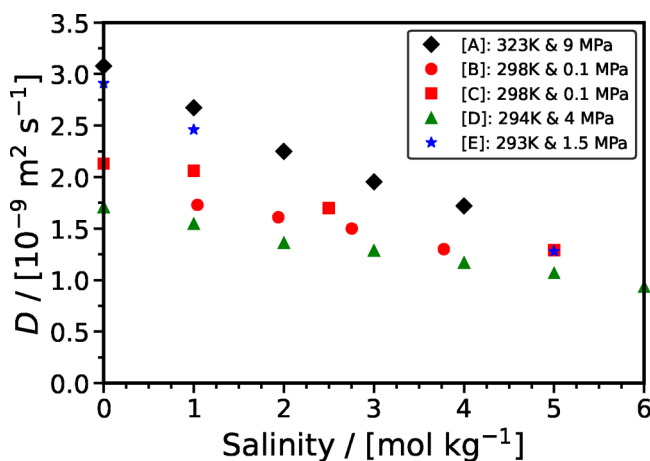


**Figure 6.** Effect of temperature and salinity [mol NaCl/(kg H<sub>2</sub>O)] on the diffusion coefficient of CO<sub>2</sub> in brines. Symbols denote the experimental data. Legend: [A] Perera et al.;<sup>172</sup> [B] Ratcliff and Holdcroft;<sup>170</sup> [C] Cadogan et al.;<sup>119</sup> [D] Belgodere et al.;<sup>117</sup> and [E] Basilio et al.<sup>124</sup>

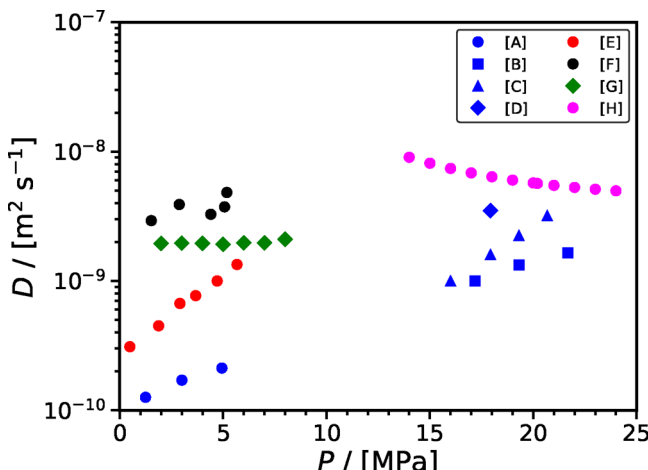


**Figure 7.** Effect of pressure and salinity on the diffusion coefficient of  $\text{CO}_2$  in aqueous brines as a function of pressure. Symbols denote the experimental data. Legend: [A] Zhang et al.<sup>182</sup> (288.15 K & 3 wt % salinity); [B] Shu et al.<sup>178</sup> (293.15 K & 3 wt % salinity); [C] Shu et al.<sup>179</sup> (293.15 K & 3 wt % salinity); [D] Shu et al.<sup>179</sup> (313.15 K & 3 wt % salinity); [E] Yang et al.<sup>125</sup> (300.15 K & 64,160 mg L<sup>-1</sup> Reservoir (Weyburn) brine); [F] Wang et al.<sup>174</sup> (311.15 and 0.2SNaCl); [G] Li et al.<sup>180</sup> (313 K & 1 M NaCl + KI); and [H] Tang et al.<sup>181</sup> (355.65 K & 243,143 mg L<sup>-1</sup> Reservoir brine).

discrepancy could be resolved by (i) either performing a new series of experiments or (ii) performing an extensive series of molecular dynamics simulations. From Figure 7, the majority of the experimental measurements for the  $\text{CO}_2$  diffusivity fall in the range  $10^{-9}$ – $10^{-8}$  m<sup>2</sup> s<sup>-1</sup>, there are also measurements in the range  $10^{-10}$ – $10^{-9}$  m<sup>2</sup> s<sup>-1</sup> (e.g., Yang et al.<sup>125</sup> using the dynamic interfacial tension method; Zhang et al.<sup>182</sup> using the pressure decay method). A systematic study at the molecular level could shed additional light into this discussion.

Figures 6 and 7 clearly show that the diffusion coefficient of  $\text{CO}_2$  in brines depends on temperature, pressure, and salinity. Nonetheless, as a result of a lack of systematic experimental measurements (completely covering the three parameter space), a scarcely populated parameter space is currently available.

Motivated by the emerging application of  $\text{CO}_2$  oceanic storage, Zhang et al.<sup>182</sup> performed a systematic study of  $\text{CO}_2$  diffusion in brines (3 wt %) under various offshore conditions covering a temperature range of 286.15–303.15 K and a pressure range 0.1–5 MPa. The  $P, T$  conditions examined cover different oceanic depths. For a scenario of oceanic sequestration, the pressure and temperature profile will change as the oceanic depth changes (i.e., the pressure increases while the temperature decreases as the depth of the water column increases). Figure 8 shows the combined effect of pressure and temperature on the  $\text{CO}_2$  diffusion coefficient. The authors concluded that the influence of the pressure on the  $\text{CO}_2$  diffusivity was stronger at the higher temperatures considered.

**2.1.8. Convection-Enhanced Effective Diffusion Coefficients.** While the molecular diffusion of  $\text{CO}_2$  in pure H<sub>2</sub>O or brines (in bulk or under confinement) is the primary focus of this review, natural convection-induced enhanced diffusion is briefly discussed in this section.

For constant temperature and salt concentration, as the pressure increases, the  $\text{CO}_2$  solubility in H<sub>2</sub>O increases as well.<sup>41,44</sup> Yang and Gu<sup>149</sup> reported that the density of  $\text{CO}_2$ -saturated brine increased linearly with  $\text{CO}_2$  concentration. Consequently, as  $\text{CO}_2$  initially gets transferred through the gas-

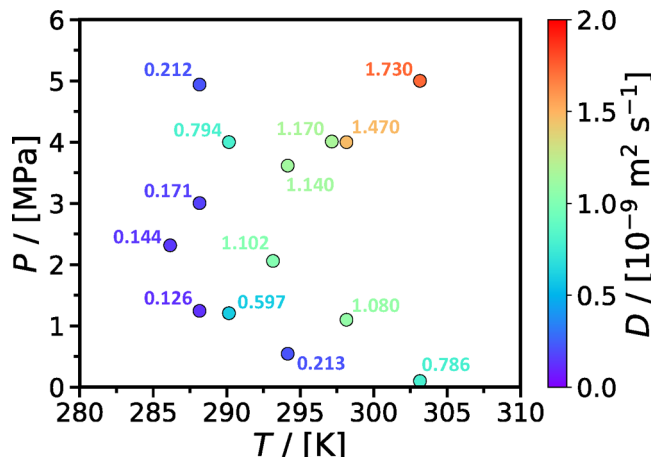


**Figure 8.** Combined effect of temperature and pressure on the diffusion coefficient of  $\text{CO}_2$  in oceanic brine (3 wt %). Symbols denote the experimental data of Zhang et al.<sup>182</sup>

liquid interface, and subsequently dissolves into the brine, a density gradient evolves in the brine phase, as a result of the concentration gradient. Namely, the brine near the interface becomes heavier than the brine further away from the interface. Instability is created in the brine which results in a natural convection flow in the brine phase. This mechanism of forced mixing results in an accelerated mass transfer of  $\text{CO}_2$  in the brine under reservoir conditions (i.e., higher pressures). Often in the literature, this behavior has been interpreted using Fick's second law:

$$\frac{\partial C(z, t)}{\partial t} = D^* \frac{\partial^2 C(z, t)}{\partial z^2} \quad (t > 0, 0 \leq z \leq H) \quad (4)$$

where  $C(z, t)$  is the  $\text{CO}_2$  concentration in the fluid,  $H$  is the height of the fluid, and  $D^*$  is a characteristic diffusion coefficient to be further discussed below. Equation 4 is subject to the following initial (eq 5) and boundary conditions (eqs 6 and 7). The initial condition is

$$C(z, t)|_{t=0} = 0 \quad (0 \leq z \leq H) \quad (5)$$

The boundary condition (B.C. 1) at the  $\text{CO}_2$ -liquid interface is

$$C(z, t)|_{z=H} = C_{\text{eq}} \quad (t > 0) \quad (6)$$

where  $C_{\text{eq}}$  is the equilibrium  $\text{CO}_2$  concentration at the interface.

The boundary condition (B.C. 2) at the bottom of the cell is

$$\left. \frac{\partial C(z, t)}{\partial z} \right|_{z=0} = C_{\text{eq}} \quad (t > 0) \quad (7)$$

By combining the solution of the diffusion equations shown above with a mass balance, an expression can be developed which connects the pressure evolution of the diffusion process with time. If pressure decay experiments are available, then by plotting the curve:

$$\ln[P(t) - P_{\text{eq}}] = \text{intercept} + \text{slope} \cdot t \quad (8)$$

we can obtain the diffusivity  $D^*$  from the slope of eq 8 (slope =  $\pi^2 D^*/(4H^2)$ ), where also intercept is a function of various parameters associated with the diffusing system.

Figure 9 shows a number of different experimental studies that followed such an approach. The  $\text{CO}_2$  diffusivity values,  $D^*$ , are

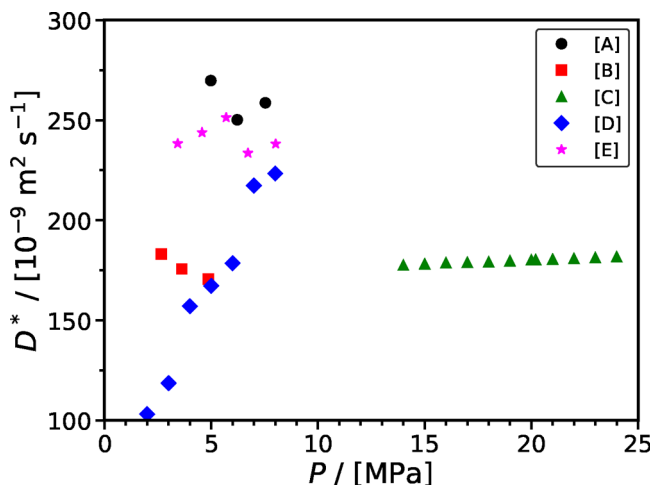


**Figure 9.** Effective diffusion coefficient,  $D^*$ , of  $\text{CO}_2$  in different brines. Legend: [A] Yang and Gu<sup>149</sup> (331.15 K & 4310 mg L<sup>-1</sup> reservoir brine), [B] Yang and Gu<sup>149</sup> (300.15 K & 4310 mg L<sup>-1</sup> reservoir brine), [C] Tang et al.<sup>181</sup> (355.65 K & 243 143 mg L<sup>-1</sup> reservoir brine), [D] Li et al.<sup>180</sup> (313 K & 1 M NaCl + KI), and [E] Wang et al.<sup>176</sup> (318.15 K & 6,778 mg L<sup>-1</sup> reservoir brine).

more than ca. 2 orders of magnitude higher than the rest of the experimental data that have been discussed earlier in Figure 7. This is due to the fact that  $D^*$  is an effective diffusivity which accounts for the combined effect of both molecular diffusion and natural convection on the mass transfer of  $\text{CO}_2$  in the liquid phase. To apply the methodology explained earlier, Wang et al.<sup>176</sup> limited their analysis to the early time values from their pressure-decay experiments instead of the late-time. Even though their pressure decay measurements extended to more than 100 min, the analysis was limited to the first 40 min. At approximately that time,  $\text{CO}_2$  arrived at the closed end of the cell, and therefore the assumption that the liquid medium is infinite (i.e., an assumption required for the analytical solution of the diffusion problem) is not valid any more. Consequently, at the initial stages of the process, the calculated effective diffusivity includes both molecular diffusion and natural convection effects.

To accurately model the complex mass-transfer process (i.e., accounting for both the molecular diffusion and the natural convection), the diffusion equation with molecular diffusivity has to be solved simultaneously with the Navier–Stokes equation, which is essential for the description of fluid flow due to natural convection. Nevertheless, this approach requires the solution of a complex numerical problem.

**2.2. Molecular Simulations.** The versatility of MD simulations has been proven in literature for computing the self-diffusivity of  $\text{CO}_2$  in various solvents, such as aqueous alkanolamine solutions,<sup>77,78,183</sup> ionic liquids,<sup>184,185</sup> and deep eutectic solvents.<sup>186,187</sup> MD simulation is a powerful method for the computation of diffusion coefficients of  $\text{CO}_2$  in  $\text{H}_2\text{O}$  that can complement experimental measurements and provide useful insight into the physical mechanisms governing diffusion at the nanoscale. MD often take less time and are less expensive than experiments, providing researchers with quicker means of studying diffusion phenomena.<sup>45,188</sup> MD simulations eliminate safety concerns associated with high-pressure and high-temperature experimental setups.<sup>45,78</sup> Furthermore, MD simulations provide the flexibility to ignore reactions between  $\text{CO}_2$  and  $\text{H}_2\text{O}$ , enabling the focus on the diffusion without considering reaction products.<sup>77,189,190</sup> Nevertheless, MD simulation results

should always be validated against experimental data to ensure accuracy and reliability in predicting diffusion coefficients under different conditions. To validate computed diffusivities, comparisons with available experimental data are performed. In the absence of experimental diffusivities, researchers often resort to assessing agreement between the computed and readily accessible experimentally obtained thermodynamic and transport properties, such as densities and viscosities.<sup>77,78,183</sup>

**2.2.1. Simulation Methods.** The computation of diffusivities can be achieved through either nonequilibrium MD (NEMD) or equilibrium MD (EMD) simulations.<sup>64,65,191</sup> NEMD involves simulating the response of molecular systems to external perturbations. The results in NEMD simulations are heavily dependent on the specific applied external perturbation.<sup>64,192</sup> Because of this reason, EMD simulations are commonly preferred for computing the diffusivity of  $\text{CO}_2$  in  $\text{H}_2\text{O}$ .<sup>45,73,191,193</sup> Two different methods can be used within EMD simulations to compute diffusivities: (i) The Green–Kubo method which involves integrating the velocity autocorrelation function over time, with this function slowly converging to zero.<sup>64,65,194</sup> (ii) The Einstein relation which establishes a linear relationship between time and the mean-square displacement (MSD) of molecules to determine diffusivity.<sup>64,65</sup> This linear relation is valid when the slope of mean-square displacement as a function of time equals 1 in a  $\log(t)$ - $\log(\text{MSD})$  plot. Open-source MD software for computing transport properties is available. The most widely used codes are GROMACS<sup>195</sup> and LAMMPS.<sup>83</sup> Recently, Jamali et al.<sup>47</sup> developed the OCTP plugin for LAMMPS which allows the on-the-fly computation of diffusivities in MD simulations. Additionally, postprocessing tools such as PyLAT<sup>196</sup> can be used to compute diffusivities using the molecular trajectories generated by MD simulations.

**2.2.2. Force Fields.** In MD simulations, the so-called force fields play a crucial role since they provide the necessary description of the interactions between atoms and molecules within a system.<sup>64,65</sup> Essentially, force fields describe the functional forms of the nonbonded potentials (e.g., van der Waals and electrostatic interactions) and bonded potential (i.e., bond stretching, angle bending, and dihedral rotations), allowing researchers to model the behavior of a molecular system. The accuracy and reliability of an MD simulation heavily depends on the accuracy of the chosen force field. Consequently, a well-parametrized force field is essential for obtaining meaningful insights into the structural and dynamic properties of molecular systems *in silico*.<sup>64,65</sup>

Although numerous force fields have been developed for  $\text{CO}_2$ , the EPM2 force field by Harris and Jung<sup>197</sup> and the TraPPE force field by Potoff and Siepmann<sup>198</sup> are the most used for computing the diffusivity of  $\text{CO}_2$  in  $\text{H}_2\text{O}$ . Both of these force fields include Lennard–Jones (LJ) interaction sites and point charges on the mass-centers of carbon and oxygen atoms of  $\text{CO}_2$ . The point charges represent the quadrupole moment of  $\text{CO}_2$  (experimentally<sup>199</sup>  $-4.3 \times 10^{-26}$  esu) and the computed quadrupole moment of both of these force fields agree with the experimental value within the statistical uncertainty (for EPM2<sup>197</sup>  $-4.1 \times 10^{-26}$  esu and for TraPPE  $-4.52 \times 10^{-26}$  esu).

In both EPM2 and TraPPE force fields, the C–O bonds are rigid. The C–O–C angle in the TraPPE force field is rigid, while in the EPM2 model, it is flexible (although the differences in the vapor liquid equilibria (VLE) and critical properties computed using a rigid angle and a flexible one are small).<sup>197</sup> TraPPE uses the Lorentz–Berthelot combining rules (arithmetic mean for  $\sigma$

and geometric mean for  $\sigma$ ), while in the EPM2 force field, a geometric mean is also used for the  $\sigma$  parameter of unlike atoms. The EPM2 force field was fitted to the VLE and critical properties of pure CO<sub>2</sub>. The change in the combining rule of the  $\sigma$  parameter between unlike atoms has a subtle impact on the  $\sigma$  parameter in interactions involving CO<sub>2</sub> and H<sub>2</sub>O. For example, using arithmetic and geometric means, the computed  $\sigma$  parameters for carbon (EPM2 CO<sub>2</sub>)<sup>197</sup> and oxygen (TIP4P/2005 H<sub>2</sub>O)<sup>85</sup> are 2.957 95 Å and 2.951 11 Å, respectively. Although the EPM2 force field consistently underestimates the liquid phase densities by 1–2% between 221–289 K, the predicted VLE, critical temperature (within 3% of experimental value), critical density (within 4% of the experimental value), and critical pressure (within 1% of the experimental value) are in good agreement with experiments.<sup>197,200</sup> The TraPPE force field was parametrized to reproduce the VLE of binary *n*-alkane/CO<sub>2</sub> mixtures, specifically the propane/CO<sub>2</sub> mixture.<sup>198</sup> The VLE of pure CO<sub>2</sub> is accurately captured by the TraPPE force field,<sup>198</sup> demonstrating a good agreement between predicted and experimental densities. Notably, there is a slight overestimation in liquid densities and a minor underestimation in gas phase densities according to the force field predictions. The TraPPE force field exhibits excellent accuracy in predicting the critical properties of CO<sub>2</sub>, with agreement within 1% for critical temperature and density, and within 4% for critical pressure when compared to the experimental values.<sup>200</sup> This shows the reliability of the TraPPE force field in capturing central thermodynamic properties.<sup>201</sup>

Het Panhuis et al.<sup>201</sup> developed a new force field which adopts the LJ parameters for carbon and oxygen atoms from GROMOS,<sup>202</sup> while partial charges were fitted to reproduce the quadrupole moment of CO<sub>2</sub>, similar to the approach used for the point charges in the EPM2 force field,<sup>197</sup> resulting in comparable point charges for these two force fields. Other force fields such as CHARMM27,<sup>203</sup> COMPASS,<sup>204</sup> and the force field from Merker et al.<sup>205</sup> have also been used to model pure CO<sub>2</sub> and mixtures.

An alternative method of designing a force field for accurately capturing the LJ interactions between CO<sub>2</sub> and H<sub>2</sub>O involves using a specific set of LJ cross-interaction parameters rather than conventional mixing rules such as the Lorentz–Berthelot rules.<sup>65</sup> Given the low solubility of CO<sub>2</sub> in H<sub>2</sub>O, this approach proves particularly advantageous, ensuring that the calculated properties of pure CO<sub>2</sub> and pure H<sub>2</sub>O remain unaffected. The study by Orozco et al.<sup>206</sup> exemplifies this strategy by tailoring the LJ cross-interaction parameters between CO<sub>2</sub> and H<sub>2</sub>O to achieve excellent agreement between the computed vapor–liquid equilibrium curve of CO<sub>2</sub>/H<sub>2</sub>O mixtures and experimental data. Vlcek et al.<sup>207</sup> used a similar approach to optimize the cross-interaction parameters between CO<sub>2</sub> and H<sub>2</sub>O to reproduce the mutual solubility of CO<sub>2</sub> and H<sub>2</sub>O. Vlcek et al.<sup>207</sup> showed that the optimized parameters were able to accurately reproduce the self-diffusivities of CO<sub>2</sub> in H<sub>2</sub>O in a temperature range of 298–353 K and 0.1 MPa. In a different, yet related context, Costandy et al.<sup>208</sup> used a modification factor (i.e.,  $\chi = 1.08$  for TIP4P/Ice water model,<sup>209</sup> and  $\chi = 1.13$  for TIP4P/2005 water model)<sup>85</sup> to correct the Lorentz–Berthelot cross interaction energy parameter for the oxygen atom in the CO<sub>2</sub> molecule and the oxygen atom in H<sub>2</sub>O. This approach has been used successfully for hydrate-related calculations in both MD<sup>208,210</sup> and MC simulations.<sup>211</sup>

As one of the most important solvents in industrial and environmental processes, many different force fields have been

developed for H<sub>2</sub>O. A few examples are SPC by Berendsen et al.,<sup>212</sup> SPC/E by Berendsen et al.,<sup>213</sup> TIP4P/2005 by Abascal and Vega,<sup>85</sup> OPC by Izadi et al.,<sup>214</sup> and TIPSP by Mahoney and Jorgensen.<sup>215</sup> Polarizable force fields have also been developed for H<sub>2</sub>O<sup>216–218</sup> and CO<sub>2</sub>.<sup>87,219</sup> Such models can be more accurate in predicting phase equilibria and transport properties of pure components and mixtures, however, as they have not been used to compute the intradiffusivity of CO<sub>2</sub> in H<sub>2</sub>O, further discussion is not provided in this review. A detailed discussion on polarizable and nonpolarizable H<sub>2</sub>O force fields falls outside the scope of this review. For more information about H<sub>2</sub>O force fields the reader is referred elsewhere.<sup>85,212–215,220–223</sup> Nevertheless, it is crucial to exercise caution when selecting a force field for H<sub>2</sub>O to compute the self-diffusion coefficient of CO<sub>2</sub> in H<sub>2</sub>O. Given the low solubility of CO<sub>2</sub> under ambient conditions,<sup>42</sup> the force field for H<sub>2</sub>O determines the density and viscosity of the solution. The self-diffusion coefficients of solutes and the solvent largely depend on these properties.

### 2.2.3. Self-Diffusivity of CO<sub>2</sub> in H<sub>2</sub>O at Ambient Pressure.

Figure 10 shows the self-diffusivity of CO<sub>2</sub> in H<sub>2</sub>O computed

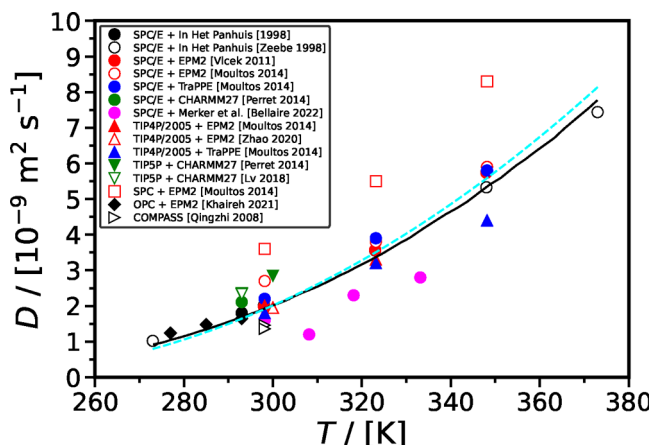
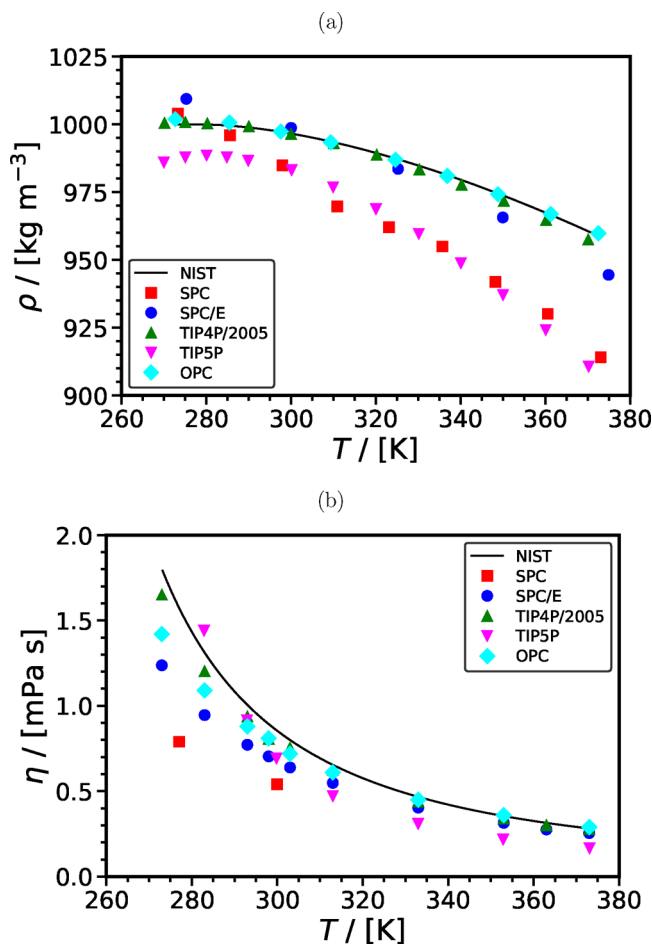


Figure 10. Intradiffusion coefficients of CO<sub>2</sub> in H<sub>2</sub>O computed using different force fields<sup>40,45,120,163,193,201,207,224–226</sup> as a function of temperature at 0.1 MPa. The black solid line and cyan dashed line represent the correlation developed by Muotoru et al.<sup>61</sup> and the correlation developed in this work (SA-type), respectively.

using different force fields<sup>40,45,120,163,193,201,207,224–226</sup> along with the correlations from Muotoru et al.<sup>61</sup> and from this work (SA-type) as a function of temperature at 0.1 MPa. The self-diffusivities of CO<sub>2</sub> computed in SPC H<sub>2</sub>O is the highest when compared with other force fields for H<sub>2</sub>O and do not agree with the experimental correlations. As shown in Figure 11, SPC force field significantly underestimates densities (up to 5% deviation from experiments) and viscosities (up to 32% deviation from experiments) of H<sub>2</sub>O. This implies that the SPC force field overestimates the free volume in the solution, leading to a significant overestimation of the self-diffusivities of the gas solute (i.e., CO<sub>2</sub>). The self-diffusivities of CO<sub>2</sub> computed in TIPSP H<sub>2</sub>O are slightly higher than those computed in SPC/E H<sub>2</sub>O, and those in SPC/E H<sub>2</sub>O are higher than in TIP4P/2005 H<sub>2</sub>O. This pattern can be attributed to the fact that TIPSP underestimates the density and viscosity of the solution to the greatest extent, followed by the SPC/E force field and then TIP4P/2005 (Figure 11). The self-diffusion coefficients of CO<sub>2</sub> computed with the EPM2 and TrapPE force fields are very similar, with TrapPE yielding slightly higher values than EPM2.



**Figure 11.** (a) Densities and (b) viscosities computed using SPC,<sup>227,228</sup> SPC/E,<sup>229–232</sup> TIP4P/2005,<sup>230,233</sup> TIP5P,<sup>233,234</sup> and OPC<sup>214,235</sup> force fields for  $\text{H}_2\text{O}$  and their comparison with the values from NIST database<sup>236</sup> as a function of temperature at 0.1 MPa.

The self-diffusivities of  $\text{CO}_2$  in  $\text{H}_2\text{O}$  computed with the same force field are generally consistent throughout literature, except in the studies by Vlcek et al.<sup>207</sup> and Moulton et al.<sup>45</sup> In both these studies, SPC/E and EPM2 force fields were used for  $\text{H}_2\text{O}$  and  $\text{CO}_2$ , respectively. Vlcek et al.,<sup>207</sup> however, computed the self-diffusivity of  $\text{CO}_2$  as  $1.98 \times 10^{-9} \text{ m}^2 \text{s}^{-1}$  at 298 K and 0.1 MPa, while at the same conditions, the self-diffusivity of  $\text{CO}_2$  was computed as  $2.7 \times 10^{-9} \text{ m}^2 \text{s}^{-1}$  by Moulton et al.<sup>45</sup> The differences between the computed self-diffusivities by Vlcek et al.<sup>207</sup> and Moulton et al.<sup>45</sup> decrease with increasing temperature. This difference may be originating from the fact that Vlcek et al.<sup>207</sup> used 512 molecules in total in their simulations and did not apply finite-size corrections. Finite-size effects were investigated by Moulton et al.<sup>45</sup> and found to be negligible for the system size used, i.e., 2000 molecules. Later in this review, a detailed discussion on the finite-size effects on the diffusivities of  $\text{CO}_2$  in  $\text{H}_2\text{O}$  is provided.

Overall, the data from literature suggest that the force field selection for  $\text{H}_2\text{O}$  has a predominant influence on the self-diffusion of  $\text{CO}_2$  in  $\text{H}_2\text{O}$ , particularly given the low concentration of  $\text{CO}_2$  in the solution due to its limited solubility in  $\text{H}_2\text{O}$ . This is in line with MD studies of other gases diffusing into  $\text{H}_2\text{O}$ , e.g., see Tsimpanogiannis et al.<sup>72</sup> for the cases of  $\text{H}_2$  and  $\text{O}_2$ . At ambient pressure, compared to the experimental correlations shown in Figure 10, the best performing

combination of force fields are TIP4P/2005-EPM2 for  $T < 323$  K and SPC/E-TraPPE for  $T > 323$  K.

**2.2.4. Self-Diffusivity of  $\text{CO}_2$  in  $\text{H}_2\text{O}$  at High Pressure.** At temperatures well below the critical point, the effect of pressure on the density and viscosity of the solution—and consequently on the self-diffusivity of  $\text{CO}_2$ —is relatively minimal, given the low compressibility of the liquid phase. For example, at a temperature of 373.15 K, the viscosity of TIP4P/2005  $\text{H}_2\text{O}$  model demonstrates a slight 8% increase from 0.1 to 100 MPa.<sup>237</sup> Similarly, the density of the TIP4P/2005  $\text{H}_2\text{O}$  model shows a 4% increase from 0.1 to 48 MPa at the same temperature.<sup>45</sup> At elevated temperatures, however, the effect of pressure on the self-diffusivity of  $\text{CO}_2$  becomes more noticeable, as the solution exhibits higher compressibility under these conditions. For instance, at 1023.15 K, the density of TIP4P/2005  $\text{H}_2\text{O}$  increases by 69% from 250 to 1000 MPa.<sup>73</sup> Figure 12 shows the available self-diffusivities of  $\text{CO}_2$  from

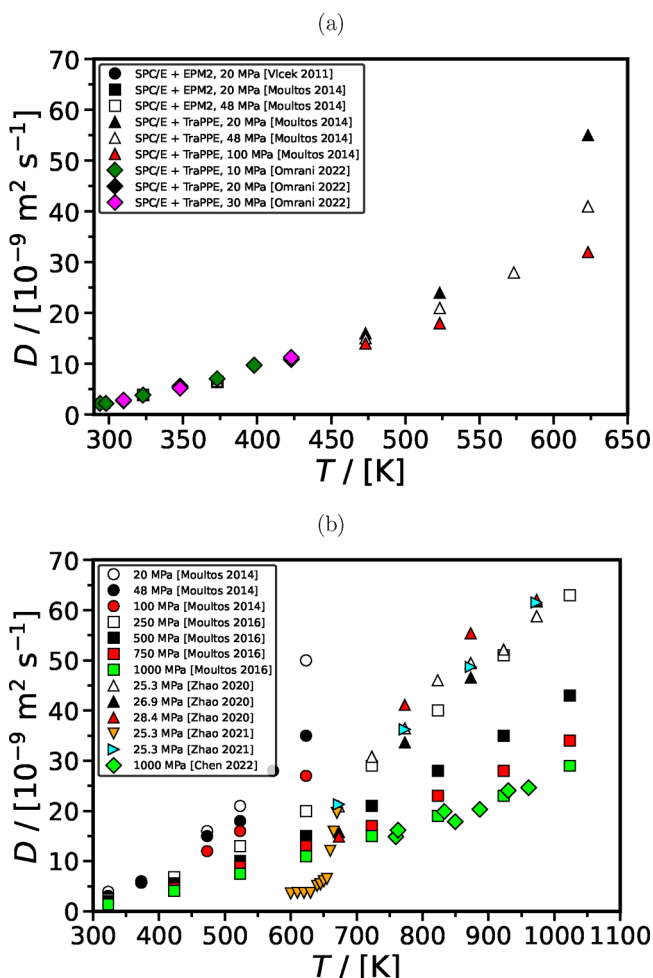


**Figure 12.** Self-diffusivities of  $\text{CO}_2$  computed using the (a) SPC/E force field for  $\text{H}_2\text{O}$  and different force fields for  $\text{CO}_2$ ,<sup>45,207,240</sup> and (b) TIP4P/2005 force field for  $\text{H}_2\text{O}$  and EPM2 force field for  $\text{CO}_2$ ,<sup>45,73,193,241–243</sup> as a function of temperature and pressure.

literature computed using MD simulations under high pressure. The data show that an increase in pressure causes a decrease in the self-diffusivities of  $\text{CO}_2$  in  $\text{H}_2\text{O}$ . This becomes significant at  $T > 500$  K. At 623.15 K, the self-diffusivity of  $\text{CO}_2$  in SPC/E  $\text{H}_2\text{O}$  and TraPPE  $\text{CO}_2$  experiences a significant decrease (42%) over the pressure range from 20 to 100 MPa.<sup>45</sup> This reduction in

self-diffusivity closely aligns with a corresponding 40% increase in the density of the solution over the same pressure range at the given temperature.<sup>45</sup>

As shown in Figure 12, toward the critical temperature of H<sub>2</sub>O (experimentally 647 K<sup>236</sup> while for TIP4P/2005 and SPC/E force fields, the critical temperatures are 623.3 K<sup>238</sup> and 640 K,<sup>239</sup> respectively), at ca. 22 MPa, the self-diffusivities of CO<sub>2</sub> in H<sub>2</sub>O computed using all combinations of force fields for H<sub>2</sub>O and CO<sub>2</sub> show a rapid increase. This is because the density of H<sub>2</sub>O changes rapidly toward the critical point.<sup>239</sup> For higher pressures ( $P > 500$  K), the computed self-diffusivities of CO<sub>2</sub> in H<sub>2</sub>O show a linear increase with increasing temperature. Comparing the computed self-diffusivities of CO<sub>2</sub> with experimental values is challenging given the scarcity of experimental data in the literature for high pressures and temperatures (relevant to CCS processes). As discussed earlier, the available experimental data by Lu et al.<sup>116</sup> and Cadogan et al.<sup>113</sup> is limited to temperatures up to 473 K and pressures up to 45 MPa. Moulton et al.<sup>45</sup> computed the self-diffusivity of CO<sub>2</sub> in H<sub>2</sub>O using the TIP4P/2005 force field for H<sub>2</sub>O and EPM2 for CO<sub>2</sub> as  $1.6 \times 10^{-8}$  m<sup>2</sup> s<sup>-1</sup> at 473.15 K and 20 MPa. In comparison, Lu et al.<sup>116</sup> experimentally measured the self-diffusivity of CO<sub>2</sub> under the same conditions as  $1.61 \times 10^{-8}$  m<sup>2</sup> s<sup>-1</sup>. The excellent agreement between the computed and experimental values, coupled with TIP4P/2005's accurate predictions of H<sub>2</sub>O density at higher temperatures and pressures,<sup>45</sup> suggests that the TIP4P/2005 and EPM2 force fields can be used for accurately predicting the intradiffusion coefficients of CO<sub>2</sub> in H<sub>2</sub>O at elevated temperatures and pressures.

**2.2.5. Finite-Size Effects.** MD simulations with periodic boundary conditions for the computation of self- and collective diffusion coefficients (as well as other properties such as activity coefficients<sup>244</sup> and thermal conductivities)<sup>245–247</sup> are susceptible to finite-size effects due to the long-range nature of hydrodynamic and electrostatic interactions.<sup>248,249</sup> To obtain the diffusivities at the thermodynamic limit, it is necessary to extrapolate the computed diffusivities which scale with  $1/L$  ( $1/L \rightarrow 0$ , where  $L$  is the simulation box length).<sup>250</sup> Commonly, the computed self-diffusivities are corrected with an analytical correction for finite-size effects derived by Yeh and Hummer.<sup>251</sup>

$$D_i = D_i^{\text{MD}} + \frac{\xi k_B T}{6\pi\eta L} \quad (9)$$

where  $D_i$  is the self-diffusivity of species  $i$  at the thermodynamic limit,  $D_i^{\text{MD}}$  is the self-diffusivity (or intradiffusivity) of species  $i$  computed from the MD simulation,  $\xi$  is a dimensionless constant equal to 2.837297 obtained by an Ewald-like summation of a periodic lattice,  $k_B$  is the Boltzmann constant,  $T$  is the absolute temperature,  $\eta$  is the viscosity computed from MD simulation, and  $L$  is the length of the simulation box. An extension of this correction was developed by Jamali et al.<sup>54,252,253</sup> for mutual diffusivities. For an in-depth understanding of the finite-size effects, readers are encouraged to refer to the review paper by Celebi et al.<sup>249</sup> and the work by Jamali et al.<sup>54</sup>

In MD literature reporting computations of CO<sub>2</sub> in H<sub>2</sub>O intradiffusivities, the system sizes used in the simulations vary from a total of 216 molecules to 4124 molecules. Many of these studies do not correct the computed diffusivities for finite-size effects.<sup>45,73,120,163,201,207,243,254</sup> In some of these studies, the diffusivities were computed using relatively big system sizes, and

finite-size effects found to be negligible.<sup>45,73,243,254</sup> However, in some studies, small system sizes were used, and thus, it is expected that the diffusivity computations are relatively inaccurate. For example, In Het Panhuis et al.<sup>201</sup> computed the self-diffusivity of CO<sub>2</sub> in H<sub>2</sub>O at 293 K and 0.1 MPa as  $1.8 \times 10^{-9}$  m<sup>2</sup> s<sup>-1</sup> using 216 molecules in total and without correcting for finite-size effects. Considering eq 9 and the densities and viscosities shown in Figure 11, the finite-size corrected self-diffusivity of CO<sub>2</sub> in H<sub>2</sub>O from this study is estimated to be  $2.3 \times 10^{-9}$  m<sup>2</sup> s<sup>-1</sup>. This corrected value is 26% higher than the originally computed value by In Het Panhuis et al.<sup>201</sup> Another example showcasing the importance of correcting for finite-size effects is found in the study by Vlcek et al.<sup>207</sup> In their work, Vlcek et al. (using 512 molecules) computed the self-diffusivity of CO<sub>2</sub> in H<sub>2</sub>O as  $1.98 \times 10^{-9}$  m<sup>2</sup> s<sup>-1</sup> at 298 K and 0.1 MPa. Interestingly, under identical conditions and using the same force field, Moulton et al. (using 2000 molecules) computed the self-diffusivity of CO<sub>2</sub> as  $2.7 \times 10^{-9}$  m<sup>2</sup> s<sup>-1</sup>.<sup>45</sup> The inconsistency between these two studies can be attributed to the fact that Vlcek et al.<sup>207</sup> did not account for finite-size effects, while using a relatively small system size. Considering eq 9, the finite-size corrected self-diffusivity of CO<sub>2</sub> from Vlcek et al.<sup>207</sup> is  $2.33 \times 10^{-9}$  (17.7% change due to finite-size effects) m<sup>2</sup> s<sup>-1</sup>, aligning better with the value computed by Moulton et al.<sup>45</sup> given the statistical uncertainty. From this discussion it becomes apparent that accounting for finite-size effects is crucial in MD simulations for accurately computing diffusivities, especially when rather small system sizes (<1000 molecules) are used.

**2.2.6. Transport Diffusivities of Aqueous CO<sub>2</sub> Solutions.** In most of the studies investigating the diffusivities of CO<sub>2</sub> in H<sub>2</sub>O, the concentration of CO<sub>2</sub> in the solvent is very low (1–5 molecules of CO<sub>2</sub> in 216–4124 water molecules), as the solubility of CO<sub>2</sub> in H<sub>2</sub>O under ambient conditions is quite low. At infinite dilution, the intradiffusivity of CO<sub>2</sub> is practically equal to transport diffusion coefficients.<sup>46,77,255</sup> A comprehensive study of transport diffusivities in aqueous solutions of CO<sub>2</sub> was performed by Zhao et al.<sup>242</sup> These authors<sup>242</sup> computed the MS and Fick diffusivities (along with intradiffusivities) of aqueous solutions containing various gases, including CO<sub>2</sub>, for a temperature range of 673–973 K and a CO<sub>2</sub> mole fraction range of 0.01–0.30. While the authors concluded that temperature and the concentration of CO<sub>2</sub> in the solution significantly influence the MS and intradiffusivities, the interpretation of MS diffusivity trends with changing CO<sub>2</sub> concentration remains challenging due to considerable scatter and uncertainties in the presented data (except for the data set at 673 K where a clear trend of increasing MS diffusivities with increasing CO<sub>2</sub> concentration can be seen). Zhao et al.<sup>242</sup> reported uncertainties up to 9% for MS diffusivities while the uncertainties for intradiffusivities were below 1%. For Fick diffusivities, Zhao et al.<sup>242</sup> noted an increase with temperature and also suggested that the concentration of CO<sub>2</sub> in the solution had no discernible effect on Fick diffusivities. The substantial scatter and uncertainties (up to 8%) in their Fick diffusivity data, potentially due to short simulation times (i.e., 1 ns), call for a careful interpretation.

Chen et al.<sup>243</sup> also computed MS diffusivities of aqueous solutions of CO<sub>2</sub> at 923 K and 25 MPa for a mole fraction range of CO<sub>2</sub> between 0.005 and 0.900. Similar to the results from Zhao et al.,<sup>242</sup> the MS diffusivities computed by Chen et al.<sup>243</sup> show substantial scatter and large uncertainties (up to 16%, potentially due to low simulation times of 3 ns). The results from these authors, however, are shown to agree well with Darken and

Vignes equations. Chen et al.<sup>243</sup> argue that the composition effect of MS diffusivities comes with a trade-off between the number of hydrogen bonds per water and CO<sub>2</sub> diffusivity, both hindering collective diffusivity in the solution. Increasing the mole fraction of CO<sub>2</sub> in the solution decreases the average number of hydrogen bonds per water molecule, which increases the collective diffusivity. As the self-diffusivity of CO<sub>2</sub> is lower than H<sub>2</sub>O, increasing the mole fraction of CO<sub>2</sub> in the solution, decreases the collective diffusivity. In summary, while the studies by Zhao et al.<sup>242</sup> and Chen et al.<sup>243</sup> offered insights into MS and Fick diffusivities of aqueous CO<sub>2</sub> solutions, further investigation including the solution structure with extended run times are essential for acquiring more robust and meaningful data.

**2.2.7. Correlations for the Diffusivity of CO<sub>2</sub> in H<sub>2</sub>O from MD Simulations.** During the design and optimization of industrial processes (e.g., CCS, EGS, EOR), calculations rely on the assessment of thermodynamic properties, such as the diffusivity of CO<sub>2</sub> in H<sub>2</sub>O, at different conditions. Despite the numerous advantages of MD simulations, their application to compute diffusivities across a very wide range of conditions is often impractical due to the long simulation times and supercomputers required. As a solution, various simpler correlations for the diffusivity of CO<sub>2</sub> in H<sub>2</sub>O have been established in the literature.<sup>45,73,163,193,241,242</sup> These correlations are derived from data obtained from MD simulations at different conditions, providing a more accessible and efficient means for estimating diffusivities at different conditions. As discussed earlier, the influence of pressure on the intradiffusivity of CO<sub>2</sub> in H<sub>2</sub>O is negligible at low temperatures ( $T < 500$  K). In literature, three pressure-independent correlations have been proposed for computing the self-diffusivities of CO<sub>2</sub> in water at  $T < 500$  K and 0.1 MPa.<sup>45,163</sup> All these correlations have the functional form of eq 3. The comparison between the correlations developed using MD simulation data<sup>45,163</sup> and the correlations developed using experimental results<sup>113,116</sup> is shown in Figure 13. The first correlation, developed by Zeebe et al.<sup>163</sup> for a temperature range of 273–373 K, used MD simulation results obtained with the SPC/E force field for water and the force field from In Het Panhuis et al.<sup>201</sup> for CO<sub>2</sub>. Zeebe et al.<sup>163</sup> demonstrated good agreement between their correlation, experimental values, and those calculated using the Stokes–Einstein equation. Moults et

al.<sup>45</sup> developed two correlations based on MD data from the force field combinations of SPC/E + TraPPE and TIP4P/2005 + EPM2. While the results from these force field combinations were similar, Moults et al.<sup>45</sup> found that the correlation using data from SPC/E + TraPPE better aligns with the correlation from Zeebe et al.<sup>163</sup> and the experimental correlation by Cadogan et al.<sup>113</sup> The correlation derived from TIP4P/2005 + EPM2 agrees well with the experimental correlation by Lu et al.<sup>116</sup> In Figure 13, the correlation from Zeebe et al.<sup>163</sup> agrees well with the experimental correlation from Cadogan et al.<sup>113</sup> within the temperature range of 273–373 K, however, when extrapolated to 473 K, it diverges from the experimental correlations. Both correlations by Moults et al.<sup>45</sup> exhibit strong agreement with experimental correlations in the temperature range of 273–473 K. The application of the correlations from Moults et al.<sup>45</sup> within this temperature range at 0.1 MPa is expected to result in more accurate self-diffusivities of CO<sub>2</sub> in H<sub>2</sub>O.

In a subsequent study Moults et al.<sup>73</sup> used the TIP4P/2005 + EPM2 force field combination for the calculation of the diffusivity of CO<sub>2</sub> in H<sub>2</sub>O at temperatures in the range 323.15–1,023.15 K and pressures equal to 250, 500, 750, and 1,000 MPa. The computed data were correlated with a Speedy–Angel type of equation (eq 3). In order to account for the effect of high pressures, the parameters  $D_0$  and  $m$  were given as functions of pressure (in MPa). Namely,

$$D_0 = a_1 \ln(P/\text{MPa}) + a_2 \quad (10)$$

and

$$m = b_1 \ln(P/\text{MPa}) + b_2 \quad (11)$$

where  $a_1 = -2.3097 \times 10^{-9}$ ,  $a_2 = 2.1064 \times 10^{-8}$ ,  $b_1 = -0.17812$ , and  $b_2 = 2.59406$ . This correlation, as clearly shown in Figure 14(a), describes the MD data very accurately at high pressures and temperatures. Furthermore, this correlation has been extrapolated to lower pressures, and compared against the MD data of an earlier study by Moults et al.,<sup>45</sup> at temperatures up to 623 K and pressures equal to 20, 48, and 100 MPa. Very good agreement was observed with these MD data, as well. Some deviations were observed for low temperatures, where the correlation reported by Moults et al.<sup>45</sup> should be used.

Two different correlations were developed for predicting the self-diffusivity of CO<sub>2</sub> in H<sub>2</sub>O at higher temperatures (water at near- and supercritical conditions). Zhao et al.<sup>193</sup> developed a temperature, density, and viscosity-dependent correlation developed at 673–973 K and 25.33 MPa for the self-diffusivities of H<sub>2</sub>, CH<sub>4</sub>, CO, O<sub>2</sub>, and CO<sub>2</sub> in supercritical H<sub>2</sub>O expressed as

$$D_i = A_{0,i} \frac{T^c}{\rho^a \eta^b} \quad (12)$$

where  $A_{0,i}$  is a gas specific constant ( $2.0078 \times 10^{-8}$  for CO<sub>2</sub>),  $\rho$  is the density,  $\eta$  is the viscosity, and  $a$ ,  $b$ ,  $c$  are the respective exponents characterizing the effect of density, viscosity, and temperature on the self-diffusivity of these gases in supercritical H<sub>2</sub>O ( $a = 0.44$ ,  $b = 1.42$ , and  $c = 2.76$ ). The higher exponent on temperature suggests that temperature has the strongest effect on self-diffusivities, with the trend following  $T > \eta > \rho$ . To validate this correlation, Zhao et al.<sup>193</sup> computed the self-diffusivities of CO<sub>2</sub> under various conditions (673 to 973 K and 26.85 MPa, and 673 to 973 K and 28.37 MPa) using MD simulations and compared the results with those predicted by the correlation. Another correlation by the same group,<sup>241</sup>

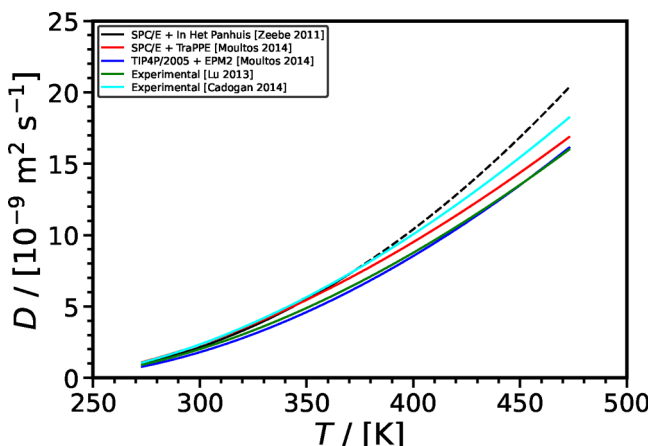


**Figure 13.** Correlations for the self-diffusivity of CO<sub>2</sub> in H<sub>2</sub>O developed using the results from MD simulations<sup>45,73,163</sup> and experimental data<sup>113,116</sup> as a function temperature at 0.1 MPa. The solid lines represent the development temperature ranges of the correlations while the dashed lines show extrapolations to higher temperatures.

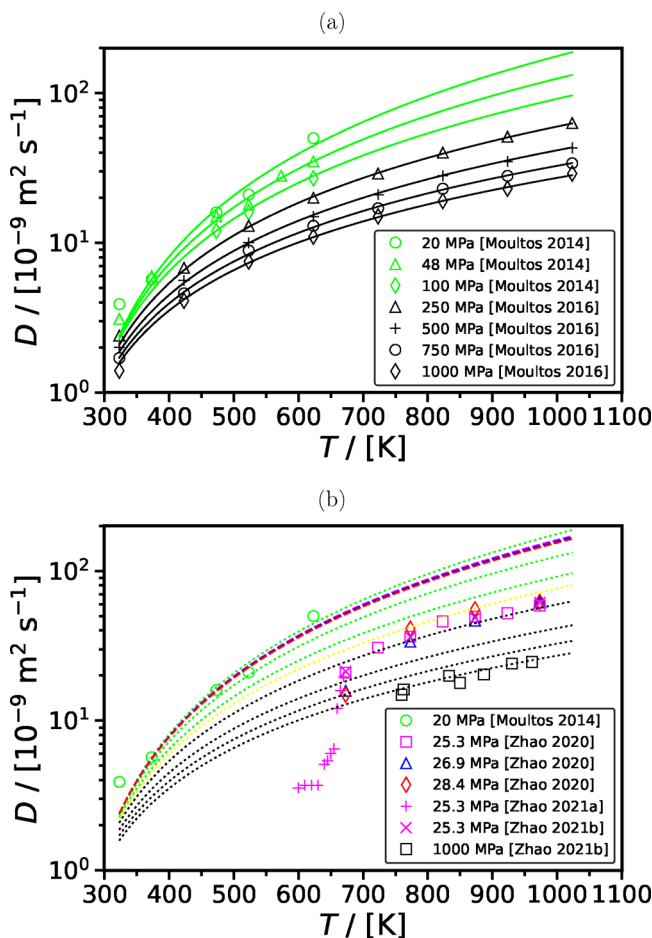


**Figure 14.** (a) Comparison of the MD data (denoted with symbols) and calculations (denoted with solid lines) using the pressure-dependent correlation of Moulton et al.<sup>73</sup> Red symbols denote the data of Moulton et al.,<sup>45</sup> while black symbols denote the data of Moulton et al.<sup>73</sup> (b) Comparison of various MD data (denoted with symbols) and calculations (denoted with dotted/dashed lines) using the pressure-dependent correlation of Moulton et al.<sup>73</sup> Notation for lines (from bottom to top): black dotted lines: 1000, 750, 500, and 250 MPa; yellow dotted line: 150 MPa; green dotted lines: 100, 48, and 20 MPa; and dashed lines: 28.4 MPa (red), 26.9 MPa (blue), 25.3 MPa (magenta).

applicable to near-critical  $\text{H}_2\text{O}$ , was developed for the self-diffusivities of  $\text{H}_2$ ,  $\text{CH}_4$ ,  $\text{CO}$ ,  $\text{O}_2$ , and  $\text{CO}_2$  at a temperature range of 600–670 K and 25.33 MPa. While utilizing the same functional form (eq 12), different parameters were fitted to the data obtained using MD simulations ( $A_{0,i} = 4.7155 \times 10^{-3}$  for  $\text{CO}_2$ ,  $a = 0.47$ ,  $b = 1.2$ , and  $c = 1.01$ ). The fitted values showed that viscosity has the most significant impact on intradiffusivities in near-critical  $\text{H}_2\text{O}$ , distinguishing it from the supercritical conditions. Although the authors<sup>241</sup> compared their results for  $\text{H}_2$  and  $\text{O}_2$  with other correlations from literature, they did not provide specific validation for the intradiffusivities of  $\text{CO}_2$ , except for limited data from MD simulations at higher pressures. Validation for both of these correlations relies on data obtained through MD simulations. Direct comparison with experimental results is essential for assessing the reliability and predictive power of the correlations in capturing the real-world behavior of the self-diffusivity of  $\text{CO}_2$  in near-critical and supercritical water.

In 2021, Zhao et al.<sup>242</sup> refined their correlation for the intradiffusivity of several gases, including  $\text{CO}_2$ , in supercritical  $\text{H}_2\text{O}$ . This enhanced correlation incorporated the effect of  $\text{CO}_2$  concentration in the solution, ranging from a mole fraction of 0.01 to 0.30. The functional form remains consistent with their prior studies (eq 12), but with additional factors accounting for solution composition and the thermodynamic factor. While these self-diffusivity correlations exhibit strong agreement with MD simulation data, direct comparisons with experimental data are challenging due to the limited availability of experimental results. Additionally, Zhao et al. extended their model to include MS and Fick diffusivities. For Fick diffusivities, the model relies solely on temperature and two gas-specific fitting parameters, while MS diffusivities are computed by dividing Fick diffusivities by the thermodynamic factor (which is a function of solution composition and temperature). As discussed earlier, the data presented by Zhao et al.<sup>242</sup> for the MS and Fick diffusivities show substantial scatter and uncertainties, emphasizing the need for cautious interpretation regarding the model's representation of reality.

Figure 14(b) shows the comparison between the calculations using the pressure-dependent correlation of Moulton et al.<sup>73</sup> and the MD simulations reported by Zhao and Jin,<sup>193</sup> Zhao et al.,<sup>241,242</sup> and Chen et al.<sup>243</sup> as a function of temperature and pressure. As can be clearly seen, the data of Chen et al. follow closely the correlation of Moulton et al. In sharp contrast, a large

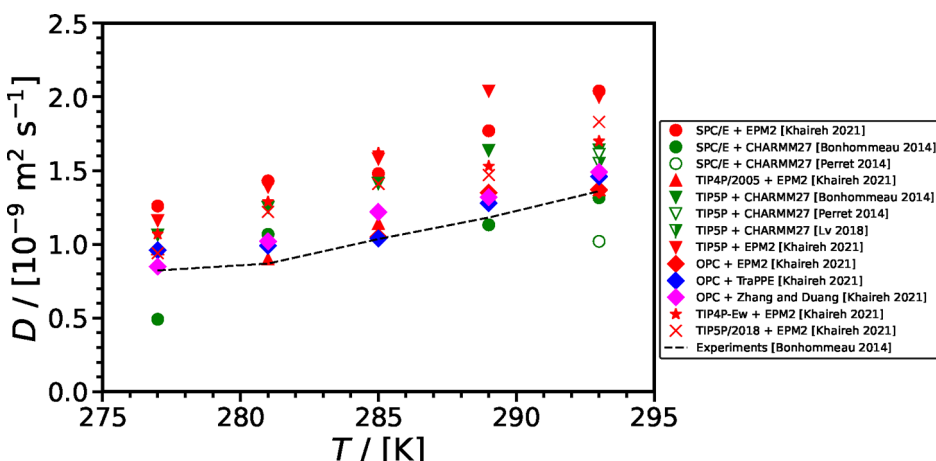


**Figure 15.** Comparison between computed<sup>40,224,225,256</sup> and experimental<sup>256</sup> self-diffusivities of  $\text{CO}_2$  in carbonated alcoholic drinks as a function of temperature at 0.1 MPa.

discrepancy is observed between the data of Zhao and Jin,<sup>193</sup> and Zhao et al.<sup>241,242</sup> Zhao and Jin<sup>193</sup> and Zhao et al.<sup>242</sup> reported data in the temperature range 673–973 K, while Zhao et al.<sup>241</sup> reported data at 600–670 K (close to the H<sub>2</sub>O critical point). From Figure 14 it is evident that the data of Zhao and Jin<sup>193</sup> and Zhao et al.<sup>242</sup> fall in-between the correlation-lines corresponding to 150 and 250 MPa, while the simulations were performed in the range 25.3–28.4 MPa. Furthermore, for the MD data Zhao et al.,<sup>242</sup> focusing on the proximity of the H<sub>2</sub>O critical point, the authors reported the diffusivity of CO<sub>2</sub> in H<sub>2</sub>O at 620 K and 25.3312 MPa to be equal to  $3.71 \times 10^{-9} \text{ m}^2 \text{ s}^{-1}$ , while Moulton et al.<sup>45</sup> reported a diffusivity value equal to  $50 \pm 4 \times 10^{-9} \text{ m}^2 \text{ s}^{-1}$  at 623 K and 20 MPa. Currently, the source of the discrepancy is not clear and further studies are required resolve it.

**2.2.8. Diffusivity of CO<sub>2</sub> in Aqueous Electrolyte Solutions.** In Figure 15, intradiffusivity data from MD simulations<sup>40,224,225,256</sup> are compared with experimental results from Bonhommeau et al.,<sup>256</sup> in a carbonated hydroalcoholic solution (representing champagne) with mole fractions of CO<sub>2</sub>, ethanol, and H<sub>2</sub>O set at ca.  $4.8 \times 10^{-3}$ , 0.042, and 0.95, respectively, at 0.1 MPa and a temperature range of 277–293 K. While MD studies using the same force fields generally exhibit consistent results, a discrepancy arises between the intradiffusivities of CO<sub>2</sub> computed by Bonhommeau et al.<sup>256</sup> and Perret et al.,<sup>40</sup> specifically when SPC/E is used for water and CHARMM for CO<sub>2</sub> and ethanol. Bonhommeau et al.<sup>256</sup> argue that the improved equilibration method used in their study (replica exchange MD) is the cause of this discrepancy and their results are more accurate.

The investigation of Khairi et al.<sup>225</sup> shows the crucial role of the H<sub>2</sub>O force field in determining the intradiffusivities of CO<sub>2</sub>. The diffusivities computed using EPM2,<sup>197</sup> TraPPE,<sup>198</sup> and Zhang-Duan<sup>257</sup> force fields are in agreement while the intradiffusivities computed using different water force fields show variations. The study by Lv et al.<sup>224</sup> further emphasizes on this point, demonstrating agreement in the intradiffusivities computed in carbonated hydroalcoholic solution, cola (in this solution, ethanol was replaced with sucrose), and club soda (in this solution, ethanol was replaced with sodium bicarbonate) at 293 K and 0.1 MPa. Comparing with the experimental data from Bonhommeau et al.,<sup>256</sup> OPC<sup>214</sup> and TIP4P/2005<sup>85</sup> H<sub>2</sub>O models exhibit excellent agreement throughout the temperature range of 277–293 K, while the other H<sub>2</sub>O force fields overestimate the self-diffusivity of CO<sub>2</sub>. This is expected since these force fields (OPC<sup>214</sup> and TIP4P/2005<sup>85</sup>) represent H<sub>2</sub>O density and transport properties (viscosity and self-diffusivity of H<sub>2</sub>O) much better than the other H<sub>2</sub>O models (see Figure 11). We suggest the usage of OPC<sup>214</sup> and TIP4P/2005<sup>85</sup> force fields for the future MD studies, while caution is advised against SPC/E,<sup>213</sup> TIP4P-Ew,<sup>258</sup> TIPSP,<sup>215</sup> and TIPSP/2018<sup>259</sup> force fields.

Garcia-Ratés et al.<sup>260</sup> investigated the diffusivity of CO<sub>2</sub> in aqueous ionic solutions using MD simulations. The authors computed self- and MS diffusivities in brine for a temperature range of 333–453 K, a pressures range of 5–50 MPa, and a salinity range of 1–4 mol kg<sup>-1</sup>. The results<sup>260</sup> showed that both self- and MS diffusivities increase with increasing temperature, while an increase in salinity from 1 mol kg<sup>-1</sup> to 4 mol kg<sup>-1</sup> led to a decrease of 34–41%. Typically to aqueous systems, the authors<sup>260</sup> show that pressure has not a significant impact on the diffusivities. Additionally, Garcia-Ratés et al.<sup>260</sup> developed a correlation linking MS diffusivities to self-diffusivities and rotational relaxation times, achieving a good agreement between predicted and computed MS diffusivities with an absolute

average deviation of 15.4%. These findings contribute insight into the complex interplay of temperature, salinity, and pressure on the diffusivity of CO<sub>2</sub> in brine which is relevant to CO<sub>2</sub> sequestration in deep saline aquifers.

Understanding the diffusivity of CO<sub>2</sub> in aqueous alkanolamine solutions is critical for absorption-based CO<sub>2</sub> capture processes.<sup>261</sup> Polat et al.<sup>78</sup> investigated the temperature and alkanolamine concentration dependencies of infinitely diluted CO<sub>2</sub> in aqueous monoethanolamine (MEA) solutions within a temperature range of 293–353 K and MEA concentrations ranging from 10 to 50 wt % using MD simulations. The results<sup>78</sup> show a significant effect of temperature and MEA concentration on the self-diffusivities of CO<sub>2</sub>, with a 72–86% decrease in self-diffusivities from 10 wt % to 50 wt % MEA concentration in the solution. This study<sup>78</sup> further revealed that the temperature dependence of the self-diffusivities in 10 wt % aqueous MEA solutions are higher than that in 50 wt % solutions. Similar observations were made by Yiannourakou et al.<sup>183</sup> for CO<sub>2</sub> in 30 wt % aqueous N-methyldiethanolamine (MDEA) solutions, demonstrating an increase in self-diffusivities from  $2.50 \times 10^{-9} \text{ m}^2 \text{ s}^{-1}$  at 300 K to  $1.03 \times 10^{-8} \text{ m}^2 \text{ s}^{-1}$  at 400 K. Polat et al.<sup>77</sup> expanded the exploration to unloaded and loaded aqueous MDEA mixtures, showing that CO<sub>2</sub> diffusion is 3.5 times faster in 10 wt % than in 50 wt % aqueous MDEA solutions within a temperature range of 288–333 K. Polat et al.<sup>77</sup> attributed the slower diffusion of CO<sub>2</sub> in concentrated MDEA solutions to stronger interactions between CO<sub>2</sub> and surrounding molecules (both water and MDEA). Additionally, investigations<sup>77</sup> into the self-diffusivities of CO<sub>2</sub> in loaded 50 wt % aqueous MDEA solutions revealed a decrease with increasing CO<sub>2</sub> loading, indicating that the CO<sub>2</sub> capture with aqueous MDEA solutions slows down as CO<sub>2</sub> loading increases. The research on CO<sub>2</sub> diffusivity in aqueous alkanolamine solutions remains limited, focusing primarily on two alkanolamines and solely on self-diffusivities. The diffusivity of CO<sub>2</sub> in aqueous solutions of other alkanolamines, such as diethanolamine (DEA) still remains unexplored, while comprehensive studies into collective diffusivities (Fick and MS) in CO<sub>2</sub>/H<sub>2</sub>O/alkanolamine mixtures are yet to be conducted, highlighting avenues for future research in the CO<sub>2</sub> capture field.

### 3. AQUEOUS CO<sub>2</sub> DIFFUSION IN CONFINED MEDIA

In applications such as gas separation and CCS in geological formations, CO<sub>2</sub> molecules are constrained by confined media. The confinement effect imposes a heterogeneous distribution of the fluid in such a way that the thermophysical properties and structure are very different from an unconfined homogeneous fluid. For instance, the solubility of confined CO<sub>2</sub> in H<sub>2</sub>O is different than that of the unconfined CO<sub>2</sub> in H<sub>2</sub>O. When confined by hydrophobic surfaces, a higher solubility is expected due to the coadsorption of CO<sub>2</sub> molecules, whereas a lower solubility is expected for the hydrophilic ones, because of the weak CO<sub>2</sub>–H<sub>2</sub>O interactions.<sup>262,263</sup> Diffusion is also affected by confinement. Overall, CO<sub>2</sub> diffusivity is expected to decrease because the mobility of molecules is reduced; preferential adsorption and steric hindrance may further decrease diffusion.<sup>264</sup>

**3.1. Experimental Studies.** **3.1.1. Experimental Measurement Techniques.** Direct experimental measurements of the molecular diffusion of confined fluids are often infeasible or nontrivial.<sup>265</sup> Nevertheless, trends can be observed through experiments, and macroscopic diffusion-related properties can be determined. Quasi-Elastic Neutron Scattering (QENS) can

be used in combination with MD simulations to investigate the stochastic motion of molecules. From the scattering signal, one can devise a model based on functions, such as Lorentzian and Gaussian, and fit parameters to determine diffusion coefficients, residence times, and correlation lengths.<sup>266</sup>

The transport diffusivity of pure CO<sub>2</sub> in silicalite has been studied with QENS and MD by Papadopoulos et al.<sup>267</sup> The same order of magnitude was obtained by both methods, however, QENS diffusivities were higher at every condition studied. The trend with loading inside the zeolite was similar for QENS and MD. The dynamics of pure CO<sub>2</sub> with QENS has been investigated in other confining materials such as the zeolite AlPO<sub>4</sub>-S<sup>268</sup> and the metal–organic frameworks (MOF) MIL-140A(Zr)<sup>269</sup> and UiO-66(Zr).<sup>270</sup> The mixtures of CO<sub>2</sub> with CH<sub>4</sub>,<sup>268,271,272</sup> C<sub>2</sub>H<sub>6</sub>,<sup>273,274</sup> and H<sub>2</sub><sup>269</sup> have also been studied. To the best of our knowledge, the only work available on the diffusion of the mixture CO<sub>2</sub>–H<sub>2</sub>O studied with QENS is from Hunvik et al.<sup>275</sup> These authors investigated the dynamics of the hydrated interlayer of hectorite with and without CO<sub>2</sub> using QENS techniques. The system has been dominated by jump-diffusion mechanisms, in which the molecule motion occurs via almost instantaneous jumps. Because individual molecule trajectories are indistinguishable, the system is characterized by a single random jump diffusion coefficient, a residence time, and a mean jump distance. Based on the diffusion parameters, the authors concluded that the dynamics in the interlayer of a hydrated smectite remains unchanged after exposure to CO<sub>2</sub>.<sup>275</sup>

Nuclear magnetic resonance (NMR) may be applied to investigate dynamic properties. By signal attenuation, one can fit a model to determine diffusion coefficients. Bowers et al.<sup>276</sup> have shown with NMR that CO<sub>2</sub> has a parallel preferential orientation when confined in the interlayer space of hectorites. The main CO<sub>2</sub> dynamics are characterized by fast-motion rotation to the normal surface at rates ca. 10<sup>5</sup> Hz. Peksa et al.<sup>277</sup> investigated the diffusion of pure CO<sub>2</sub> confined by DMOF-1 with the <sup>13</sup>C pulsed field gradient (PFG) NMR technique. They discovered that CO<sub>2</sub> is highly mobile in this MOF with diffusion trace tensor of  $(6.2 \pm 1.0) \times 10^{-9} \text{ m}^2 \text{ s}^{-1}$ . The anisotropy (ratio between the parallel and perpendicular diffusion coefficient) is equal to 3.<sup>277</sup> Using similar techniques, Forse et al.<sup>278</sup> have shown that this anisotropy is equal to ca. 30 for the CO<sub>2</sub> diffusion in the Zn<sub>2</sub>(dobpdc) MOF. The diffusion coefficient of CO<sub>2</sub> confined by pores of silica is at least 1 order of magnitude lower than in the bulk. By modifying the silica surface, further decrement in the CO<sub>2</sub> diffusivity occurs due to higher adsorption.<sup>279</sup> Despite the numerous NMR studies of CO<sub>2</sub> diffusion in various confining materials,<sup>276–281</sup> to the best of our knowledge no studies investigating the CO<sub>2</sub>–H<sub>2</sub>O mixture exist in the open literature.

Microfluidics can be applied along with fluorescence techniques to investigate CO<sub>2</sub> diffusion in aqueous mixtures. By the spatial evolution of the pH measured by fluorescence emissions, one determines the CO<sub>2</sub> concentration profile with time. The diffusion coefficient is obtained by fitting the profiles with analytical diffusion models.<sup>121,282</sup> Sell et al.<sup>121</sup> developed a microfluidic device capable of measuring diffusivity in less than 90 s. The authors determined the CO<sub>2</sub> diffusion coefficient in a wide range of pressure (0.5 to 5 MPa) and salinity (0 to 5 M NaCl) and showed that their results are in good agreement with previous experiments and models: CO<sub>2</sub> diffusivity is almost independent of the pressure, and decay exponentially with salinity. Peñas López et al.<sup>282</sup> have investigated the CO<sub>2</sub> radial diffusion from a CO<sub>2</sub> bubble to an air-saturated H<sub>2</sub>O solution confined by a horizontal Hele-Shaw cell via pH-sensitive planar

laser-induced fluorescence (PLIF). Different analytical models were able to successfully describe the diffusion-driven transport, and the characteristic length of the isoconcentration front evolves proportionally to  $\sqrt{Dt}$ , with  $t$  being time.

Finally, chromatographic techniques may also provide insights into macroscopic diffusion. Suzuki et al.<sup>283</sup> performed chromatographic experiments in a zeolite bed with different humidity contents. The authors showed that the contribution of the macropore diffusion on the interparticle diffusion is dominant compared to the micropore diffusion. The CO<sub>2</sub> interparticle diffusion in hydrophobic zeolites has shown no dependency on the moisture level.<sup>283</sup>

**3.1.2. Core Flooding Experiments.** Core flooding experiments are a common approach when the effect of confinement, via a porous medium, on different thermodynamic or transport properties is of interest. For the case of CO<sub>2</sub> diffusion in liquid H<sub>2</sub>O under confinement, core flooding experiments usually provide an effective diffusivity, which is different than the molecular diffusivity in bulk fluids, that also includes the effect of the porous medium.

Macroscopically, core flooding experiments may also provide insights related to CO<sub>2</sub> transport in a confined environment, for instance, through the rock permeability calculation.<sup>284–286</sup> Moortgat et al.<sup>287</sup> have shown that, to represent the core-flooding experiments, the applied numerical model needs to take into account the CO<sub>2</sub> Fickian diffusion. Busch et al.<sup>288</sup> measured the effective diffusion coefficient of CO<sub>2</sub> in a H<sub>2</sub>O-saturated shale sample under subsurface conditions by fitting the cumulative amount of CO<sub>2</sub> passing through the pores to a nonstationary diffusion model. The diffusivity is estimated at 3.08 and  $4.81 \times 10^{-11} \text{ m}^2 \text{ s}^{-1}$  for the first and second run of the experiment, respectively. The difference between runs is attributed to CO<sub>2</sub> partial sorption in the first run. By comparing the effective diffusivity with the diffusion of CO<sub>2</sub> in bulk H<sub>2</sub>O, the sample tortuosity is estimated to be between 40 and 70.<sup>288</sup> Si et al.<sup>289</sup> conducted a similar experimental study for the measurement of the effective diffusion coefficient of CO<sub>2</sub> in water-saturated coal.

Renner<sup>290</sup> used Berea cores and examined the diffusivity of CO<sub>2</sub> in 0.25 N NaCl (i.e., 14.625 g per L H<sub>2</sub>O) brines at 311 K and pressures up to 5.86 MPa. The author concluded that for the chosen conditions there was no difference identified between diffusion coefficients measured for vertical or horizontal positioning of the cores (i.e., the gravity-induced convection had minimal effects on the measured diffusivities). Shi et al.<sup>154</sup> reported experimental measurements for water-saturated or brine-saturated packs of two different porous materials. Namely, (i) 1.6 mm soda lime glass beads with 40% porosity and  $250.11 \times 10^{-11} \text{ m}^2$  permeability, and 125–150  $\mu\text{m}$  quartz particles with 45% porosity and  $0.48 \times 10^{-11} \text{ m}^2$  permeability. Seyyedi et al.<sup>291</sup> performed experiments in brines (0–20 wt %) at temperatures in the range 311.15–331.15 K, in a bead pack cell, with 37% porosity and  $2.95 \times 10^{-9} \text{ m}^2$  permeability. The authors used a mathematical model to account for the density-driven convection and investigated the effect of temperature and brine salinity on the convection mechanism. They reported that an increase in salinity results in reduction of the diffusion coefficient, while an increase in the temperature results in an increase of the diffusion coefficient, which is consistent with previous studies. Additionally, they reported that an increase in temperature or brine salinity has an unfavorable effect on the convection mechanism. Zhang et al.<sup>182</sup> used Berea cores and examined the effect of the core permeability (10, 50, and 100

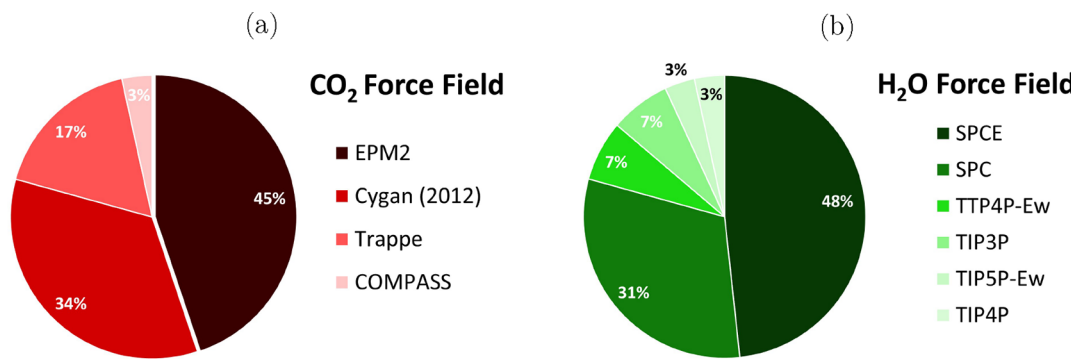


**Figure 16.** Overview of the relative popularity of (a) CO<sub>2</sub> and (b) H<sub>2</sub>O force fields used in the literature for the computation of CO<sub>2</sub>–H<sub>2</sub>O diffusion in confinement.

mD) on the CO<sub>2</sub> diffusivity in brine-saturated (3 wt %) cores at  $T, P$  conditions equal to 290.15 K and 4 MPa, respectively. They reported effective diffusion coefficients of CO<sub>2</sub> in the brine-saturated cores equal to  $1.22 \times 10^{-15}$ ,  $3.87 \times 10^{-15}$ , and  $4.81 \times 10^{-15}$ , m<sup>2</sup>/s for the aforementioned permeabilities, respectively. Li et al.<sup>292</sup> reported effective diffusion coefficients in brine-saturated (0.5–2 mol L<sup>-1</sup> NaCl) Berea cores. The authors examined temperatures in the range 313.15–373.15 K and pressures in the range 8.28–30.94 MPa, and provided empirical pressure–temperature-based correlations for the CO<sub>2</sub> diffusivities in brines under reservoir conditions. Li et al.<sup>150</sup> reported experiments using Berea and Bentheimer core samples. The authors introduced a new method for the measurement of effective gas diffusion coefficients in brine-saturated consolidated cores based on a radial diffusion model. To this purpose, mathematical models were developed to obtain the gas effective diffusion coefficient from the measured pressure decay curve. Li et al.<sup>150</sup> concluded that the diffusive tortuosity factor of the examined cores was about 10. Basilio et al.<sup>124</sup> used the pressure decay method to measure the molecular CO<sub>2</sub> diffusion coefficients in pure water, at 293.15 K, using capillary tubes, packed with glass beads with three different grain size ranges: (i) 45–90  $\mu$ m, (ii) 200–300  $\mu$ m, and (iii) 425–560  $\mu$ m. The use of capillary tubes in this experimental approach allows for the disregard of density-induced convection during the diffusion process. Moghaddam et al.<sup>293</sup> used different unconsolidated sand packs with permeabilities in a range of ca. 3.1–2.546 m<sup>2</sup> to measure the effective CO<sub>2</sub> diffusion coefficients in pure water at 310.15 K. The experimental diffusivities were subsequently correlated with the dimensionless Rayleigh number.

**3.1.3. The Challenge of Comparing Experimental and Computed Diffusivities in Confined Media.** The comparison of diffusion data from experiments and theoretical models is not always straightforward. The multiple definitions of diffusivities (e.g., self-, Fickian, Maxwell-Stefan) makes the comparison even harder, since one needs to be very careful on how the diffusion coefficient is defined, which depends on the proposed driving force (concentration, mole fraction, or chemical potential). Only few techniques, such as NMR<sup>294</sup> and QENS<sup>295</sup> can provide essential insight into diffusion mechanisms under confinement. More difficulties emerge when comparing real materials (with defects, different geometries, shapes, and crystallographic planes) with the simulations, which are usually carried out with perfect materials (e.g., no defects). Due to this, the experimentally determined diffusion tensor is different from the diffusion tensor computed with MD simulations. The latter is a diagonal tensor even for anisotropic materials, whereas the

former exhibits off-diagonal components in anisotropic materials.<sup>296</sup> This is a direct consequence of the spatial scale at which the experiment and the simulations are conducted. When confined in a idealized shape (e.g., slit, cylindrical, or spherical pores), the diffusion tensor of the fluid is necessarily diagonal.<sup>296,297</sup> Another issue is related to Darcy's law, widely applied to describe porous media flow. For highly confined media with low permeability (e.g., some nanoporous materials), due to the strong adsorption, Darcy's law may fail, as shown via molecular simulations for kerogen.<sup>298</sup> Such discrepancies between experiments and simulations could be tackled to some degree by a more systematic effort by the scientific community in determining diffusion coefficients, and transport properties more generally, in confined media.

**3.2. Molecular Simulations.** For a full description of the microscopic diffusion under confinement, molecular simulation techniques can be a very helpful approach. From MD simulations, we obtain the trajectories of the molecules from which the diffusion of each species can be computed. The initial configuration of MD simulations of confined fluids may be obtained with Grand-Canonical Monte Carlo (GCMC) simulations, in which the temperature  $T$ , the volume  $V$ , and the chemical potential of each species  $\mu_i$  are fixed.<sup>264,299–302</sup> At equilibrium, the chemical potential of confined species is equal to their chemical potential in the bulk, and the number of molecules is defined based on insertion/deletion techniques. Performing GCMC to generate initial configurations for MD simulations, one guarantees a confined fluid distribution that is in equilibrium with an unconfined fluid at the specified bulk pressure.

Via MD simulations, the diffusion of confined CO<sub>2</sub> has been investigated as part of various mixtures, such as shale gas,<sup>303</sup> CH<sub>4</sub>,<sup>304–306</sup>  $n$ -C<sub>4</sub>H<sub>10</sub>,<sup>307</sup>  $n$ -C<sub>7</sub>H<sub>16</sub>,<sup>308</sup>  $n$ -C<sub>8</sub>H<sub>18</sub>,<sup>309</sup> and ionic liquids.<sup>310,311</sup> The diffusivity of pure CO<sub>2</sub> has also been investigated under confinement by different materials, such as MOF,<sup>312–314</sup> graphene sheets,<sup>315</sup> zeolites,<sup>316</sup> calcites,<sup>317,318</sup> silicalites<sup>314,319</sup> and clays.<sup>320</sup> In this review, we focus only on the results related to diffusion of the confined mixture of CO<sub>2</sub> and H<sub>2</sub>O.

**3.2.1. Force Fields.** As we extensively discussed earlier, in MD (and GCMC) simulations, accurate force fields are required for the description of the interactions between the species. Similarly to the bulk phase, to study transport properties of confined CO<sub>2</sub>–H<sub>2</sub>O mixtures, the EPM2<sup>197</sup> and SPCE<sup>213</sup> force fields for CO<sub>2</sub> and H<sub>2</sub>O, respectively, are the ones more commonly used in the literature (see Figure 16). These force fields were developed to reproduce bulk properties at homogeneous

conditions, and thus, they may not always be a good representation of the interactions of the molecules in confinement, especially taking into account the solid–fluid interactions. Cygan et al.<sup>321</sup> have developed a fully flexible force field for CO<sub>2</sub> based on vibrational data of confined CO<sub>2</sub>. This force field has been widely used to study CO<sub>2</sub> diffusion in confinement.<sup>263,264,301,322–328</sup>

The choice of force field representing the confining material is also crucial. CLAYFF<sup>329</sup> is the most used force field to represent natural confining media. CLAYFF has been shown to be suitable for representing hydrated minerals, such as hydroxides, oxyhydroxides, and clays, in contact with fluids. CLAYFF is based on metal–oxygen ionic interactions and the only bonded interactions are in the terminal groups.<sup>329</sup> To investigate CO<sub>2</sub> diffusion under confinement, CLAYFF has been used to represent the mineral structure of montmorillonite,<sup>264,265,301,323,325,327</sup> hectorite,<sup>330</sup> beidellite,<sup>302</sup> forsterite,<sup>331</sup> kaolinite,<sup>262</sup> sepiolite,<sup>328</sup> palygorskite,<sup>328</sup> and hydrocalcite.<sup>322</sup> To represent kerogen<sup>332</sup> and calcite<sup>263,333,334</sup> structures, COMPASS<sup>204</sup> and the force field developed by Xiao et al.<sup>335</sup> are the ones commonly used.

To represent artificial materials, various force fields can be used. For carbon-derived materials such as carbon nanotubes<sup>300,336</sup> the LJ carbon is commonly represented by the chargeless FF from Steele.<sup>337</sup> The CVFF<sup>338</sup> has also been applied to model graphene sheets.<sup>339</sup> This force field, however, has been originally parametrized to represent proteins.<sup>338</sup> Sizova et al.<sup>340</sup> applied the Steele FF<sup>337</sup> combined with the OPLS-AA<sup>341</sup> to represent, respectively, the carbon atoms and the functional groups in the structure of the CMK-5 mesoporous.

The representation of MOF usually is made by the generic DREIDING force field<sup>342</sup> and the universal force field (UFF).<sup>343</sup> Both these models have already been used to investigate CO<sub>2</sub> diffusion.<sup>344–347</sup> Bendt et al.<sup>344</sup> devised a force field based on Density Functional Theory (DFT) calculations capable of better predicting the potential energy surface around the open metal sites of Mg-MOF-74.<sup>348</sup> The authors have investigated the effect of accounting for flexibility in the solid framework on the CO<sub>2</sub> diffusion. Although the adsorption energy in the flexible material is about the same as in the rigid one, the equilibrium distance between guest molecules and the open metal site is enlarged in the former, which increases the diffusivity of CO<sub>2</sub> molecules when flexibility is taken into account.<sup>344</sup>

**3.2.2. Methods.** When confined, the fluid density is no longer spatially homogeneous, and the diffusion coefficient exhibits a tensorial nature. Following Einstein's method, diffusion coefficients may be obtained from the mean squared displacement evolution with time if the medium is homogeneous. For inhomogeneous fluids, however, Einstein's equation is no longer valid, not only because of the inherent inhomogeneity, but also because Einstein's solution to the mass balance equation is found by considering boundary conditions at infinity, which does not hold for confined systems. In this case, both parallel and perpendicular components of diffusion coefficients should be computed using other methods. For parallel self-diffusion coefficients, the method proposed by Liu et al.,<sup>349</sup> based on the solution of the Smoluchowski equation and the calculation of the survival probability, is adequate and has been applied in the literature.<sup>317,350</sup> Similar to Einstein's relation, the method is based on the computation of diffusivity from the mean squared displacement, but, to account for the medium inhomogeneity, the mean squared displacement must be divided by the survival

probability of molecules to stay in the reference layer in which the diffusivity is evaluated.

For the perpendicular self-diffusion coefficient, some methods have been proposed in the literature. Liu et al.<sup>349</sup> proposed a method that requires two simulations in parallel, one of them using Langevin dynamics.<sup>65</sup> Mittal et al.<sup>351</sup> proposed a method based on a discretized version of Smoluchowski equation. The Mean First-Passage Time has been applied by von Hansen et al.<sup>352</sup> to compute the diffusion of H<sub>2</sub>O in a lipid bilayer. Carmer et al.<sup>353</sup> proposed the steady-state color reaction-counter-diffusion method. Finally, Franco et al.<sup>297</sup> analytically solved the Smoluchowski equation deriving a method to compute the perpendicular self-diffusion coefficient. It is important to note that although these methods have been applied in the literature, many authors continue to apply Einstein's relation to compute diffusion coefficients in confined media. Overall, the perpendicular component of CO<sub>2</sub> diffusion is lower than the parallel one due to the constraints imposed by the surface in that direction.<sup>262,326,327,339</sup> Usually, the diffusion coefficient tensor is dependent on the distance from the surface, in such a way that the Smoluchowski equation needs to be solved for each direction in layers parallel to the confining media. When a molecule goes from one layer to another, it no longer contributes to the calculation of the diffusion in its initial layer. This effect is accounted for by the survival probability of molecules in space.<sup>349</sup>

Using the method proposed by Liu et al.<sup>349</sup> for the parallel self-diffusion coefficient, Chialvo et al.<sup>354</sup> computed the H<sub>2</sub>O and CO<sub>2</sub> self-diffusion coefficients parallel ( $D_{\parallel}^s$ ) to a silica surface in a H<sub>2</sub>O-rich environment. They have computed  $D_{\parallel}^s$  in both external and internal (confined) interfacial regions. Externally, the diffusion coefficient of H<sub>2</sub>O decreases monotonically with decreasing distance from the silica surface.<sup>263,354</sup> In the confined region of hydrophobic surfaces, the diffusivity is no longer monotonic due to the local fluctuations of density and composition. Under severe confinement of hydrophobic silica (distance of 0.6 nm between plates), CO<sub>2</sub> concentrates in a single peak in the middle of the pore and achieves a diffusivity ( $2.8 \times 10^{-9} \text{ m}^2 \text{ s}^{-1}$ ) close to the bulk value ( $3.2 \times 10^{-9} \text{ m}^2 \text{ s}^{-1}$ ). Santos et al.<sup>334</sup> have also computed the parallel diffusion of CO<sub>2</sub> with low H<sub>2</sub>O concentration at calcite and silica surfaces, accounting for the inhomogeneity of the confined fluid. All other studies available on the confined CO<sub>2</sub>–H<sub>2</sub>O diffusion have computed the diffusion coefficients from the slope of the mean squared displacement with time, following Einstein's relation, which could lead to misleading conclusions and inaccurate results.

The self-diffusion coefficient relates to the thermal energy of particles through Brownian motion. The presence of other particles, especially a different component, may interfere with the particle motion. Transport diffusivity, such as Maxwell–Stephan or Fick diffusion coefficients, accounts for the influence of collective interactions on the fluid motion. Transport diffusion coefficients can be computed from EMD or NEMD. The former may converge very slowly because it needs to account for cross-correlation between all particles.<sup>355</sup> Various nonequilibrium techniques may be applied to investigate diffusion flux under confinement. With gradient relaxation molecular dynamics (GRMD), an initial concentration gradient is established and the transport diffusivity is obtained by fitting the diffusion equation with the system relaxation with time.<sup>356</sup> In the dual control volume grand canonical molecular dynamics (DCV-GCMD), two bulk reservoirs with distinct chemical

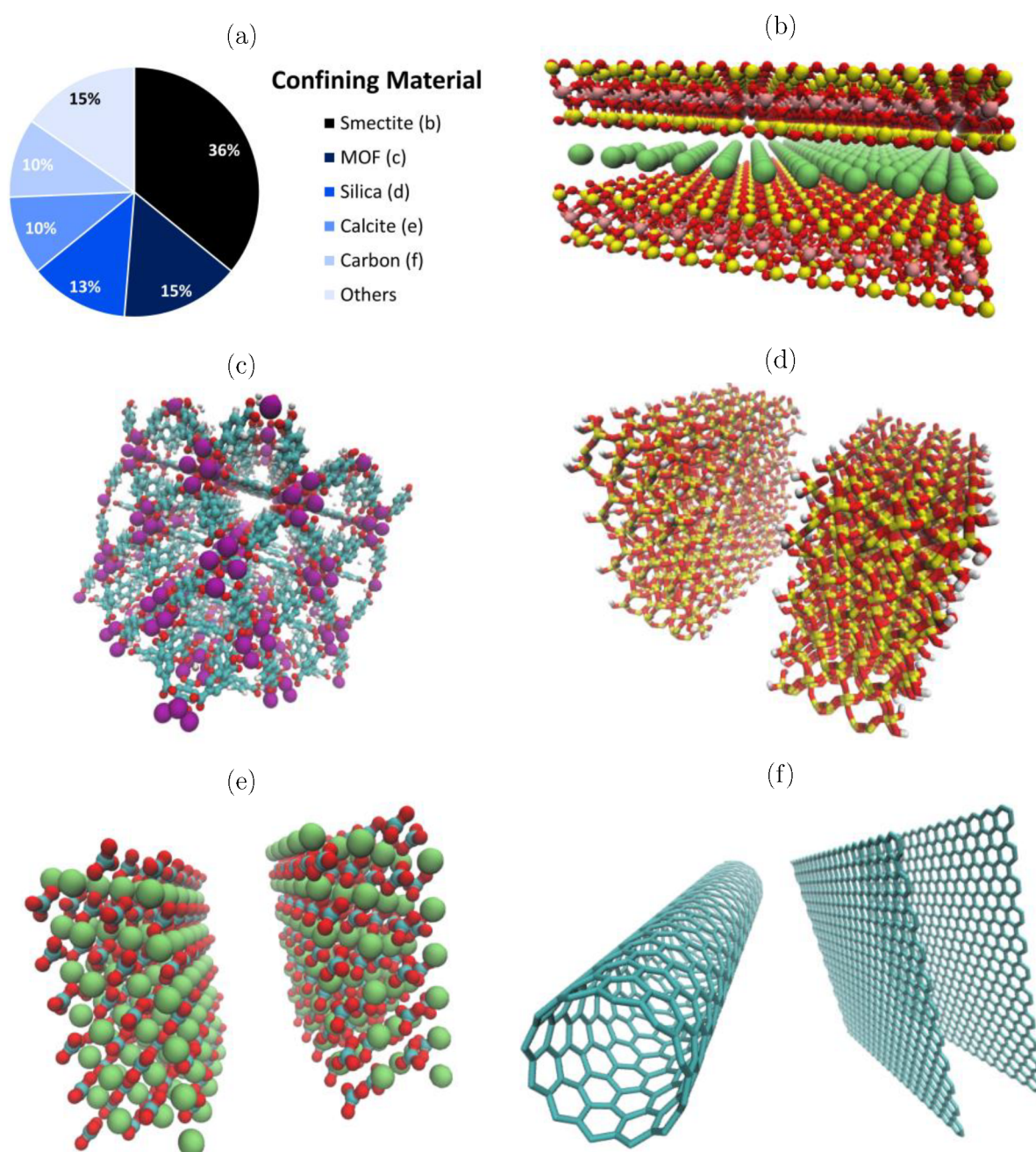


**Figure 17.** (a) Overview of the relative popularity of confining materials used in molecular simulations in the literature for the investigation of CO<sub>2</sub>–H<sub>2</sub>O diffusion in confinement. An example of the structure of the main confining material is shown: (b) Ca-montmorillonite representing a smectite crystal; (c) UiO-66(Zr) MOF; (d) [001] quartz representing a silica crystal; (e) [1014] calcite crystal; and (f) carbon nanotube and graphene sheets representing carbon materials. The colors red, white, yellow, cyan, green, pink, and purple represent oxygen, hydrogen, silicon, carbon, calcium, aluminum, and zirconium atoms, respectively.

potential are coupled to opposite edges of the confined system; the chemical potential gradient is kept constant via particle creation/destruction in the reservoirs, in such a way that a steady state flux is established and the diffusion coefficients can be obtained.<sup>357</sup> An external field (EF-NEMD) can also be applied in the fluid particles to induce a mass flux in a predefined direction.<sup>358</sup> Care should be taken because the effect of an external field on the interaction between particles may not be negligible.<sup>355</sup>

Magnin et al.<sup>346</sup> have computed both self-and MS diffusivity of CO<sub>2</sub> and H<sub>2</sub>O confined by a MOF using Einstein's method (EMD) and applying a constant force on the guest molecules

(NEMD), respectively. They found that  $D_{MS}^{CO_2} \approx D_s^{CO_2}$ , which indicates that for CO<sub>2</sub> the cross-interaction effects on diffusion may be negligible compared to the strong effect imposed by the confinement. The same does not apply for H<sub>2</sub>O at all conditions: by increasing the pressure, and consequently the loading, the self-diffusivity deviates from the Maxwell-Stephan one, and collective interactions may no longer be neglected.<sup>346</sup> Yang et al.<sup>300</sup> related the self- and transport diffusion coefficients in the CO<sub>2</sub>–H<sub>2</sub>O mixture confined in carbon nanotubes (CNT). The authors have used the pure component sorption and diffusion data, and the saturation loading, and derived a loading-

independent self-exchange coefficient. They found that the MS diffusivity of CO<sub>2</sub> is almost independent of the loading. Overall, good agreement is obtained with the correlation. At low loading (or high H<sub>2</sub>O content), this approach is less reliable.<sup>300</sup>

As in the bulk phase, finite-size effects may also be present when computing diffusivities under confinement. Considering  $z$  as the confinement direction, Simonnin et al.<sup>359</sup> have shown that for a LJ fluid the use of periodic boundary conditions in  $x$  and  $y$  directions leads to finite-size effects due to the hydrodynamic interactions between periodic images and the constraint of total momentum conservation. Elongated simulation boxes in  $x$  and  $y$  directions ( $L_x \approx L_y \gg L_z$ ) should be used to avoid such effects. When this is not an option (it is often computationally expensive), analytical expressions may be applied to correct diffusion coefficients.<sup>249,359</sup> To the best of our knowledge, there is no investigation available in the literature regarding finite-size effects on CO<sub>2</sub> diffusion under confinement.

**3.2.3. Confinement in Natural Media.** The effect of confinement on CO<sub>2</sub> depends on the confining material. Figure 17 shows the distribution of confining media used to investigate the CO<sub>2</sub> diffusion in studies available in the literature.

**3.2.3.1. Smectites.** Smectites are the most studied material due to their importance in carbon sequestration applications. This clay is a layered aluminosilicate composed of one octahedral (O) sheet with Al as central atom and two adjacent tetrahedral (T) sheets with Si, creating a T–O–T structure. Some of these central atoms are substituted by divalent metals. This creates a partial negative charge in the structure that is balanced by positive counterions located in the interlayer region between two T–O–T structures.<sup>323</sup> Because of the high hydration energy of counterions, smectites may swell to accommodate H<sub>2</sub>O molecules in the interlayer. It has been experimentally observed that hydrated smectites may also swell in contact with CO<sub>2</sub>, depending on the initial confined H<sub>2</sub>O concentration.<sup>360</sup> The confinement effect in these conditions is significant, and the molecules distribute themselves in one or two layers.<sup>321</sup>

The different types of smectite can be classified depending on the main substitution of metal atoms and its location.<sup>302</sup> Montmorillonite (MMT) is the most common smectite and also the most investigated one in regards to CO<sub>2</sub> diffusion.<sup>264,265,299,301,302,323,325,327,361</sup> CO<sub>2</sub> diffusion has also been investigated in the interlayer of hectorite (HEC)<sup>275,326,330</sup> and beidellite (BEI).<sup>302</sup>

The basal  $d$ -spacing in the interlayer depends on its relative humidity.<sup>301,323</sup> For a monolayer (1W), a bilayer (2W), and three layer (3W) H<sub>2</sub>O arrangement, the basal  $d$ -spacing is expected to be around 12, 15, and 18.5 Å, respectively.<sup>362</sup> Care should be taken when defining the basal  $d$ -spacing in MD simulations because not all hydrate states are stable for all clays.<sup>361</sup> By predefining the basal  $d$ -spacing, the final equilibrated composition may not correspond to a thermodynamically stable state.<sup>264</sup> From MD and MC simulations, the stability of the clay can be analyzed through the swelling free energy.<sup>299,323</sup>

Swelling may also occur due to the intercalation of CO<sub>2</sub> molecules within interlayers.<sup>323,330</sup> At low CO<sub>2</sub> concentration and low hydration state, CO<sub>2</sub> molecules organize themselves parallel to the surface.<sup>276,325,330</sup> By increasing the H<sub>2</sub>O concentration, CO<sub>2</sub> adopts other orientations, with some of them pointing perpendicular to the surface.<sup>322,330</sup> Swelling is not always expected to happen due to CO<sub>2</sub> intercalation. No evidence of swelling is observed in the presence of CO<sub>2</sub> for 1W Na-HEC.<sup>275</sup> The effect of swelling increases CO<sub>2</sub> diffusivity in

the interlayers of smectites.<sup>301,322–324,327</sup> Transition from 1W to 2W hydration state increases both CO<sub>2</sub> and H<sub>2</sub>O mobility. The increment is more pronounced on CO<sub>2</sub> diffusivity because molecules are no longer trapped in a single preferential orientation.<sup>324</sup> At the same hydration state, H<sub>2</sub>O mobility is higher at lower concentrations of CO<sub>2</sub> due to the hindering caused by the latter.<sup>327,361</sup> Kadoura et al.<sup>264</sup> showed that for a fixed basal  $d$ -spacing, CO<sub>2</sub> diffusivity decreases with loading of both CO<sub>2</sub> and H<sub>2</sub>O due to steric hindrance, but does not depend significantly on the loading of CH<sub>4</sub>. Both CO<sub>2</sub> and H<sub>2</sub>O molecules simultaneously adsorb in the clay surface and occupy the center region of the interlayer, whereas CH<sub>4</sub> does not present preferential adsorption. Therefore, the effect of both H<sub>2</sub>O and CO<sub>2</sub> loading on the CH<sub>4</sub> diffusion is more pronounced than the effect of CH<sub>4</sub> loading on CO<sub>2</sub> diffusion.<sup>264</sup>

The ions in the interlayer reduce the diffusivity of both H<sub>2</sub>O and CO<sub>2</sub>.<sup>263,363</sup> Severe confinement at 1W structure decreases the mobility of ions the most due to the strong electrostatic interactions with the mineral wall (the diffusion coefficient can be up to 4 orders of magnitude lower than the bulk).<sup>301</sup> Different cations may occupy the interlayer space to balance the surface charge. By fixing an ion-independent basal  $d$ -spacing, Kadoura et al.<sup>301</sup> have concluded that the diffusion of CO<sub>2</sub> is mostly independent of the cation type. Cations with different hydration energies could lead to different hydration and swelling of the clay, which may affect the diffusion of CO<sub>2</sub>.<sup>324</sup> The residence time between CO<sub>2</sub> and ions is short, and the activation energy for H<sub>2</sub>O molecules to move out of the first coordination shell of ions is 5 times larger than the activation energy for CO<sub>2</sub>.<sup>325,330</sup> The CO<sub>2</sub>–ion interaction is weak compared to their respective interaction with H<sub>2</sub>O molecules. Due to the repulsions, CO<sub>2</sub> may change the clay wettability.<sup>324</sup> In the presence of CO<sub>2</sub>, ion migration to the clay basal surface may screen part of the surface charge, increasing the surface hydrophobicity.<sup>323</sup>

Zhang et al.<sup>327</sup> have performed a compression test in MMT intercalated with CO<sub>2</sub> and H<sub>2</sub>O by deforming the cell parameters. The self-diffusion coefficient of both species decreases drastically with compression loading and approaches zero at the end of the test. The mineral stiffness is increased by the process of intercalation of both CO<sub>2</sub> and H<sub>2</sub>O.<sup>327</sup>

Owusu et al.<sup>265</sup> have investigated the diffusion of different gases (CO<sub>2</sub> included) in H<sub>2</sub>O confined by MMT. By increasing the pore size, CO<sub>2</sub> diffusion coefficient converges asymptotically to CO<sub>2</sub> unconfined diffusion. The diffusion is inversely proportional to the hydrodynamic radius of the gas. The authors have investigated the temperature influence on diffusion. As expected, by increasing temperature, the mobility of both CO<sub>2</sub> and H<sub>2</sub>O increases. The diffusion activation energy is changed by the confinement: for polyatomic molecules such as CO<sub>2</sub> and CH<sub>4</sub>, the activation energy is higher than in the bulk H<sub>2</sub>O,<sup>265</sup> which means that CO<sub>2</sub> diffusion is less dependent on temperature under confinement.

Figure 18 shows a compilation of the results reported for CO<sub>2</sub> diffusion coefficient in the interlayer of MMT. In  $D_{CO_2}^s$  is plotted as a function of  $1/T$  to verify the correspondence to Arrhenius equation (i.e.,  $D = D_0 \exp\left(-\frac{E_a}{RT}\right)$ ). A wide range of diffusivities is obtained for similar temperatures and hydration states. The main factors that may cause this dispersion are the fluid composition and density, the force field selection, the definition of the basal distance, and the method of computing the diffusion coefficient. At the same temperature and hydration state (2W), Kadoura et al.<sup>264</sup> have obtained diffusion coefficients different

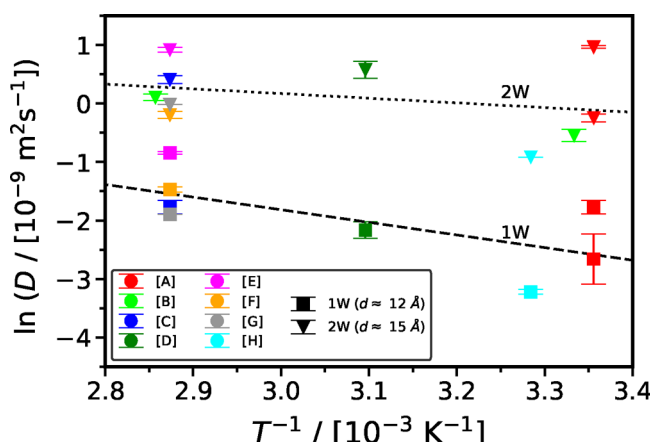


**Figure 18.**  $\text{CO}_2$  self-diffusion coefficient in Na-MMT at different temperatures for the 1W (square symbols) and 2W (triangle symbols) hydration states. The black dashed and dotted lines represent linear interpolation of Arrhenius equation for the 1W and 2W states, which are given by  $\ln D/D_0 = -2157.2/T + 4.7$  and  $\ln D/D_0 = -798.1/T + 2.6$ , respectively, where  $D_0 = 10^{-9} \text{ m}^2 \text{s}^{-1}$ . Legend: [A] Kadoura et al.; [B] Owusu et al.; [C] Botan et al.; [D] Kadoura et al.; [E] Makaremi et al.; [F] Myshakin et al.; [G] Rahromostaqim and Sahimi;<sup>324</sup> and [H] Zhang et al.<sup>327</sup>

from each other by a factor of 3. The lower the  $\text{H}_2\text{O}$  concentration (400 compared to  $600 \text{ kg m}^{-3}$ ), the higher the diffusivity. The number of  $\text{H}_2\text{O}$  and  $\text{CO}_2$  molecules should be defined in GCMC simulations before the MD simulation, to avoid simulation artifacts caused by an arbitrary choice of the number of particles. The usual basal  $d$ -space definition is the pore distance plus half the width of each T–O–T structure. Owusu et al.<sup>265</sup> have considered only the pore distance, which could cause some disparity when compared to other works if no correction is made. Finally, if the perpendicular component is accounted for in the trace of the diffusion coefficient,<sup>327</sup> then lower values are obtained compared with the parallel-only diffusion coefficients. By linear interpolation of the  $\ln D_{\text{CO}_2}^s$  vs  $1/T$  plot, the activation energy ( $E_a$ ) of  $\text{CO}_2$  diffusion in the 1W and 2W hydration states are 17.9 and  $6.6 \text{ kJ mol}^{-1}$ , respectively. The activation energy computed by Owusu et al.<sup>265</sup> for  $\text{CO}_2$  diffusion in MMT is ca.  $11.1 \text{ kJ mol}^{-1}$  (no difference caused by the pore size was accounted for).

**3.2.3.2. Calcite.** Despite the abundance of carbonate-bearing subsurface formations, only a few works have investigated the diffusion of  $\text{CO}_2$  confined by calcite.<sup>263,317,318,322,334</sup>  $\text{CO}_2$  solubility is reduced by the hydrophilic surface of calcite and the presence of salts, such as  $\text{NaCl}$ , may further reduce it.<sup>263</sup>  $\text{H}_2\text{O}$  at low concentrations increases  $\text{CO}_2$  diffusion by displacing  $\text{CO}_2$  toward the center of the pore due to  $\text{H}_2\text{O}$  preferential adsorption.<sup>333,334</sup> Increasing the concentration of both components, the species mobility decreases due to steric hindrance and molecular collisions.<sup>322,333</sup> For  $\text{CO}_2$  confined between parallel calcite minerals, an anisotropy in the  $\text{CO}_2$  parallel diffusion coefficients is observed due to the calcite plane morphology.<sup>317</sup> The same anisotropy is also observed in the  $\text{CO}_2\text{--H}_2\text{O}$  mixture.<sup>333,334</sup>

**3.2.3.3. Silica.**  $\text{CO}_2$  diffusion has been also investigated in silica nanopores.<sup>328,334,340,354</sup> The mobility of  $\text{CO}_2$  increases in regions with larger pores. For this reason,  $\text{CO}_2$  diffusion is higher in sepiolite channels than in palygorskite,<sup>328</sup> and larger in mesopores than micropores of the SBA-15 structure.<sup>340</sup> Molecules located close to the porous medium surface have

low mobility. The displacement of  $\text{CO}_2$  molecules caused by low concentrations of  $\text{H}_2\text{O}$  in hydrophilic surfaces increase  $\text{CO}_2$  diffusivity.<sup>334,340</sup> Under severe confinement (6 Å),  $\text{CO}_2$  diffusion coefficient is five times higher in hydrophobic silica than in the hydrophilic silica because of the lower  $\text{H}_2\text{O}$  content.<sup>354</sup>

**3.2.3.4. Other Materials.** Others confining materials include kerogen,<sup>332</sup> kaolinite,<sup>262</sup> forsterite,<sup>331</sup> Illite,<sup>324</sup> and zeolites.<sup>364</sup> As with the materials discussed earlier, the diffusivity of  $\text{CO}_2$  increases with temperature in kerogen. In the presence of  $\text{H}_2\text{O}$ , adsorption of  $\text{CO}_2$  onto functional groups of kerogen is reduced.<sup>332</sup> The hydrophobic surfaces of kaolinite promote a slightly higher parallel diffusion of  $\text{CO}_2$  than the hydrophilic surfaces for pressures up to 35 MPa.<sup>262</sup> Rahromostaqim and Sahimi<sup>324</sup> have investigated  $\text{CO}_2\text{--H}_2\text{O}$  diffusion confined by mixed layers of MMT and Illite, a mica mineral. They showed that the swelling and ion hydration depends on the charge location of the mineral. Within the bilayer space, the diffusivities of both  $\text{CO}_2$  and  $\text{H}_2\text{O}$  increase with the  $\text{H}_2\text{O}$ -to- $\text{CO}_2$  ratio.<sup>324</sup> Kerisit et al.<sup>331</sup> have studied the behavior of  $\text{CO}_2\text{--H}_2\text{O}$  in the interface of a forsterite mineral. A phase separation occurs, and a  $\text{H}_2\text{O}$  film forms at this mineral surface. The diffusivity of  $\text{CO}_2$  and  $\text{H}_2\text{O}$  are similar in both aqueous and  $\text{CO}_2$ -rich phase. In the transition interface region,  $\text{CO}_2$  is less hydrated by other  $\text{H}_2\text{O}$  molecules compared to their hydration in the bulk region, which results in a higher  $\text{CO}_2$  diffusivity than  $\text{H}_2\text{O}$  diffusivity in this region.<sup>331</sup> Wang et al.<sup>364</sup> have investigated the diffusion of flue gas ( $\text{CO}_2$ ,  $\text{NO}$ ,  $\text{NO}_2$ ,  $\text{N}_2$ ,  $\text{O}_2$ ,  $\text{SO}_2$  and  $\text{H}_2\text{O}$ ) in zeolites (13X and SA). The authors reported a correlation between the guest molecule size and its diffusivity, with triatomic molecules obtaining a lower diffusion coefficient. Due to the strong binding force between water molecules and the zeolite framework, no detectable  $\text{H}_2\text{O}$  diffusion was obtained with reasonable accuracy. As expected, the higher the temperature or the pore sizes (zeolite 13X), the higher the mobility and the diffusion coefficient of all molecules.<sup>364</sup>

**3.2.4. Confinement in Artificial Media.** **3.2.4.1. Metal–Organic Frameworks.** MOFs are crystal-like structures composed of metal clusters and organic linkers. Due to their potential to separate  $\text{CO}_2$  from flue gas, the diffusion of  $\text{CO}_2$  in various MOFs at different conditions have been investigated.<sup>344–347</sup> The diffusion behavior of  $\text{CO}_2$  in this confining medium depends on the crystal structure and the loading.

Diffusion and adsorption show opposite trends, i.e., the species with higher adsorption energy tend to have lower mobility. Mera et al.<sup>347</sup> investigated the diffusion of the  $\text{CO}_2\text{--N}_2\text{--H}_2\text{O}$  mixture in three MOFs (IRMOF-1, Cu-BTC, and MIL-47). Although Cu-BTC has the narrowest pores, the reduction in pure  $\text{CO}_2$  diffusion is higher in the confinement imposed by MIL-47 due to the stronger interactions between the adsorbate and the framework. In the presence of  $\text{H}_2\text{O}$ ,  $\text{CO}_2$  diffusion coefficient in MIL-47 is increased by 1 order of magnitude. The competition between  $\text{CO}_2$  and  $\text{H}_2\text{O}$  for the active sites increases the mobility of both species. The opposite occurs in the mixture diffusion in Cu-BTC, in which the species have a lower diffusivity compared to its pure components diffusion.<sup>347</sup>

Magnin et al.<sup>345</sup> investigated the  $\text{CO}_2$  diffusion in UiO-66 at different loadings of  $\text{CO}_2$  and  $\text{H}_2\text{O}$ . At lower pressures (lower loadings),  $\text{CO}_2$  preferentially adsorbs in the tetrahedral cages and the diffusion mechanism is mainly cage hopping.<sup>345,346</sup> By increasing  $\text{CO}_2$  loading, its mobility is reduced due to the increase of  $\text{CO}_2\text{--CO}_2$  collisions and reduction in the MOF free

volume. In a different MOF, CALF-20, further increment in  $\text{CO}_2$  loading could actually increase  $\text{CO}_2$  diffusivity because of the presence of more than one  $\text{CO}_2$  per cage could make their interaction with the solid surface weaker.<sup>346</sup>

In UiO-66 MOF,  $\text{H}_2\text{O}$  acts as an extra sorbent medium for  $\text{CO}_2$  diffusion. The tortuosity created by the  $\text{H}_2\text{O}$  network, the  $\text{CO}_2-\text{H}_2\text{O}$  attractive interactions, and the occupied pore volume at high  $\text{H}_2\text{O}$  loading are some of the reasons for the reduction in  $\text{CO}_2$  mobility in the presence of  $\text{H}_2\text{O}$ .<sup>345</sup> In CALF-20, the enthalpies of adsorption of  $\text{CO}_2$  and  $\text{H}_2\text{O}$  have similar magnitudes, which results in similar values for their diffusion coefficients.<sup>346</sup> On the other hand, in the Mg-MOF-74, where the adsorption energy between water and the open metal sites is stronger,  $\text{CO}_2$  diffusion coefficient can be an order of magnitude higher than  $\text{H}_2\text{O}$ .<sup>345</sup>

Darcy's law describing the fluid flow in the porous media, fails to predict the fluid transport in nanopores by neglecting the adsorption. Magnin et al.<sup>345</sup> have computed the permeance, which corrects Darcy's law, using the confined fluid diffusivity. From the nano-Darcy expression, they show that the macroscopic fluid flow in UiO-66 MOF decreases with  $\text{H}_2\text{O}$  loading, following the behavior predicted by the diffusion mechanisms.<sup>345</sup>

Figure 19 shows at which conditions the  $\text{CO}_2$  diffusion in MOFs has been investigated by the studies available in literature. The  $\text{CO}_2$  mole fraction here accounts only for the presence of  $\text{CO}_2$  and  $\text{H}_2\text{O}$  as guest molecules (not accounting for the  $\text{N}_2$  in the work of Mera et al.,<sup>347</sup> for instance). The focus so far has been mainly on temperatures ca. 300 K and low loadings (low pressure), with few exceptions. In the future, it could be interesting to further investigate the temperature and pressure effects, because by changing these conditions one can control the adsorption/release of guest molecules in gas capture applications.

**3.2.4.2. Carbon Materials.** Carbon nanotubes (CNTs) allow for faster  $\text{CO}_2$  diffusion compared to other nanoporous materials.<sup>336</sup> The larger the pore, the higher the  $\text{CO}_2$  mobility.<sup>300,336,339</sup> Contrary to other materials,  $\text{CO}_2$  diffusion coefficients in CNTs is almost space-independent. Svoboda et al.<sup>336</sup> attribute the abnormal higher diffusivity close to the wall to the  $\text{CO}_2$  parallel orientation to the nanotube. The effect of  $\text{H}_2\text{O}$  on  $\text{CO}_2$  diffusion is a balance between  $\text{CO}_2$  displacement and  $\text{CO}_2-\text{H}_2\text{O}$  interactions.<sup>300,336</sup> Because these interactions are stronger than  $\text{CH}_4-\text{H}_2\text{O}$  interactions, the effect of preadsorbed  $\text{H}_2\text{O}$  is less pronounced on  $\text{CO}_2$  diffusion than on methane diffusion.<sup>300</sup> In hydrophobic carbon mesoporous surfaces, such as CMK-5, at high pressures (high loading) the  $\text{CO}_2$  diffusivity is decreased in the presence of  $\text{H}_2\text{O}$  due to the reduction in the pore free volume.<sup>340</sup> In most cases, the mobility of species increases with temperature. Zhao et al.<sup>339</sup> discovered, however, that the diffusion coefficient of hydrogen decreases with temperature in the mixture of  $\text{CO}_2-\text{H}_2-\text{H}_2\text{O}$  confined by graphene sheets. The increment in the thermal motion of  $\text{CO}_2$  and  $\text{H}_2\text{O}$  molecules with temperature acts like an extra obstruction to small  $\text{H}_2$  molecules.<sup>339</sup>

#### 4. OUTLOOK

In light of the discussion we provided in this review and the currently available data (experimental and MD) on the diffusivity of  $\text{CO}_2$  in  $\text{H}_2\text{O}$ , we propose several promising directions for future research for both cases of diffusivity in bulk or under confinement.

##### 4.1. $\text{CO}_2-\text{H}_2\text{O}$ Diffusion in Bulk.

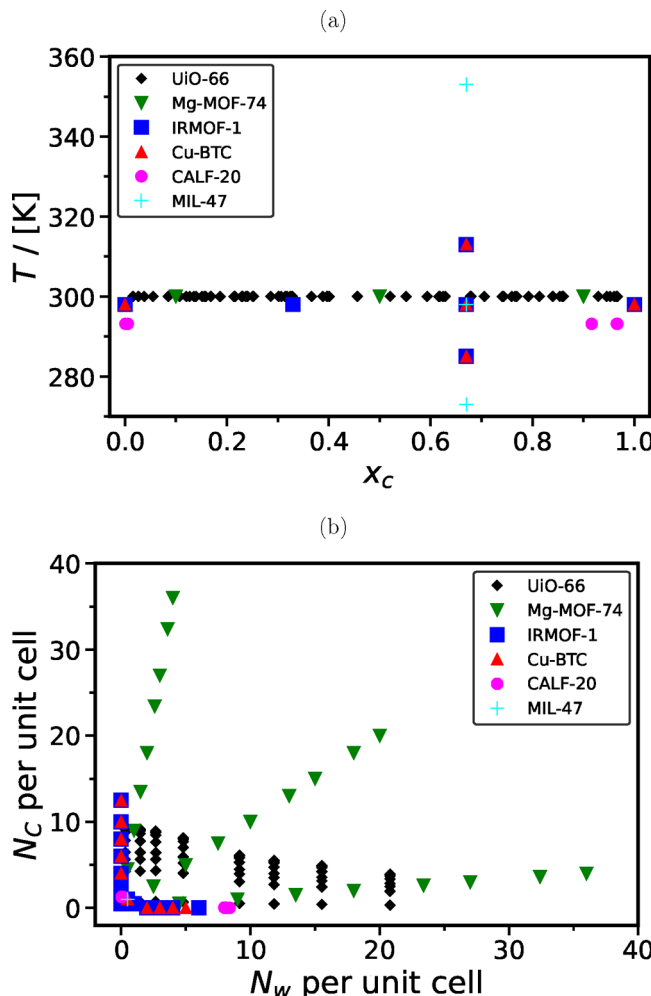


**Figure 19.** Conditions with available data in the literature for  $\text{CO}_2$  diffusion confined in metal organic frameworks UiO-66,<sup>345</sup> IRMOF-1,<sup>347</sup> Cu-BTC,<sup>347</sup> MIL-47,<sup>347</sup> Mg-MOF-74,<sup>344</sup> and CALF-20.<sup>346</sup> (a) Temperature as a function of  $\text{CO}_2$  composition ( $x_{\text{CO}_2} = N_{\text{CO}_2}/(N_{\text{CO}_2} + N_{\text{H}_2\text{O}})$ ), and (b) loading as a function of the number of  $\text{CO}_2$  and  $\text{H}_2\text{O}$  per unit cell.

- The effect of pressure on the diffusion of  $\text{CO}_2$  in brines needs to be further investigated via: (i) additional experimental measurements, and/or (ii) extensive MD simulations;
- Additional experimental measurements for  $\text{CO}_2$  diffusion in brines are required to provide adequate data for the development of accurate correlations. Emphasis should be given to aqueous salt-solutions (other than NaCl solutions), as well as to geologic formation brines;
- In addition to useful engineering-type correlations of the experimental data, there is a need for the development of theoretically based models for the diffusivity of  $\text{CO}_2$  in pure  $\text{H}_2\text{O}$  and brines;
- A call for closer collaboration between experimental and simulation groups is stressed to rigorously validate simulation results, thereby deepening the insights into  $\text{CO}_2$  diffusion in  $\text{H}_2\text{O}$ . Currently in literature, for many systems the experimental data are insufficient for validating the results from MD studies, especially at high temperatures and pressures. An enhanced synergy

- between experiments and simulations can pave the way for more accurate simulations of CO<sub>2</sub> in H<sub>2</sub>O;
- Polarizable force fields may offer the potential for a more precise representation of electrostatic interactions in aqueous solutions of CO<sub>2</sub>, increasing the accuracy of MD simulations.<sup>216–218,365,366</sup> Simulations are needed toward this direction since no data exist for the diffusivity of CO<sub>2</sub> in H<sub>2</sub>O using polarizable force fields;
  - Ab initio MD (AIMD) simulation is another possible method to study the diffusivity of CO<sub>2</sub> in H<sub>2</sub>O, yielding a more comprehensive understanding of electronic structure in the solution.<sup>367</sup> Although AIMD simulations have already been used to investigate the reaction mechanism and dynamics of CO<sub>2</sub> in different solvents,<sup>367–372</sup> their applicability to computing transport properties is largely hindered by the significant additional computational cost, compared to classical MD, that does not allow for accessing the time scale required to capture the diffusive regime. Nevertheless, with the ever-increasing computational power being available, AIMD could be an interesting route to explore further;
  - Introducing machine learning techniques into force field parametrization is possible to increase the predictive accuracy by discerning patterns in extensive data sets.<sup>373</sup> This field is already very active, nevertheless, more efforts can focus on the CO<sub>2</sub>–H<sub>2</sub>O system;
  - Currently, the behavior of CO<sub>2</sub> diffusivity at near-critical H<sub>2</sub>O is not well understood. Additional MD simulations are required to produce the necessary data at these conditions. An advancement in this area will facilitate the refinement of the engineering-type correlations, and thus, allow for the development of more accurate predictive tools.

#### 4.2. CO<sub>2</sub>–H<sub>2</sub>O Diffusion under Confinement.

- Experimental investigation of the mixture diffusion mechanisms with techniques such as QENS and NMR would be a powerful route to explore;
- When performing MD simulations, care should be taken to choose the initial configuration and the method. We advocate the use of GCMC to determine the composition and loading for a giving state, and the use of methods that account for the nonhomogeneity of the confined fluid to compute the diffusion coefficients;
- From a methodological perspective, the study of transport diffusion coefficients using NEMD simulations to account for the collective transport and the investigation of possible finite-size effects in the confined CO<sub>2</sub> diffusion is an interesting future directive;
- Diffusion within confining materials, such as smectites, have been extensively studied. Others, however, such as calcite, which is a mineral abundant in subsurface formations, needs further investigation since it is important for many applications, e.g., CCS.

### 5. CONCLUSIONS

In this review paper, experimental data for the diffusion coefficient of CO<sub>2</sub> in pure H<sub>2</sub>O are collected and discussed in detail. The experimental data are used to develop simple and computationally efficient correlations. These correlations are applicable to temperatures from 273 K and 0.1 MPa to 473 K and pressures up to 45 MPa. At this pressure and temperature range, the diffusion coefficient of CO<sub>2</sub> in H<sub>2</sub>O has a very weak

dependence on pressure. Therefore, the proposed correlations are only temperature-dependent. The proposed correlations could be useful for engineering calculations that are related to a number of industrial and environmental processes. Finally, experimental data for the diffusion coefficient of CO<sub>2</sub> in brines are collected and their dependency on temperature, pressure and salinity have been thoroughly examined and reported.

Along with the experimental data, in this review, a detailed discussion on the available MD studies of CO<sub>2</sub> diffusivity in aqueous solutions is provided. The focus is on the force field combinations, the data for diffusivities at low and high pressures, the finite-size effects, and the correlations using MD data. The vast majority of the available MD studies of CO<sub>2</sub> diffusivity in H<sub>2</sub>O report data at the infinite dilution limit (i.e., 1 to 5 solute molecules). The very few data available for higher CO<sub>2</sub> compositions are also provided and useful analysis is performed. A short discussion related to CO<sub>2</sub> diffusivity in carbonated hydroalcoholic drinks is also available.

For certain applications, e.g., CCS, a confining structure can constrain the CO<sub>2</sub> mobility, and consequently reduce CO<sub>2</sub> diffusion coefficients. Here, the main methods to compute the diffusivity of confined CO<sub>2</sub> are reviewed and the main natural and artificial confining media (i.e., smectites, calcites, silica, MOFs, and carbon materials), focusing primarily on MD simulations and secondarily on experimental studies are discussed. Smectites were found to be the most studied material due to their swelling, which generates an interlayer space capable of intercalating CO<sub>2</sub> and H<sub>2</sub>O. The diffusion of CO<sub>2</sub> and H<sub>2</sub>O under confinement is driven by a balance between adsorption and steric hindrance. For hydrophilic surfaces, water at lower concentrations increases CO<sub>2</sub> mobility due to preferential adsorption of H<sub>2</sub>O. Based on the analysis and discussion, an outlook containing possible, useful, future research paths for advancing the field of CO<sub>2</sub> diffusivity in H<sub>2</sub>O at the bulk phase and in confinement is devised.

### ■ ASSOCIATED CONTENT

#### SI Supporting Information

The Supporting Information is available free of charge at <https://pubs.acs.org/doi/10.1021/acs.jced.3c00778>.

Raw experimental and simulation data shown in the figures, along with the available statistical uncertainties ([XLSX](#))

### ■ AUTHOR INFORMATION

#### Corresponding Authors

Othonas A. Moultsos – *Engineering Thermodynamics, Process & Energy Department, Faculty of Mechanical Engineering, Delft University of Technology, 2628CB Delft, The Netherlands; [orcid.org/0000-0001-7477-9684](#); Email: o.moultsos@tudelft.nl*

Ioannis N. Tsimpanogiannis – *Chemical Process & Energy Resources Institute (CPERI)/Centre for Research & Technology Hellas (CERTH), 57001 Thermi-Thessaloniki, Greece; [orcid.org/0000-0002-3466-1873](#); Email: i.n.tsimpanogiannis@certh.gr*

Luis Fernando Mercier Franco – *Universidade Estadual de Campinas (UNICAMP), Faculdade de Engenharia Química, Campinas CEP: 13083-852, Brazil; Email: lmfranco@unicamp.br*

**Authors**

H. Mert Polat – *Engineering Thermodynamics, Process & Energy Department, Faculty of Mechanical Engineering, Delft University of Technology, 2628CB Delft, The Netherlands*

Felipe M. Coelho – *Universidade Estadual de Campinas (UNICAMP), Faculdade de Engenharia Química, Campinas CEP: 13083-852, Brazil; [orcid.org/0000-0002-7572-1991](#)*

Thijs J. H. Vlugt – *Engineering Thermodynamics, Process & Energy Department, Faculty of Mechanical Engineering, Delft University of Technology, 2628CB Delft, The Netherlands; [orcid.org/0000-0003-3059-8712](#)*

Complete contact information is available at:

<https://pubs.acs.org/10.1021/acs.jced.3c00778>

**Author Contributions**

<sup>¶</sup>These authors contributed equally to this work.

**Notes**

The authors declare no competing financial interest.

**ACKNOWLEDGMENTS**

This work was sponsored by NWO Domain Science for the use of supercomputer facilities. O.A.M., H.M.P., and T.J.H.V. acknowledge the use of computational resources of DelftBlue supercomputer provided by Delft High Performance Computing Centre (<https://www.tudelft.nl/dhpc>). O.A.M. gratefully acknowledges the support of NVIDIA Corporation with the donation of the Titan V GPU used for this research. F.M.C. and L.F.M.F. are grateful for the support provided by São Paulo Research Foundation (FAPESP) grants #2018/02713-8 and #2020/13300-6, CNPq (The Brazilian National Council for Scientific and Technological Development), and CAPES (Coordination of Superior Level Staff Improvement). The work of I.N.T. has received partial funding from the European Union HORIZON Europe project “CEEGS—Novel CO<sub>2</sub>—based Electrothermal Energy and Geological Storage System”, under Grand Agreement Number: 101084376. Views and opinions expressed are however those of the author(s) only and do not necessarily reflect those of the European Union or CINEA. Neither the European Union nor the granting authority can be held responsible for them.

**REFERENCES**

- (1) Marchetti, C. On geoengineering and the CO<sub>2</sub> problem. *Climatic Change* **1977**, *1*, 59–68.
- (2) Turkenburg, W. C. Sustainable development, climate change, and carbon dioxide removal (CDR). *Energy Conversion and Management* **1997**, *38*, S3–S12.
- (3) Herzog, H.; Caldeira, K.; Reilly, J. An issue of permanence: Assessing the effectiveness of temporary carbon storage. *Climatic Change* **2003**, *59*, 293–310.
- (4) Metz, B.; Davidson, O.; De Coninck, H.; Loos, M.; Meyer, L. *IPCC Special Report on Carbon Dioxide Capture and Storage*; Cambridge University Press: Cambridge, U.K., 2005.
- (5) Kenarsari, S. D.; Yang, D.; Jiang, G.; Zhang, S.; Wang, J.; Russell, A. G.; Wei, Q.; Fan, M. Review of recent advances in carbon dioxide separation and capture. *RSC Adv.* **2013**, *3*, 22739–22773.
- (6) Skovholt, O. CO<sub>2</sub> transportation system. *Energy Conversion and Management* **1993**, *34*, 1095–1103.
- (7) Aursand, P.; Hammer, M.; Munkejord, S. T.; Wilhelmsen, Ø. Pipeline transport of CO<sub>2</sub> mixtures: Models for transient simulation. *International Journal of Greenhouse Gas Control* **2013**, *15*, 174–185.
- (8) Schiermeier, Q. Putting the carbon back: The hundred billion tonne challenge. *Nature* **2006**, *442*, 620–624.
- (9) Goodman, A.; Hakala, A.; Bromhal, G.; Deel, D.; Rodosta, T.; Frailey, S.; Small, M.; Allen, D.; Romanov, V.; Fazio, J.; Huerta, N.; McIntyre, D.; Kutchko, B.; Guthrie, G. others US DOE methodology for the development of geologic storage potential for carbon dioxide at the national and regional scale. *Int. J. Greenhouse Gas Control* **2011**, *5*, 952–965.
- (10) Middleton, R. S.; Keating, G. N.; Stauffer, P. H.; Jordan, A. B.; Viswanathan, H. S.; Kang, Q. J.; Carey, J. W.; Mulkey, M. L.; Sullivan, E. J.; Chu, S. P.; Esposito, R.; Meckel, T. A. others The cross-scale science of CO<sub>2</sub> capture and storage: from pore scale to regional scale. *Energy Environ. Sci.* **2012**, *5*, 7328–7345.
- (11) Bergman, P. D.; Winter, E. M.; Chen, Z.-Y. Disposal of power plant CO<sub>2</sub> in depleted oil and gas reservoirs in Texas. *Energy Conversion and Management* **1997**, *38*, S211–S216.
- (12) Holtz, M. H.; Nance, P. K.; Finley, R. J. Reduction of greenhouse gas emissions through CO<sub>2</sub> EOR in Texas. *Environmental Geosciences* **2001**, *8*, 187–199.
- (13) Kovsek, A. R. Screening criteria for CO<sub>2</sub> storage in oil reservoirs. *Petroleum Science and Technology* **2002**, *20*, 841–866.
- (14) Oldenburg, C.; Pruess, K.; Benson, S. M. Process modeling of CO<sub>2</sub> injection into natural gas reservoirs for carbon sequestration and enhanced gas recovery. *Energy Fuels* **2001**, *15*, 293–298.
- (15) Bachu, S.; Gunter, W.; Perkins, E. Aquifer disposal of CO<sub>2</sub>: hydrodynamic and mineral trapping. *Energy Conversion and Management* **1994**, *35*, 269–279.
- (16) Holt, T.; Jensen, J.-I.; Lindeberg, E. Underground storage of CO<sub>2</sub> in aquifers and oil reservoirs. *Energy Conversion and Management* **1995**, *36*, 535–538.
- (17) Bachu, S.; Adams, J. J. Sequestration of CO<sub>2</sub> in geological media in response to climate change: capacity of deep saline aquifers to sequester CO<sub>2</sub> in solution. *Energy Conversion and Management* **2003**, *44*, 3151–3175.
- (18) Michael, K.; Golab, A.; Shulakova, V.; Ennis-King, J.; Allinson, G.; Sharma, S.; Aiken, T. Geological storage of CO<sub>2</sub> in saline aquifers—A review of the experience from existing storage operations. *International Journal of Greenhouse Gas Control* **2010**, *4*, 659–667.
- (19) Keating, E. H.; Newell, D. L.; Viswanathan, H.; Carey, J.; Zyvoloski, G.; Pawar, R. CO<sub>2</sub>/brine transport into shallow aquifers along fault zones. *Environ. Sci. Technol.* **2013**, *47*, 290–297.
- (20) Steele-MacInnis, M.; Capobianco, R. M.; Dilmore, R.; Goodman, A.; Guthrie, G.; Rimstidt, J. D.; Bodnar, R. J. Volumetrics of CO<sub>2</sub> storage in deep saline formations. *Environ. Sci. Technol.* **2013**, *47*, 79–86.
- (21) Coelho, F. M.; Franco, L. F. M.; Firoozabadi, A. Thermodiffusion of CO<sub>2</sub> in Water by Nonequilibrium Molecular Dynamics Simulations. *Journal Physical Chemistry B* **2023**, *127*, 2749–2760.
- (22) Coelho, F. M.; Franco, L. F. M.; Firoozabadi, A. Effect of Salinity on CO<sub>2</sub> Thermodiffusion in Aqueous Mixtures by Molecular Dynamics Simulations. *ACS Sustainable Chem. Eng.* **2023**, *11*, 17086–17097.
- (23) Gale, J.; Freund, P. Coal-bed methane enhancement with CO<sub>2</sub> sequestration worldwide potential. *Environmental Geosciences* **2001**, *8*, 210–217.
- (24) Stevens, S. H.; Kuuskraa, V. A.; Gale, J.; Beecy, D. CO<sub>2</sub> injection and sequestration in depleted oil and gas fields and deep coal seams: worldwide potential and costs. *Environmental Geosciences* **2001**, *8*, 200–209.
- (25) White, C. M.; Smith, D. H.; Jones, K. L.; Goodman, A. L.; Jikich, S. A.; LaCount, R. B.; DuBose, S. B.; Ozdemir, E.; Morsi, B. I.; Schroeder, K. T. Sequestration of carbon dioxide in coal with enhanced coalbed methane recovery a review. *Energy Fuels* **2005**, *19*, 659–724.
- (26) Mazumder, S.; Van Hemert, P.; Bruining, J.; Wolf, K.-H.; Drabe, K. In situ CO<sub>2</sub>—coal reactions in view of carbon dioxide storage in deep unminable coal seams. *Fuel* **2006**, *85*, 1904–1912.
- (27) Pruess, K. Enhanced geothermal systems (EGS) using CO<sub>2</sub> as working fluid—A novel approach for generating renewable energy with simultaneous sequestration of carbon. *Geothermics* **2006**, *35*, 351–367.
- (28) Pruess, K. On production behavior of enhanced geothermal systems with CO<sub>2</sub> as working fluid. *Energy Conversion and Management* **2008**, *49*, 1446–1454.

- (29) Kyriakides, A.-S.; Stoikos, A.; Trigkas, D.; Gravanis, G.; Tsimpanogiannis, I. N.; Papadopoulou, S.; Voutetakis, S. Modelling and Evaluation of CO<sub>2</sub>-based Electrothermal Energy Storage System. *Chem. Eng. Trans.* **2023**, *103*, 505–510.
- (30) Carro, A.; Chacartegui, R.; Ortiz, C.; Carneiro, J.; Becerra, J. Energy storage system based on transcritical CO<sub>2</sub> cycles and geological storage. *Applied Thermal Engineering* **2021**, *193*, No. 116813.
- (31) Carro, A.; Chacartegui, R.; Ortiz, C.; Carneiro, J.; Becerra, J. Integration of energy storage systems based on transcritical CO<sub>2</sub>: Concept of CO<sub>2</sub> based electrothermal energy and geological storage. *Energy* **2022**, *238*, No. 121665.
- (32) Tsimpanogiannis, I. N.; Yortsos, Y. C.; Stubos, A. K. Evaporation of a stagnant liquid. *Ind. Eng. Chem. Res.* **2000**, *39*, 1505–1513.
- (33) Yiotis, A.; Boudouvis, A.; Stubos, A.; Tsimpanogiannis, I.; Yortsos, Y. Effect of liquid films on the drying of porous media. *AICHE J.* **2004**, *50*, 2721–2737.
- (34) Pruess, K.; Müller, N. Formation dry-out from CO<sub>2</sub> injection into saline aquifers: 1. Effects of solids precipitation and their mitigation. *Water Resour. Res.* **2009**, *45*, No. W03402.
- (35) Ott, H.; Roels, S.; De Kloe, K. Salt precipitation due to supercritical gas injection: I. Capillary-driven flow in unimodal sandstone. *International Journal of Greenhouse Gas Control* **2015**, *43*, 247–255.
- (36) Lake, L. W. *Enhanced Oil Recovery; Old Tappan*, Prentice Hall Inc.: Hoboken, NJ, 1989.
- (37) Khatiwala, S.; Tanhua, T.; Mikaloff Fletcher, S.; Gerber, M.; Doney, S. C.; Graven, H. D.; Gruber, N.; McKinley, G. A.; Murata, A.; Rios, A. F.; Sabine, C. L. Global ocean storage of anthropogenic carbon. *Biogeosciences* **2013**, *10*, 2169–2191.
- (38) DeVries, T. The oceanic anthropogenic CO<sub>2</sub> sink: Storage, air-sea fluxes, and transports over the industrial era. *Global Biogeochemical Cycles* **2014**, *28*, 631–647.
- (39) DeVries, T.; Holzer, M.; Primeau, F. Recent increase in oceanic carbon uptake driven by weaker upper-ocean overturning. *Nature* **2017**, *542*, 215–218.
- (40) Perret, A.; Bonhommeau, D. A.; Liger-Belair, G.; Cours, T.; Alijah, A. CO<sub>2</sub> diffusion in champagne wines: A molecular dynamics study. *J. Phys. Chem. B* **2014**, *118*, 1839–1847.
- (41) Duan, Z.; Sun, R. An improved model calculating CO<sub>2</sub> solubility in pure water and aqueous NaCl solutions from 273 to 533 K and from 0 to 2000 bar. *Chem. Geol.* **2003**, *193*, 257–271.
- (42) Carroll, J. J.; Slupsky, J. D.; Mather, A. E. The Solubility of Carbon Dioxide in Water at Low Pressure. *J. Phys. Chem. Ref. Data* **1991**, *20*, 1201–1209.
- (43) Gallagher, J.; Crovotto, R.; Sengers, J. L. The thermodynamic behavior of the CO<sub>2</sub>-H<sub>2</sub>O system from 400 to 1000 K, up to 100 MPa and 30% mole fraction of CO<sub>2</sub>. *J. Phys. Chem. Ref. Data* **1993**, *22*, 431–513.
- (44) Duan, Z.; Sun, R.; Zhu, C.; Chou, I.-M. An improved model for the calculation of CO<sub>2</sub> solubility in aqueous solutions containing Na<sup>+</sup>, K<sup>+</sup>, Ca<sup>2+</sup>, Mg<sup>2+</sup>, Cl<sup>-</sup>, and SO<sub>4</sub><sup>2-</sup>. *Marine Chemistry* **2006**, *98*, 131–139.
- (45) Mourtos, O. A.; Tsimpanogiannis, I. N.; Panagiotopoulos, A. Z.; Economou, I. G. Atomistic molecular dynamics simulations of CO<sub>2</sub> diffusivity in H<sub>2</sub>O for a wide range of temperatures and pressures. *J. Phys. Chem. B* **2014**, *118*, 5532–5541.
- (46) Taylor, R.; Krishna, R. *Multicomponent Mass Transfer*, 1<sup>st</sup> ed.; John Wiley & Sons: New York, 1993.
- (47) Jamali, S. H.; Wolff, L.; Becker, T. M.; de Groen, M.; Ramdin, M.; Hartkamp, R.; Bardow, A.; Vlugt, T. J. H.; Mourtos, O. A. OCTP: A Tool for On-the-fly Calculation of Transport Properties of Fluids with the Order-n Algorithm in LAMMPS. *J. Chem. Inf. Model.* **2019**, *59*, 1290–1294.
- (48) Janzen, T.; Zhang, S.; Mialdun, A.; Guevara-Carrion, G.; Vrabec, J.; He, M.; Shevtsova, V. Mutual Diffusion Governed by Kinetics and Thermodynamics in the Partially Miscible Mixture Methanol + Cyclohexane. *Phys. Chem. Chem. Phys.* **2017**, *19*, 31856–31873.
- (49) Liu, X.; Schnell, S. K.; Simon, J.-M.; Krüger, P.; Bedeaux, D.; Kjelstrup, S.; Bardow, A.; Vlugt, T. J. H. Diffusion Coefficients from Molecular Dynamics Simulations in Binary and Ternary Mixtures. *Int. J. Thermophys.* **2013**, *34*, 1169–1196.
- (50) Cussler, E. L. *Diffusion: Mass Transfer in Fluid Systems*, 3<sup>rd</sup> ed.; Cambridge University Press: Cambridge, U.K., 2009.
- (51) Krishna, R.; Wesselingh, J. The Maxwell-Stefan Approach to Mass Transfer. *Chem. Eng. Sci.* **1997**, *52*, 861–911.
- (52) Wolff, L.; Jamali, S. H.; Becker, T. M.; Mourtos, O. A.; Vlugt, T. J. H.; Bardow, A. Prediction of Composition-Dependent Self-Diffusion Coefficients in Binary Liquid Mixtures: The Missing Link for Darken-Based Models. *Ind. Eng. Chem. Res.* **2018**, *57*, 14784–14794.
- (53) Poling, B. E.; Prausnitz, J. M.; O'Connal, J. P. *The Properties of Gases and Liquids*, 5<sup>th</sup> ed.; McGraw-Hill: Singapore, 2001.
- (54) Jamali, S. H.; Bardow, A.; Vlugt, T. J. H.; Mourtos, O. A. Generalized Form for Finite-Size Corrections in Mutual Diffusion Coefficients of Multicomponent Mixtures Obtained from Equilibrium Molecular Dynamics Simulation. *J. Chem. Theory Comput.* **2020**, *16*, 3799–3806.
- (55) Krüger, P.; Schnell, S. K.; Bedeaux, D.; Kjelstrup, S.; Vlugt, T. J. H.; Simon, J.-M. Kirkwood–Buff Integrals for Finite Volumes. *J. Phys. Chem. Lett.* **2013**, *4*, 235–238.
- (56) Dawass, N.; Krüger, P.; Schnell, S. K.; Simon, J.-M.; Vlugt, T. J. H. Kirkwood–Buff Integrals from Molecular Simulation. *Fluid Phase Equilib.* **2019**, *486*, 21–36.
- (57) Dawass, N.; Krüger, P.; Schnell, S. K.; Mourtos, O. A.; Economou, I. G.; Vlugt, T. J. H.; Simon, J.-M. Kirkwood–Buff Integrals Using Molecular Simulation: Estimation of Surface Effects. *Nanomaterials* **2020**, *10*, 771.
- (58) Simon, J.-M.; Krüger, P.; Schnell, S. K.; Vlugt, T. J. H.; Kjelstrup, S.; Bedeaux, D. Kirkwood–Buff integrals: From fluctuations in finite volumes to the thermodynamic limit. *J. Chem. Phys.* **2022**, *157*, No. 130901.
- (59) Hulikal Chakrapani, T.; Hajibeygi, H.; Mourtos, O. A.; Vlugt, T. J. H. Calculating Thermodynamic Factors for Diffusion Using the Continuous Fractional Component Monte Carlo Method. *J. Chem. Theory Comput.* **2024**, *20*, 333–347.
- (60) Himmelblau, D. M. Diffusion of Dissolved Gases in Liquids. *Chem. Rev.* **1964**, *64*, 527–550.
- (61) Mutoru, J. W.; Leahy-Dios, A.; Firoozabadi, A. Modeling infinite dilution and Fickian diffusion coefficients of carbon dioxide in water. *AICHE J.* **2011**, *57*, 1617–1627.
- (62) Wilke, C. R.; Chang, P. Correlation of Diffusion Coefficients in Dilute Solutions. *AICHE J.* **1955**, *1*, 264–270.
- (63) Bird, R. B.; Stewart, W. E.; Lightfoot, E. N. *Transport Phenomena*, 2<sup>nd</sup> ed.; John Wiley & Sons: New York, 2007.
- (64) Allen, M. P.; Tildesley, D. J. *Computer Simulation of Liquids*, 2<sup>nd</sup> ed.; Oxford University Press: Oxford, UK, 2017.
- (65) Frenkel, D.; Smit, B. *Understanding Molecular Simulation: From Algorithms to Applications*, 3<sup>rd</sup> ed.; Academic Press: San Diego, CA, 2023.
- (66) Chatwell, R. S.; Guevara-Carrion, G.; Gaponenko, Y.; Shevtsova, V.; Vrabec, J. Diffusion of the carbon dioxide–ethanol mixture in the extended critical region. *Phys. Chem. Chem. Phys.* **2021**, *23*, 3106–3115.
- (67) Erdős, M.; Frangou, M.; Vlugt, T. J. H.; Mourtos, O. A. Diffusivity of α-, β-, γ-cyclodextrin and the inclusion complex of β-cyclodextrin: Ibuprofen in aqueous solutions: A molecular dynamics simulation study. *Fluid Phase Equilib.* **2021**, *528*, No. 112842.
- (68) Kozlova, S.; Mialdun, A.; Ryzhkov, I.; Janzen, T.; Vrabec, J.; Shevtsova, V. Do ternary liquid mixtures exhibit negative main Fick diffusion coefficients? *Phys. Chem. Chem. Phys.* **2019**, *21*, 2140–2152.
- (69) Michalis, V. K.; Mourtos, O. A.; Tsimpanogiannis, I. N.; Economou, I. G. Molecular dynamics simulations of the diffusion coefficients of light n-alkanes in water over a wide range of temperature and pressure. *Fluid Phase Equilib.* **2016**, *407*, 236–242.
- (70) Perez, S.; Guevara-Carrion, G.; Hasse, H.; Vrabec, J. Mutual diffusion in the ternary mixture of water + methanol + ethanol and its binary subsystems. *Phys. Chem. Chem. Phys.* **2013**, *15*, 3985–4001.
- (71) Liu, X.; Bardow, A.; Vlugt, T. J. H. Multicomponent Maxwell–Stefan Diffusivities at Infinite Dilution. *Ind. Eng. Chem. Res.* **2011**, *50*, 4776–4782.

- (72) Tsimpanogiannis, I. N.; Maity, S.; Celebi, A. T.; Moultsos, O. A. Engineering Model for Predicting the Intradiffusion Coefficients of Hydrogen and Oxygen in Vapor, Liquid, and Supercritical Water based on Molecular Dynamics Simulations. *Journal of Chemical & Engineering Data* **2021**, *66*, 3226–3244.
- (73) Moultsos, O. A.; Tsimpanogiannis, I. N.; Panagiotopoulos, A. Z.; Economou, I. G. Self-diffusion coefficients of the binary ( $\text{H}_2\text{O} + \text{CO}_2$ ) mixture at high temperatures and pressures. *J. Chem. Thermodyn.* **2016**, *93*, 424–429.
- (74) Moultsos, O. A.; Orozco, G. A.; Tsimpanogiannis, I. N.; Panagiotopoulos, A. Z.; Economou, I. G. Atomistic molecular dynamics simulations of  $\text{H}_2\text{O}$  diffusivity in liquid and supercritical  $\text{CO}_2$ . *Mol. Phys.* **2015**, *113*, 2805–2814.
- (75) van Rooijen, W. A.; Habibi, P.; Xu, K.; Dey, P.; Vlugt, T. J. H.; Hajibeygi, H.; Moultsos, O. A. Interfacial Tensions, Solubilities, and Transport Properties of the  $\text{H}_2/\text{H}_2\text{O}/\text{NaCl}$  System: A Molecular Simulation Study. *J. Chem. Eng. Data* **2024**, *69*, 307–319.
- (76) Habibi, P.; Rahbari, A.; Blazquez, S.; Vega, C.; Dey, P.; Vlugt, T. J. H.; Moultsos, O. A. A New Force Field for  $\text{OH}^-$  for Computing Thermodynamic and Transport Properties of  $\text{H}_2$  and  $\text{O}_2$  in Aqueous NaOH and KOH Solutions. *J. Phys. Chem. B* **2022**, *126*, 9376–9387.
- (77) Polat, H. M.; van der Geest, C.; de Meyer, F.; Houriez, C.; Vlugt, T. J. H.; Moultsos, O. A. Densities, viscosities, and diffusivities of loaded and unloaded aqueous  $\text{CO}_2/\text{H}_2\text{S}/\text{MDEA}$  mixtures: A molecular dynamics simulation study. *Fluid Phase Equilib.* **2023**, *575*, No. 113913.
- (78) Polat, H. M.; de Meyer, F.; Houriez, C.; Coquelet, C.; Moultsos, O. A.; Vlugt, T. J. H. Transport properties of mixtures of acid gases with aqueous monoethanolamine solutions: A molecular dynamics study. *Fluid Phase Equilib.* **2023**, *564*, No. 113587.
- (79) Moultsos, O. A.; Tsimpanogiannis, I. N.; Panagiotopoulos, A. Z.; Trusler, J. P. M.; Economou, I. G. Atomistic Molecular Dynamics Simulations of Carbon Dioxide Diffusivity in n-Hexane, n-Decane, n-Hexadecane, Cyclohexane, and Squalane. *J. Phys. Chem. B* **2016**, *120*, 12890–12900.
- (80) Fang, B.; Habibi, P.; Moultsos, O. A.; Lü, T.; Ning, F.; Vlugt, T. J. H. Solubilities and Self-Diffusion Coefficients of Light n-Alkanes in  $\text{NaCl}$  Solutions at the Temperature Range (278.15–308.15) K and Pressure Range (1–300) bar and Thermodynamics Properties of Their Corresponding Hydrates at (150–290) K and (1–7000) bar. *Journal of Chemical & Engineering Data*, In Press DOI: [10.1021/acs.jced.3c00225](https://doi.org/10.1021/acs.jced.3c00225).
- (81) Ma, L.; Salehi, H. S.; Jing, R.; Erkens, S.; Vlugt, T. J. H.; Moultsos, O. A.; Greenfield, M. L.; Varveri, A. Water diffusion mechanisms in bitumen studied through molecular dynamics simulations. *Construction and Building Materials* **2023**, *409*, No. 133828.
- (82) Habibi, P.; Postma, J. R. T.; Padding, J. T.; Dey, P.; Vlugt, T. J. H.; Moultsos, O. A. Thermodynamic and Transport Properties of  $\text{H}_2/\text{H}_2\text{O}/\text{NaB(OH)}_4$  Mixtures Using the Delft Force Field (DFF/B (OH) $^+$ ). *Ind. Eng. Chem. Res.* **2023**, *62*, 11992–12005.
- (83) Plimpton, S. Fast Parallel Algorithms for Short-Range Molecular Dynamics. *J. Comput. Phys.* **1995**, *117*, 1–19.
- (84) Van Der Spoel, D.; Lindahl, E.; Hess, B.; Groenhof, G.; Mark, A. E.; Berendsen, H. J. C. GROMACS: Fast, flexible, and free. *J. Comput. Chem.* **2005**, *26*, 1701–1718.
- (85) Abascal, J. L. F.; Vega, C. A general purpose model for the condensed phases of water: TIP4P/2005. *J. Chem. Phys.* **2005**, *123*, No. 234505.
- (86) Martin, M. G.; Siepmann, J. I. Transferable Potentials for Phase Equilibria. 1. United-Atom Description of n-Alkanes. *J. Phys. Chem. B* **1998**, *102*, 2569–2577.
- (87) Jiang, H.; Moultsos, O. A.; Economou, I. G.; Panagiotopoulos, A. Z. Gaussian-charge Polarizable and Nonpolarizable Models for  $\text{CO}_2$ . *J. Phys. Chem. B* **2016**, *120*, 984–994.
- (88) Lyra, E. P.; Franco, L. F. M. Deriving force fields with a multiscale approach: From ab initio calculations to molecular-based equations of state. *J. Chem. Phys.* **2022**, *157*, No. 114107.
- (89) Tsimpanogiannis, I. N.; Moultsos, O. A. Is Stokes-Einstein relation valid for the description of intra-diffusivity of hydrogen and oxygen in liquid water? *Fluid Phase Equilib.* **2023**, *563*, No. 113568.
- (90) Moultsos, O. A.; Tsimpanogiannis, I. N. Predictive model for the intra-diffusion coefficients of  $\text{H}_2$  and  $\text{O}_2$  in vapour  $\text{H}_2\text{O}$  based on data from molecular dynamics simulations. *Mol. Phys.* **2023**, *121*, No. e2211889.
- (91) Saeki, S.; Tsubokawa, M.; Yamanaka, J.; Yamaguchi, T. Correlation between equation of state and temperature and pressure dependence of self-diffusion coefficient of polymers and simple liquids. *Polymer* **1990**, *31*, 2338–2345.
- (92) Zhu, Y.; Lu, X.; Zhou, J.; Wang, Y.; Shi, J. Prediction of diffusion coefficients for gas, liquid and supercritical fluid: application to pure real fluids and infinite dilute binary solutions based on the simulation of Lennard-Jones fluid. *Fluid Phase Equilif.* **2002**, *194–197*, 1141–1159.
- (93) Zuo, Z.; Lu, X.; Ji, X. Modeling Self-Diffusion Coefficient and Viscosity of Chain-like Fluids Based on ePC-SAFT. *J. Chem. Eng. Data* **2024**, *69*, 348.
- (94) Hopp, M.; Mele, J.; Gross, J. Self-Diffusion Coefficients from Entropy Scaling Using the PCP-SAFT Equation of State. *Ind. Eng. Chem. Res.* **2018**, *57*, 12942–12950.
- (95) Dehlouz, A.; Jaubert, J.-N.; Galliero, G.; Bonnissel, M.; Privat, R. Entropy Scaling-Based Correlation for Estimating the Self-Diffusion Coefficients of Pure Fluids. *Ind. Eng. Chem. Res.* **2022**, *61*, 14033–14050.
- (96) Li, B.; Xiao, X.; Lou, K.; Wang, S.; Wen, W.; Wang, Z. Breakdown of diffusivity–entropy scaling in colloidal glass-forming liquids. *Communications Physics* **2018**, *1*, 79.
- (97) Tyrrell, H. J. V.; Harris, K. *Diffusion in Liquids: A Theoretical and Experimental Study*; Butterworth-Heinemann: Oxford, U.K., 2013.
- (98) Upadhyay, S. R.; Mehrotra, A. K. Experimental determination of gas diffusivity in liquids—A review. *Canadian Journal of Chemical Engineering* **2021**, *99*, 1239–1267.
- (99) Rezk, M. G.; Foroozesh, J.; Abdulrahman, A.; Gholinezhad, J.  $\text{CO}_2$  diffusion and dispersion in porous media: Review of advances in experimental measurements and mathematical models. *Energy Fuels* **2022**, *36*, 133–155.
- (100) Tham, M.; Bhatia, K.; Gubbins, K. Steady-state method for studying diffusion of gases in liquids. *Chem. Eng. Sci.* **1967**, *22*, 309–311.
- (101) Takeuchi, H.; Fujine, M.; Sato, T.; Onda, K. Simultaneous determination of diffusion coefficient and solubility of gas in liquid by a diaphragm cell. *J. Chem. Eng. Jpn.* **1975**, *8*, 252–253.
- (102) Jähne, B.; Heinz, G.; Dietrich, W. Measurement of the diffusion coefficients of sparingly soluble gases in water. *Journal of Geophysical Research: Oceans* **1987**, *92*, 10767–10776.
- (103) Al-Ghawas, H. A.; Hagewiesche, D. P.; Ruiz-Ibanez, G.; Sandall, O. C. Physicochemical properties important for carbon dioxide absorption in aqueous methyl-diethanolamine. *Journal of Chemical & Engineering Data* **1989**, *34*, 385–391.
- (104) Tamimi, A.; Rinker, E. B.; Sandall, O. C. Diffusion coefficients for hydrogen sulfide, carbon dioxide, and nitrous oxide in water over the temperature range 293–368 K. *Journal of Chemical & Engineering Data* **1994**, *39*, 330–332.
- (105) Unver, A.; Himmelblau, D. Diffusion Coefficients of  $\text{CO}_2$ ,  $\text{C}_2\text{H}_4$ ,  $\text{C}_3\text{H}_6$  and  $\text{C}_4\text{H}_8$  in Water from 6° to 65° C. *Journal of Chemical & Engineering Data* **1964**, *9*, 428–431.
- (106) Thomas, W.; Adams, M. Measurement of the diffusion coefficients of carbon dioxide and nitrous oxide in water and aqueous solutions of glycerol. *Trans. Faraday Soc.* **1965**, *61*, 668–673.
- (107) Duda, J.; Vrentas, J. Laminar liquid jet diffusion studies. *AIChE J.* **1968**, *14*, 286–294.
- (108) Diaz, J.; Vega, A.; Coca, J. Diffusivities of carbon dioxide and nitrous oxide in aqueous alcohol solutions. *Journal of Chemical & Engineering Data* **1988**, *33*, 10–12.
- (109) Ross, M.; Hildebrand, J. H. Diffusion of hydrogen, deuterium, nitrogen, argon, methane, and carbon tetrafluoride in carbon tetrachloride. *J. Chem. Phys.* **1964**, *40*, 2397–2399.
- (110) Malik, V.; Hayduk, W. A steady-state capillary cell method for measuring gas-liquid diffusion coefficients. *Canadian Journal of Chemical Engineering* **1968**, *46*, 462–466.

- (111) Taylor, G. I. Dispersion of soluble matter in solvent flowing slowly through a tube. *Proc. R. Soc. London. Ser. A* **1953**, *219*, 186–203.
- (112) Aris, R. On the dispersion of a solute in a fluid flowing through a tube. *Proc. R. Soc. London. Ser. A* **1956**, *235*, 67–77.
- (113) Cadogan, S. P.; Maitland, G. C.; Trusler, J. M. Diffusion coefficients of CO<sub>2</sub> and N<sub>2</sub> in water at temperatures between 298.15 and 423.15 K at pressures up to 45 MPa. *Journal of Chemical & Engineering Data* **2014**, *59*, 519–525.
- (114) Hirai, S.; Okazaki, K.; Yazawa, H.; Ito, H.; Tabe, Y.; Hijikata, K. Measurement of CO<sub>2</sub> diffusion coefficient and application of LIF in pressurized water. *Energy* **1997**, *22*, 363–367.
- (115) Wu, W.; Klein, T.; Kerscher, M.; Rausch, M. H.; Koller, T. M.; Giraudet, C.; Fröba, A. P. Diffusivities in 1-alcohols containing dissolved H<sub>2</sub>, He, N<sub>2</sub>, CO, or CO<sub>2</sub> close to infinite dilution. *J. Phys. Chem. B* **2019**, *123*, 8777–8790.
- (116) Lu, W.; Guo, H.; Chou, I.-M.; Burruss, R.; Li, L. Determination of diffusion coefficients of carbon dioxide in water between 268 and 473 K in a high-pressure capillary optical cell with in situ Raman spectroscopic measurements. *Geochim. Cosmochim. Acta* **2013**, *115*, 183–204.
- (117) Belgodere, C.; Dubessy, J.; Vautrin, D.; Caumon, M.-C.; Sterpenich, J.; Pironon, J.; Robert, P.; Randi, A.; Birat, J.-P. Experimental determination of CO<sub>2</sub> diffusion coefficient in aqueous solutions under pressure at room temperature via Raman spectroscopy: impact of salinity (NaCl). *J. Raman Spectrosc.* **2015**, *46*, 1025–1032.
- (118) Liger-Belair, G.; Prost, E.; Parmentier, M.; Jeandet, P.; Nuzillard, J.-M. Diffusion coefficient of CO<sub>2</sub> molecules as determined by <sup>13</sup>C NMR in various carbonated beverages. *J. Agric. Food Chem.* **2003**, *51*, 7560–7563.
- (119) Cadogan, S. P.; Hallett, J. P.; Maitland, G. C.; Trusler, J. M. Diffusion coefficients of carbon dioxide in brines measured using <sup>13</sup>C pulsed-field gradient nuclear magnetic resonance. *Journal of Chemical & Engineering Data* **2015**, *60*, 181–184.
- (120) Bellaire, D.; Großmann, O.; Münnemann, K.; Hasse, H. Diffusion coefficients at infinite dilution of carbon dioxide and methane in water, ethanol, cyclohexane, toluene, methanol, and acetone: A PFG-NMR and MD simulation study. *J. Chem. Thermodyn.* **2022**, *166*, No. 106691.
- (121) Sell, A.; Fadaei, H.; Kim, M.; Sinton, D. Measurement of CO<sub>2</sub> Diffusivity for Carbon Sequestration: A Microfluidic Approach for Reservoir-Specific Analysis. *Environ. Sci. Technol.* **2013**, *47*, 71–78.
- (122) Haugen, K. B.; Firoozabadi, A. Mixing of two binary nonequilibrium phases in one dimension. *AIChE J.* **2009**, *55*, 1930–1936.
- (123) Yang, Z.; Bryant, S.; Dong, M.; Hassanzadeh, H. An analytical method of estimating diffusion coefficients of gases in liquids from pressure decay tests. *AIChE J.* **2019**, *65*, 434–445.
- (124) Basilio, E.; Addassi, M.; Al-Juaied, M.; Hassanzadeh, S. M.; Hoteit, H. Improved Pressure Decay Method for Measuring CO<sub>2</sub>-Water Diffusion Coefficient without Convection Interference. *Advances in Water Resources* **2024**, *183*, No. 104608.
- (125) Yang, D.; Tontiwachwuthikul, P.; Gu, Y. Dynamic interfacial tension method for measuring gas diffusion coefficient and interface mass transfer coefficient in a liquid. *Ind. Eng. Chem. Res.* **2006**, *45*, 4999–5008.
- (126) Yang, C.; Gu, Y. New experimental method for measuring gas diffusivity in heavy oil by the dynamic pendant drop volume analysis (DPDVA). *Ind. Eng. Chem. Res.* **2005**, *44*, 4474–4483.
- (127) Yang, C.; Gu, Y. A new method for measuring solvent diffusivity in heavy oil by dynamic pendant drop shape analysis (DPDSA). *SPE Journal* **2006**, *11*, 48–57.
- (128) Wen, Y.; Kantzas, A. Monitoring bitumen-solvent interactions with low-field nuclear magnetic resonance and X-Ray computer-assisted tomography. *Energy Fuels* **2005**, *19*, 1319–1326.
- (129) Eide, Ø.; Fernø, M. A.; Alcorn, Z.; Graue, A. Visualization of carbon dioxide enhanced oil recovery by diffusion in fractured chalk. *SPE Journal* **2016**, *21*, 112–120.
- (130) Muir, C.; Lowry, B.; Balcom, B. Measuring diffusion using the differential form of Fick's law and magnetic resonance imaging. *New J. Phys.* **2011**, *13*, No. 015005.
- (131) Tang, Y.-P.; Himmelblau, D. Interphase mass transfer for laminar concurrent flow of carbon dioxide and water between parallel plates. *AIChE J.* **1963**, *9*, 630–635.
- (132) Lee, S.; Song, H.-J.; Maken, S.; Shin, H.-C.; Song, H.-C.; Park, J.-W. Physical solubility and diffusivity of N<sub>2</sub>O and CO<sub>2</sub> in aqueous sodium glycinate solutions. *Journal of Chemical & Engineering Data* **2006**, *51*, 504–509.
- (133) Olbrich, W.; Wild, J. Diffusion from the free surface into a liquid film in laminar flow over defined shapes. *Chem. Eng. Sci.* **1969**, *24*, 25–32.
- (134) Davidson, J. The determination of diffusion coefficient for sparingly soluble gases in liquids. *Trans. Inst. Chem. Eng.* **1957**, *35*, 51–60.
- (135) Danckwerts, P.; Kennedy, A. The kinetics of absorption of carbon dioxide into neutral and alkaline solutions. *Chem. Eng. Sci.* **1958**, *8*, 201–215.
- (136) Goodgame, T.; Sherwood, T. The additivity of resistances in mass transfer between phases. *Chem. Eng. Sci.* **1954**, *3*, 37–42.
- (137) Warner, N. Gas-phase mass-transfer in a disk-column. *Chem. Eng. Sci.* **1959**, *11*, 130–137.
- (138) Alizadeh, A.; Nieto de Castro, C.; Wakeham, W. The theory of the Taylor dispersion technique for liquid diffusivity measurements. *Int. J. Thermophys.* **1980**, *1*, 243–284.
- (139) Ferrell, R. T.; Himmelblau, D. M. Diffusion coefficients of nitrogen and oxygen in water. *Journal of Chemical & Engineering Data* **1967**, *12*, 111–115.
- (140) Snijder, E. D.; te Riele, M. J.; Versteeg, G. F.; van Swaaij, W. P. Diffusion Coefficients of CO, CO<sub>2</sub>, N<sub>2</sub>O, and N<sub>2</sub> in Ethanol and Toluene. *Journal of Chemical & Engineering Data* **1995**, *40*, 37–39.
- (141) Frank, M. J.; Kuipers, J. A.; van Swaaij, W. P. Diffusion coefficients and viscosities of CO<sub>2</sub> + H<sub>2</sub>O, CO<sub>2</sub> + CH<sub>3</sub>OH, NH<sub>3</sub> + H<sub>2</sub>O, and NH<sub>3</sub> + CH<sub>3</sub>OH liquid mixtures. *Journal of Chemical & Engineering Data* **1996**, *41*, 297–302.
- (142) Klein, T.; Wu, W.; Rausch, M. H.; Giraudet, C.; Koller, T. M.; Fröba, A. P. Influence of liquid structure on Fickian diffusion in binary mixtures of n-hexane and carbon dioxide probed by dynamic light scattering, Raman spectroscopy, and molecular dynamics simulations. *J. Phys. Chem. B* **2018**, *122*, 7122–7133.
- (143) Price, W. S. Pulsed-field gradient nuclear magnetic resonance as a tool for studying translational diffusion: Part 1. Basic theory. *Concepts in Magnetic Resonance: An Educational Journal* **1997**, *9*, 299–336.
- (144) Price, W. S. Pulsed-field gradient nuclear magnetic resonance as a tool for studying translational diffusion: Part II. Experimental aspects. *Concepts in Magnetic Resonance: An Educational Journal* **1998**, *10*, 197–237.
- (145) Riazi, M. R. A new method for experimental measurement of diffusion coefficients in reservoir fluids. *J. Pet. Sci. Eng.* **1996**, *14*, 235–250.
- (146) Ghaderi, S. M.; Tabatabaie, S. H.; Hassanzadeh, H.; Pooladi-Darvish, M. Estimation of concentration-dependent diffusion coefficient in pressure-decay experiment of heavy oils and bitumen. *Fluid Phase Equilib.* **2011**, *305*, 132–144.
- (147) Farajzadeh, R.; Barati, A.; Delil, H. A.; Bruining, J.; Zitha, P. L. Mass transfer of CO<sub>2</sub> into water and surfactant solutions. *Petroleum Science and Technology* **2007**, *25*, 1493–1511.
- (148) Rongy, L.; Haugen, K. B.; Firoozabadi, A. Mixing from Fickian diffusion and natural convection in binary non-equilibrium fluid phases. *AIChE J.* **2012**, *58*, 1336–1345.
- (149) Yang, C.; Gu, Y. Accelerated mass transfer of CO<sub>2</sub> in reservoir brine due to density-driven natural convection at high pressures and elevated temperatures. *Ind. Eng. Chem. Res.* **2006**, *45*, 2430–2436.
- (150) Li, Z.; Dong, M.; Li, S.; Dai, L. A new method for gas effective diffusion coefficient measurement in water-saturated porous rocks under high pressures. *Journal of Porous Media* **2006**, *9*, 445–461.

- (151) Azin, R.; Mahmoudy, M.; Raad, S. M. J.; Osfouri, S. Measurement and modeling of CO<sub>2</sub> diffusion coefficient in saline aquifer at reservoir conditions. *Cent. Eur. J. Eng.* **2013**, *3*, 585–594.
- (152) Jafari Raad, S. M.; Azin, R.; Osfouri, S. Measurement of CO<sub>2</sub> diffusivity in synthetic and saline aquifer solutions at reservoir conditions: the role of ion interactions. *Heat and Mass Transfer* **2015**, *51*, 1587–1595.
- (153) Zhang, W.; Wu, S.; Ren, S.; Zhang, L.; Li, J. The modeling and experimental studies on the diffusion coefficient of CO<sub>2</sub> in saline water. *J. CO<sub>2</sub> Utili.* **2015**, *11*, 49–53.
- (154) Shi, Z.; Wen, B.; Hesse, M.; Tsotsis, T.; Jessen, K. Measurement and modeling of CO<sub>2</sub> mass transfer in brine at reservoir conditions. *Advances in Water Resources* **2018**, *113*, 100–111.
- (155) Tharanivasan, A. K.; Yang, C.; Gu, Y. Comparison of three different interface mass transfer models used in the experimental measurement of solvent diffusivity in heavy oil. *J. Pet. Sci. Eng.* **2004**, *44*, 269–282.
- (156) Etminan, S. R.; Maini, B. B.; Chen, Z. Determination of mass transfer parameters in solvent-based oil recovery techniques using a non-equilibrium boundary condition at the interface. *Fuel* **2014**, *120*, 218–232.
- (157) Rasmussen, M. L.; Civan, F. Parameters of gas dissolution in liquids obtained by isothermal pressure decay. *AIChE J.* **2009**, *55*, 9–23.
- (158) Magalhães, A. L.; Lito, P. F.; Da Silva, F. A.; Silva, C. M. Simple and accurate correlations for diffusion coefficients of solutes in liquids and supercritical fluids over wide ranges of temperature and density. *J. Supercrit. Fluids* **2013**, *76*, 94–114.
- (159) Aziz, K.; Settari, A. *Petroleum Reservoir Simulation*; Applied Science Publishers: Basel, Switzerland, 1979.
- (160) Islam, A. W.; Carlson, E. S. Viscosity models and effects of dissolved CO<sub>2</sub>. *Energy Fuels* **2012**, *26*, 5330–5336.
- (161) Versteeg, G. F.; Van Swaaij, W. P. Solubility and diffusivity of acid gases (carbon dioxide, nitrous oxide) in aqueous alkanolamine solutions. *Journal of Chemical & Engineering Data* **1988**, *33*, 29–34.
- (162) Speedy, R.; Angell, C. Isothermal compressibility of super-cooled water and evidence for a thermodynamic singularity at –45 C. *J. Chem. Phys.* **1976**, *65*, 851–858.
- (163) Zeebe, R. E. On the molecular diffusion coefficients of dissolved CO<sub>2</sub>, HCO<sub>3</sub><sup>-</sup>, and CO<sub>3</sub><sup>2-</sup> and their dependence on isotopic mass. *Geochim. Cosmochim. Acta* **2011**, *75*, 2483–2498.
- (164) Shimizu, K. *Measurement of the Diffusion Coefficient of CO<sub>2</sub>-Aqueous Solutions Systems under High Pressure by the Taylor Dispersion Method*. Proc. of the Fourth Asian Thermophysical Properties Conference; 1995; pp 771–774.
- (165) Tomita, S.; Shimizu, K.; Nagashima, A. *Measurement of the diffusion coefficient of CO<sub>2</sub> in high pressure water by the Taylor dispersion method*. Physical Chemistry of Aqueous Systems: Meeting the Needs of Industry; 1994.
- (166) Chiquet, P. *Mécanismes Thermophysiques Déterminant la Sécurité du Stockage Géologique du CO<sub>2</sub>*; Ph.D. thesis: Pau, 2006.
- (167) Tewes, F.; Boury, F. Formation and rheological properties of the supercritical CO<sub>2</sub>-water pure interface. *J. Phys. Chem. B* **2005**, *109*, 3990–3997.
- (168) Li, B.; Zhang, Q.; Cao, A.; Bai, H.; Xu, J. Experimental and Numerical Studies on the Diffusion of CO<sub>2</sub> from Oil to Water. *Journal of Thermal Science* **2020**, *29*, 268–278.
- (169) Ahmadi, H.; Jamialahmadi, M.; Soulhani, B. S.; Dinarvand, N.; Sharafi, M. S. Experimental study and modelling on diffusion coefficient of CO<sub>2</sub> in water. *Fluid Phase Equilib.* **2020**, *523*, No. 112584.
- (170) Ratcliff, G.; Holdcroft, J. Diffusivities of gases in aqueous electrolyte solutions. *Trans. Inst. Chem. Eng.* **1963**, *41*, 315–319.
- (171) Mutoru, J. W.; Leahy-Dios, A.; Firoozabadi, A. Modeling infinite dilution and Fickian diffusion coefficients of carbon dioxide in water. *AIChE J.* **2011**, *57*, 1617–1627.
- (172) Perera, P. N.; Deng, H.; Schuck, P. J.; Gilbert, B. Diffusivity of carbon dioxide in aqueous solutions under geologic carbon sequestration conditions. *J. Phys. Chem. B* **2018**, *122*, 4566–4572.
- (173) Nijsing, R.; Hendriksz, R.; Kramers, H. Absorption of CO<sub>2</sub> in jets and falling films of electrolyte solutions, with and without chemical reaction. *Chem. Eng. Sci.* **1959**, *10*, 88–104.
- (174) Wang, L.-S.; Lang, Z.-X.; Guo, T.-M. Measurement and correlation of the diffusion coefficients of carbon dioxide in liquid hydrocarbons under elevated pressures. *Fluid Phase Equilib.* **1996**, *117*, 364–372.
- (175) Bahar, M. M.; Liu, K. *Measurement of the Diffusion Coefficient of CO<sub>2</sub> in Formation Water under Reservoir Conditions: Implications for CO<sub>2</sub> Storage*; SPE Asia Pacific Oil and Gas Conference and Exhibition, 2008.
- (176) Wang, S.; Hou, J.; Liu, B.; Zhao, F.; Yuan, G.; Liu, G. The pressure-decay method for nature convection accelerated diffusion of CO<sub>2</sub> in oil and water under elevated pressures. *Energy Sources, Part A: Recovery, Utilization, and Environmental Effects* **2013**, *35*, 538–545.
- (177) Zarghami, S.; Boukadi, F.; Al-Wahaibi, Y. Diffusion of carbon dioxide in formation water as a result of CO<sub>2</sub> enhanced oil recovery and CO<sub>2</sub> sequestration. *Journal of Petroleum Exploration and Production Technology* **2017**, *7*, 161–168.
- (178) Shu, G.; Dong, M.; Chen, S.; Hassanzadeh, H. Mass transfer of CO<sub>2</sub> in a carbonated water–oil system at high pressures. *Ind. Eng. Chem. Res.* **2017**, *56*, 404–416.
- (179) Shu, G.; Dong, M.; Hassanzadeh, H.; Chen, S. Effects of operational parameters on diffusion coefficients of CO<sub>2</sub> in a carbonated water–oil system. *Ind. Eng. Chem. Res.* **2017**, *56*, 12799–12810.
- (180) Li, X.; Liu, Y.; Jiang, L.; Song, Y. Diffusion properties for CO<sub>2</sub>–brine system under sequestration-related pressures with consideration of the swelling effect and interfacial area. *Ind. Eng. Chem. Res.* **2018**, *57*, 15556–15564.
- (181) Tang, Y.; Li, Z.; Wang, R.; Cui, M.; Wang, X.; Lun, Z.; Lu, Y. Experimental study on the density-driven carbon dioxide convective diffusion in formation water at reservoir conditions. *ACS Omega* **2019**, *4*, 11082–11092.
- (182) Zhang, Y.; Geng, W.; Chen, M.; Xu, X.; Jiang, L.; Song, Y. Experimental Measurements of the Diffusion Coefficient and Effective Diffusion Coefficient of CO<sub>2</sub>–Brine under Offshore CO<sub>2</sub> Storage Conditions. *Energy Fuels* **2023**, *37*, 19695–19703.
- (183) Yiannourakou, M.; Rozanska, X.; Minisini, B.; de Meyer, F. Molecular simulations for improved process modeling of an acid gas removal unit. *Fluid Phase Equilib.* **2022**, *560*, No. 113478.
- (184) Perez-Blanco, M. E.; Maginn, E. J. Molecular Dynamics Simulations of CO<sub>2</sub> at an Ionic Liquid Interface: Adsorption, Ordering, and Interfacial Crossing. *J. Phys. Chem. B* **2010**, *114*, 11827–11837.
- (185) Yu, T.; Cai, Q.; Lian, G.; Liu, L. Molecular dynamics studies on separation of CO<sub>2</sub>/CH<sub>4</sub> by the ionic liquids encapsulated ZIF-8. *J. Membr. Sci.* **2022**, *644*, No. 120117.
- (186) Dokoochaki, M. H.; Zolghadr, A. R. Significant Improvement in CO<sub>2</sub> Absorption by Deep Eutectic Solvents as Immobilized Sorbents: Computational Analysis. *J. Phys. Chem. B* **2021**, *125*, 10035–10046.
- (187) Xin, K.; van Sint Annaland, M. Diffusivities and solubilities of carbon dioxide in deep eutectic solvents. *Sep. Purif. Technol.* **2023**, *307*, No. 122779.
- (188) Geng, H.; Chen, F.; Ye, J.; Jiang, F. Applications of Molecular Dynamics Simulation in Structure Prediction of Peptides and Proteins. *Computational and Structural Biotechnology Journal* **2019**, *17*, 1162–1170.
- (189) Chen, Q.; Balaji, S. P.; Ramdin, M.; Gutierrez-Sevillano, J. J.; Bardow, A.; Goetheer, E.; Vlugt, T. J. H. Validation of the CO<sub>2</sub>/N<sub>2</sub>O analogy using molecular simulation. *Ind. Eng. Chem. Res.* **2014**, *53*, 18081–18090.
- (190) Kohns, M.; Werth, S.; Horsch, M.; von Harbou, E.; Hasse, H. Molecular simulation study of the CO<sub>2</sub>-N<sub>2</sub>O analogy. *Fluid Phase Equilib.* **2017**, *442*, 44–52.
- (191) Maginn, E. J.; Messerly, R. A.; Carlson, D. J.; Roe, D. R.; Elliott, J. R. Best Practices for Computing Transport Properties 1. Self-Diffusivity and Viscosity from Equilibrium Molecular Dynamics. *Living J. Comp. Mol. Sci.* **2020**, *2*, 6324.
- (192) Tenney, C. M.; Maginn, E. J. Limitations and recommendations for the calculation of shear viscosity using reverse nonequilibrium molecular dynamics. *J. Chem. Phys.* **2010**, *132*, No. 014103.

- (193) Zhao, X.; Jin, H. Correlation for self-diffusion coefficients of H<sub>2</sub>, CH<sub>4</sub>, CO, O<sub>2</sub> and CO<sub>2</sub> in supercritical water from molecular dynamics simulation. *Applied Thermal Engineering* **2020**, *171*, No. 114941.
- (194) van der Hoef, M. A.; Frenkel, D. Long-time tails of the velocity autocorrelation function in two- and three-dimensional lattice-gas cellular automata: A test of mode-coupling theory. *Phys. Rev. A* **1990**, *41*, 4277–4284.
- (195) Abraham, M. et al. GROMACS 2023.3 Manual; 2023; DOI: 10.5281/zenodo.10017699.
- (196) Humbert, M. T.; Zhang, Y.; Maginn, E. J. PyLAT: Python LAMMPS Analysis Tools. *J. Chem. Inf. Model.* **2019**, *59*, 1301–1305.
- (197) Harris, J. G.; Yung, K. H. Carbon Dioxide's Liquid-Vapor Coexistence Curve And Critical Properties as Predicted by a Simple Molecular Model. *J. Phys. Chem.* **1995**, *99*, 12021–12024.
- (198) Potoff, J. J.; Siepmann, J. I. Vapor–liquid equilibria of mixtures containing alkanes, carbon dioxide, and nitrogen. *AIChE J.* **2001**, *47*, 1676–1682.
- (199) Buckingham, A. D.; Disch, R. L. The quadrupole moment of the carbon dioxide molecule. *Proc. R. Soc. London A* **1963**, *273*, 275–289.
- (200) Moldover, M. R.; Gallagher, J. S. Critical points of mixtures: An analogy with pure fluids. *AIChE J.* **1978**, *24*, 267–278.
- (201) Panhuis, M. I. H.; Patterson, C. H.; Lynden-Bell, R. M. A molecular dynamics study of carbon dioxide in water: Diffusion, structure and thermodynamics. *Mol. Phys.* **1998**, *94*, 963–972.
- (202) van Gunsteren, W. F.; Berendsen, H. J. Groningen molecular simulation (GROMOS) library manual. *Biomos, Groningen* **1987**, *24*, 13.
- (203) Brooks, B. R.; et al. CHARMM: The biomolecular simulation program. *J. Comput. Chem.* **2009**, *30*, 1545–1614.
- (204) Sun, H. COMPASS: An ab Initio Force-Field Optimized for Condensed-Phase ApplicationsOverview with Details on Alkane and Benzene Compounds. *J. Phys. Chem. B* **1998**, *102*, 7338–7364.
- (205) Merker, T.; Engin, C.; Vrabec, J.; Hasse, H. Molecular model for carbon dioxide optimized to vapor-liquid equilibria. *J. Chem. Phys.* **2010**, *132*, No. 234512.
- (206) Orozco, G. A.; Economou, I. G.; Panagiotopoulos, A. Z. Optimization of intermolecular potential parameters for the CO<sub>2</sub>/H<sub>2</sub>O mixture. *J. Phys. Chem. B* **2014**, *118*, 11504–11511.
- (207) Vlcek, L.; Chialvo, A. A.; Cole, D. R. Optimized unlike-pair interactions for water-carbon dioxide mixtures described by the SPC/E and EPM2 models. *J. Phys. Chem. B* **2011**, *115*, 8775–8784.
- (208) Costandy, J.; Michalis, V. K.; Tsipmanogiannis, I. N.; Stubos, A. K.; Economou, I. G. The role of intermolecular interactions in the prediction of the phase equilibria of carbon dioxide hydrates. *J. Chem. Phys.* **2015**, *143*, 094506.
- (209) Abascal, J.; Sanz, E.; García Fernández, R.; Vega, C. A potential model for the study of ices and amorphous water: TIP4P/Ice. *J. Chem. Phys.* **2005**, *122*, No. 234511.
- (210) Costandy, J.; Michalis, V. K.; Tsipmanogiannis, I. N.; Stubos, A. K.; Economou, I. G. Molecular dynamics simulations of pure methane and carbon dioxide hydrates: lattice constants and derivative properties. *Mol. Phys.* **2016**, *114*, 2672–2687.
- (211) Waage, M. H.; Vlugt, T. J. H.; Kjelstrup, S. Phase diagram of methane and carbon dioxide hydrates computed by Monte Carlo simulations. *J. Phys. Chem. B* **2017**, *121*, 7336–7350.
- (212) Berendsen, H. J. C.; Postma, J. P. M.; van Gunsteren, W. F.; Hermans, J. In *Intermolecular Forces: Proceedings of the Fourteenth Jerusalem Symposium on Quantum Chemistry and Biochemistry Held in Jerusalem, Israel, April 13–16, 1981*; Pullman, B., Ed.; Springer Netherlands: Dordrecht, 1981; pp 331–342.
- (213) Berendsen, H. J. C.; Grigera, J. R.; Straatsma, T. P. The missing term in effective pair potentials. *J. Phys. Chem.* **1987**, *91*, 6269–6271.
- (214) Izadi, S.; Anandakrishnan, R.; Onufriev, A. V. Building Water Models: A Different Approach. *J. Phys. Chem. Lett.* **2014**, *5*, 3863–3871.
- (215) Mahoney, M. W.; Jorgensen, W. L. A five-site model for liquid water and the reproduction of the density anomaly by rigid, nonpolarizable potential functions. *J. Chem. Phys.* **2000**, *112*, 8910–8922.
- (216) Paricaud, P.; Predota, M.; Chialvo, A. A.; Cummings, P. T. From dimer to condensed phases at extreme conditions: Accurate predictions of the properties of water by a Gaussian charge polarizable model. *J. Chem. Phys.* **2005**, *122*, No. 244511.
- (217) Kiss, P. T.; Baranyai, A. A systematic development of a polarizable potential of water. *J. Chem. Phys.* **2013**, *138*, No. 204507.
- (218) Jiang, H.; Moultsos, O. A.; Economou, I. G.; Panagiotopoulos, A. Z. Hydrogen-Bonding Polarizable Intermolecular Potential Model for Water. *J. Phys. Chem. B* **2016**, *120*, 12358–12370.
- (219) Wang, F.-F.; Kumar, R.; Jordan, K. D. A distributed point polarizable force field for carbon dioxide. *Theor. Chem. Acc.* **2012**, *131*, 1132.
- (220) Jiang, H.; Mester, Z.; Moultsos, O. A.; Economou, I. G.; Panagiotopoulos, A. Z. Thermodynamic and Transport Properties of H<sub>2</sub>O + NaCl from Polarizable Force Fields. *J. Chem. Theory Comput.* **2015**, *11*, 3802–3810.
- (221) Gallo, P.; et al. Water: A Tale of Two Liquids. *Chem. Rev.* **2016**, *116*, 7463–7500.
- (222) Tsipmanogiannis, I. N.; Moultsos, O. A.; Franco, L. F.; Spera, M. B. d. M.; Erdős, M.; Economou, I. G. Self-diffusion Coefficient of Bulk and Confined Water: A Critical Review of Classical Molecular Simulation Studies. *Mol. Simul.* **2019**, *45*, 425–453.
- (223) Tsipmanogiannis, I. N.; Jamali, S. H.; Economou, I. G.; Vlugt, T. J. H.; Moultsos, O. A. On the validity of the Stokes–Einstein relation for various water force fields. *Mol. Phys.* **2020**, *118*, No. e1702729.
- (224) Lv, J.; Ren, K.; Chen, Y. CO<sub>2</sub> Diffusion in Various Carbonated Beverages: A Molecular Dynamics Study. *J. Phys. Chem. B* **2018**, *122*, 1655–1661.
- (225) Khaireh, M. A.; Liger-Belair, G.; Bonhommeau, D. A. Toward *in Silico* Prediction of CO<sub>2</sub> Diffusion in Champagne Wines. *ACS Omega* **2021**, *6*, 11231–11239.
- (226) Liu, Q.; Hu, Y. Application of the clustering method in molecular dynamics simulation of the diffusion coefficient. *Journal of Ocean University of China* **2008**, *7*, 43–47.
- (227) Jorgensen, W. L.; Jenson, C. Temperature dependence of TIP3P, SPC, and TIP4P water from NPT Monte Carlo simulations: Seeking temperatures of maximum density. *J. Comput. Chem.* **1998**, *19*, 1179–1186.
- (228) Smith, P. E.; van Gunsteren, W. F. The viscosity of SPC and SPC/E water at 277 and 300 K. *Chem. Phys. Lett.* **1993**, *215*, 315–318.
- (229) Krouskop, P. E.; Madura, J. D.; Paschek, D.; Krukau, A. Solubility of simple, nonpolar compounds in TIP4P-Ew. *J. Chem. Phys.* **2006**, *124*, No. 016102.
- (230) Fanourgakis, G. S.; Medina, J. S.; Prosmitsi, R. Determining the Bulk Viscosity of Rigid Water Models. *J. Phys. Chem. A* **2012**, *116*, 2564–2570.
- (231) Medina, J.; Prosmitsi, R.; Villarreal, P.; Delgado-Barrio, G.; Winter, G.; González, B.; Alemán, J.; Collado, C. Molecular dynamics simulations of rigid and flexible water models: Temperature dependence of viscosity. *Chem. Phys.* **2011**, *388*, 9–18.
- (232) Holmboe, M.; Bourg, I. C. Molecular Dynamics Simulations of Water and Sodium Diffusion in Smectite Interlayer Nanopores as a Function of Pore Size and Temperature. *J. Phys. Chem. C* **2014**, *118*, 1001–1013.
- (233) Ashbaugh, H. S.; Collett, N. J.; Hatch, H. W.; Staton, J. A. Assessing the thermodynamic signatures of hydrophobic hydration for several common water models. *J. Chem. Phys.* **2010**, *132*, No. 124504.
- (234) Song, Y.; Dai, L. L. The shear viscosities of common water models by non-equilibrium molecular dynamics simulations. *Mol. Simul.* **2010**, *36*, 560–567.
- (235) Ando, T. Shear viscosity of OPC and OPC3 water models. *J. Chem. Phys.* **2023**, *159*, 159.
- (236) Lemmon, E. W.; Bell, I. H.; Huber, M. L.; McLinden, M. O. *NIST Standard Reference Database 23: Reference Fluid Thermodynamic and Transport Properties-REFPROP, Version 10.0*; National Institute of Standards and Technology, 2018.
- (237) González, M. A.; Abascal, J. L. F. The shear viscosity of rigid water models. *J. Chem. Phys.* **2010**, *132*, No. 096101.

- (238) Brovchenko, I.; Geiger, A.; Oleinikova, A. Liquid-liquid phase transitions in supercooled water studied by computer simulations of various water models. *J. Chem. Phys.* **2005**, *123*, No. 044515.
- (239) Vega, C.; Abascal, J. L. F.; Nezbeda, I. Vapor-liquid equilibria from the triple point up to the critical point for the new generation of TIP4P-like models: TIP4P/Ew, TIP4P/2005, and TIP4P/ice. *J. Chem. Phys.* **2006**, *125*, No. 034503.
- (240) Omrani, S.; Ghasemi, M.; Mahmoodpour, S.; Shafiei, A.; Rostami, B. Insights from molecular dynamics on CO<sub>2</sub> diffusion coefficient in saline water over a wide range of temperatures, pressures, and salinity: CO<sub>2</sub> geological storage implications. *J. Mol. Liq.* **2022**, *345*, No. 117868.
- (241) Zhao, X.; Jin, H.; Chen, Y.; Ge, Z. Numerical study of H<sub>2</sub>, CH<sub>4</sub>, CO, O<sub>2</sub> and CO<sub>2</sub> diffusion in water near the critical point with molecular dynamics simulation. *Computers and Mathematics with Applications* **2021**, *81*, 759–771.
- (242) Zhao, X.; Luo, T.; Jin, H. A predictive model for self-, Maxwell-Stefan, and Fick diffusion coefficients of binary supercritical water mixtures. *J. Mol. Liq.* **2021**, *324*, No. 114735.
- (243) Chen, L.; Liu, D.; Li, Q. CO<sub>2</sub> Diffusivity in H<sub>2</sub>O for Supercritical Conditions: A Molecular Dynamics Study. *Journal of Thermal Science* **2022**, *31*, 1407–1415.
- (244) Young, J. M.; Panagiotopoulos, A. Z. System-Size Dependence of Electrolyte Activity Coefficients in Molecular Simulations. *J. Phys. Chem. B* **2018**, *122*, 3330–3338.
- (245) Sellan, D. P.; Landry, E. S.; Turney, J. E.; McGaughey, A. J. H.; Amon, C. H. Size effects in molecular dynamics thermal conductivity predictions. *Phys. Rev. B* **2010**, *81*, No. 214305.
- (246) Chantrenne, P.; Barrat, J.-L. Finite Size Effects in Determination of Thermal Conductivities: Comparing Molecular Dynamics Results With Simple Models. *Journal of Heat Transfer* **2004**, *126*, 577–585.
- (247) Celebi, A. T.; Vlugt, T. J. H.; Moulton, O. A. Thermal conductivity of aqueous solutions of reline, ethaline, and glyceline deep eutectic solvents; a molecular dynamics simulation study. *Mol. Phys.* **2021**, *119*, No. e1876263.
- (248) Dünweg, B.; Kremer, K. Molecular dynamics simulation of a polymer chain in solution. *J. Chem. Phys.* **1993**, *99*, 6983–6997.
- (249) Celebi, A. T.; Jamali, S. H.; Bardow, A.; Vlugt, T. J. H.; Moulton, O. A. Finite-size effects of diffusion coefficients computed from molecular dynamics: a review of what we have learned so far. *Mol. Simul.* **2021**, *47*, 831–845.
- (250) Moulton, O. A.; Zhang, Y.; Tsimpanogiannis, I. N.; Economou, I. G.; Maginn, E. J. System-size Corrections for Self-diffusion Coefficients Calculated from Molecular Dynamics Simulations: The Case of CO<sub>2</sub>, n-alkanes, and Poly (Ethylene Glycol) Dimethyl Ethers. *J. Chem. Phys.* **2016**, *145*, No. 074109.
- (251) Yeh, I.-C.; Hummer, G. System-Size Dependence of Diffusion Coefficients and Viscosities from Molecular Dynamics Simulations with Periodic Boundary Conditions. *J. Phys. Chem. B* **2004**, *108*, 15873–15879.
- (252) Jamali, S. H.; Wolff, L.; Becker, T. M.; Bardow, A.; Vlugt, T. J. H.; Moulton, O. A. Finite-size Effects of Binary Mutual Diffusion Coefficients from Molecular Dynamics. *J. Chem. Theory Comput.* **2018**, *14*, 2667–2677.
- (253) Jamali, S. H.; Hartkamp, R.; Bardas, C.; Söhl, J.; Vlugt, T. J. H.; Moulton, O. A. Shear viscosity computed from the finite-size effects of self-diffusivity in equilibrium molecular dynamics. *J. Chem. Theory Comput.* **2018**, *14*, 5959–5968.
- (254) Cai, S.; Hu, Z. C.; Li, J.; Zhang, Y. L.; Zhang, X. R. Molecular dynamics simulation of infinite dilution diffusivity of carbon dioxide in supercritical water. *International Journal of Modern Physics B* **2018**, *32*, No. 1850296.
- (255) Janzen, T.; Vrabec, J. Diffusion Coefficients of a Highly Nonideal Ternary Liquid Mixture: Cyclohexane–Toluene–Methanol. *Ind. Eng. Chem. Res.* **2018**, *57*, 16508–16517.
- (256) Bonhommeau, D. A.; Perret, A.; Nuzillard, J. M.; Cilindre, C.; Cours, T.; Alijah, A.; Liger-Belair, G. Unveiling the interplay between diffusing CO<sub>2</sub> and ethanol molecules in champagne wines by classical molecular dynamics and <sup>13</sup>C NMR spectroscopy. *J. Phys. Chem. Lett.* **2014**, *5*, 4232–4237.
- (257) Zhang, Z.; Duan, Z. An optimized molecular potential for carbon dioxide. *J. Chem. Phys.* **2005**, *122*, No. 214507.
- (258) Horn, H. W.; Swope, W. C.; Pitera, J. W.; Madura, J. D.; Dick, T. J.; Hura, G. L.; Head-Gordon, T. Development of an improved four-site water model for biomolecular simulations: TIP4P-Ew. *J. Chem. Phys.* **2004**, *120*, 9665–9676.
- (259) Khalak, Y.; Baumeier, B.; Karttunen, M. Improved general-purpose five-point model for water: TIP5P/2018. *J. Chem. Phys.* **2018**, *149*, No. 224507.
- (260) Garcia-Ratés, M.; de Hemptinne, J.-C.; Avalos, J. B.; Nieto-Draghi, C. Molecular Modeling of Diffusion Coefficient and Ionic Conductivity of CO<sub>2</sub> in Aqueous Ionic Solutions. *J. Phys. Chem. B* **2012**, *116*, 2787–2800.
- (261) Polat, H. M.; de Meyer, F.; Houriez, C.; Moulton, O. A.; Vlugt, T. J. H. Solving Chemical Absorption Equilibria using Free Energy and Quantum Chemistry Calculations: Methodology, Limitations, and New Open-Source Software. *J. Chem. Theory Comput.* **2023**, *19*, 2616–2629.
- (262) Li, W.; Nan, Y.; Zhang, Z.; You, Q.; Jin, Z. Hydrophilicity/hydrophobicity driven CO<sub>2</sub> solubility in kaolinite nanopores in relation to carbon sequestration. *Chemical Engineering Journal* **2020**, *398*, No. 125449.
- (263) Ali, A.; Striolo, A.; Cole, D. R. CO<sub>2</sub> Solubility in Aqueous Electrolyte Solutions Confined in Calcite Nanopores. *J. Phys. Chem. C* **2021**, *125*, 12333–12341.
- (264) Kadoura, A.; Narayanan Nair, A. K.; Sun, S. Molecular Dynamics Simulations of Carbon Dioxide, Methane, and Their Mixture in Montmorillonite Clay Hydrates. *J. Phys. Chem. C* **2016**, *120*, 12517–12529.
- (265) Owusu, J. P.; Karalis, K.; Prasianakis, N. I.; Churakov, S. V. Mobility of Dissolved Gases in Smectites under Saturated Conditions: Effects of Pore Size, Gas Types, Temperature, and Surface Interaction. *J. Phys. Chem. C* **2022**, *126*, 17441–17455.
- (266) Gautam, S.; Le, T. T. B.; Rother, G.; Jalarvo, N.; Liu, T.; Mamontov, E.; Dai, S.; Qiao, Z.-A.; Striolo, A.; Cole, D. Effects of water on the stochastic motions of propane confined in MCM-41-S pores. *Phys. Chem. Chem. Phys.* **2019**, *21*, 25035–25046.
- (267) Papadopoulos, G. K.; Jobic, H.; Theodorou, D. N. Transport Diffusivity of N<sub>2</sub> and CO<sub>2</sub> in Silicalite: Coherent Quasielastic Neutron Scattering Measurements and Molecular Dynamics Simulations. *J. Phys. Chem. B* **2004**, *108*, 12748–12756.
- (268) Rives, S.; Jobic, H.; Beale, A.; Maurin, G. Diffusion of CH<sub>4</sub>, CO<sub>2</sub>, and Their Mixtures in AlPO<sub>4</sub>-5 Investigated by QENS Experiments and MD Simulations. *J. Phys. Chem. C* **2013**, *117*, 13530–13539.
- (269) Prakash, M.; Jobic, H.; Ramsahye, N. A.; Nouar, F.; Damasceno Borges, D.; Serre, C.; Maurin, G. Diffusion of H<sub>2</sub>, CO<sub>2</sub>, and Their Mixtures in the Porous Zirconium Based Metal–Organic Framework MIL-140A(Zr): Combination of Quasi-Elastic Neutron Scattering Measurements and Molecular Dynamics Simulations. *J. Phys. Chem. C* **2015**, *119*, 23978–23989.
- (270) Yang, Q.; Jobic, H.; Salles, F.; Kolokolov, D.; Guillerm, V.; Serre, C.; Maurin, G. Probing the Dynamics of CO<sub>2</sub> and CH<sub>4</sub> within the Porous Zirconium Terephthalate UiO-66(Zr): A Synergic Combination of Neutron Scattering Measurements and Molecular Simulations. *Chemistry -Eur. J.* **2011**, *17*, 8882–8889.
- (271) Chattoth, S.; He, L.; Mamontov, E.; Melnichenko, Y. Effect of carbon dioxide and nitrogen on the diffusivity of methane confined in nano-porous carbon aerogel. *Microporous Mesoporous Mater.* **2012**, *148*, 101–106.
- (272) Salles, F.; Jobic, H.; Devic, T.; Guillerm, V.; Serre, C.; Koza, M. M.; Ferey, G.; Maurin, G. Diffusion of Binary CO<sub>2</sub>/CH<sub>4</sub> Mixtures in the MIL-47(V) and MIL-53(Cr) Metal–Organic Framework Type Solids: A Combination of Neutron Scattering Measurements and Molecular Dynamics Simulations. *J. Phys. Chem. C* **2013**, *117*, 11275–11284.
- (273) Liu, T.; Gautam, S.; Cole, D. R.; Patankar, S.; Tomasko, D.; Zhou, W.; Rother, G. Structure and dynamics of ethane confined in

- silica nanopores in the presence of CO<sub>2</sub>. *J. Chem. Phys.* **2020**, *152*, No. 084707.
- (274) Patankar, S.; Gautam, S.; Rother, G.; Podlesnyak, A.; Ehlers, G.; Liu, T.; Cole, D. R.; Tomasko, D. L. Role of Confinement on Adsorption and Dynamics of Ethane and an Ethane–CO<sub>2</sub> Mixture in Mesoporous CPG Silica. *J. Phys. Chem. C* **2016**, *120*, 4843–4853.
- (275) Hunvik, K. W. Bø; Lima, R. J. d. S.; Kirch, A.; Loch, P.; Monceyron Røren, P.; Hoffmann Petersen, M.; Rudic, S.; Garcia Sakai, V.; Knudsen, K. D.; Rodrigues Miranda, C.; Breu, J.; Fossum, J. O.; Bordallo, H. N. Influence of CO<sub>2</sub> on Nanoconfined Water in a Clay Mineral. *J. Phys. Chem. C* **2022**, *126*, 17243–17254.
- (276) Bowers, G. M.; Schaeff, H. T.; Loring, J. S.; Hoyt, D. W.; Burton, S. D.; Walter, E. D.; Kirkpatrick, R. J. Role of Cations in CO<sub>2</sub> Adsorption, Dynamics, and Hydration in Smectite Clays under in Situ Supercritical CO<sub>2</sub> Conditions. *J. Phys. Chem. C* **2017**, *121*, 577–592.
- (277) Peksa, M.; Lang, J.; Stallmach, F. <sup>13</sup>C NMR study of diffusion anisotropy of carbon dioxide adsorbed in nanoporous DMOF-1. *Microporous Mesoporous Mater.* **2015**, *205*, 11–15.
- (278) Forse, A. C.; Gonzalez, M. I.; Siegelman, R. L.; Witherspoon, V. J.; Jawahery, S.; Mercado, R.; Milner, P. J.; Martell, J. D.; Smit, B.; Blümich, B.; Long, J. R.; Reimer, J. A. Unexpected Diffusion Anisotropy of Carbon Dioxide in the Metal–Organic Framework Zn<sub>2</sub>(dobpc). *J. Am. Chem. Soc.* **2018**, *140*, 1663–1673.
- (279) Hu, Y.; Pan, X.; Han, X.; Bao, X. Displacement and Diffusion of Methane and Carbon Dioxide in SBA-15 Studied by NMR. *J. Phys. Chem. C* **2017**, *121*, 2481–2486.
- (280) Díaz, K.; Garrido, L.; López-González, M.; del Castillo, L. F.; Riande, E. CO<sub>2</sub> Transport in Polysulfone Membranes Containing Zeolitic Imidazolate Frameworks As Determined by Permeation and PFG NMR Techniques. *Macromolecules* **2010**, *43*, 316–325.
- (281) Policicchio, A.; Conte, G.; Agostino, R. G.; Caputo, P.; Oliviero Rossi, C.; Godbert, N.; Nicotera, I.; Simari, C. Hexagonal Mesoporous Silica for carbon capture: Unrevealing CO<sub>2</sub> microscopic dynamics by Nuclear Magnetic Resonance. *J. CO<sub>2</sub> Utili.* **2022**, *55*, No. 101809.
- (282) Peñas López, P.; van Elburg, B.; Parrales, M. A.; Rodríguez-Rodríguez, J. Diffusion of dissolved CO<sub>2</sub> in water propagating from a cylindrical bubble in a horizontal Hele-Shaw cell. *Physical Review Fluids* **2017**, *2*, No. 063602.
- (283) Suzuki, T.; Sakoda, A.; Suzuki, M.; Izumi, J. Adsorption of Carbon Dioxide onto Hydrophobic Zeolite under High Moisture. *J. Chem. Eng. Jpn.* **1997**, *30*, 954–958.
- (284) Shiraki, R.; Dunn, T. L. Experimental study on water–rock interactions during CO<sub>2</sub> flooding in the Tensleep Formation, Wyoming, USA. *Appl. Geochim.* **2000**, *15*, 265–279.
- (285) Hou, L.; Elsworth, D. Mechanisms of tripartite permeability evolution for supercritical CO<sub>2</sub> in propped shale fractures. *Fuel* **2021**, *292*, No. 120188.
- (286) Zhang, T.; Tang, M.; Ma, Y.; Zhu, G.; Zhang, Q.; Wu, J.; Xie, Z. Experimental study on CO<sub>2</sub>/Water flooding mechanism and oil recovery in ultralow - Permeability sandstone with online LF-NMR. *Energy* **2022**, *252*, No. 123948.
- (287) Moortgat, J.; Firoozabadi, A.; Li, Z.; Espósito, R. Experimental Coreflooding and Numerical Modeling of CO<sub>2</sub> Injection With Gravity and Diffusion Effects. In *SPE Annual Technical Conference and Exhibition*; SPE, 2010, pp SPE-135563.
- (288) Busch, A.; Alles, S.; Gensterblum, Y.; Prinz, D.; Dewhurst, D. N.; Raven, M. D.; Stanjek, H.; Krooss, B. M. Carbon dioxide storage potential of shales. *International Journal of Greenhouse Gas Control* **2008**, *2*, 297–308.
- (289) Si, L.; Zhang, H.; Wei, J.; Li, B.; Han, H. Modeling and experiment for effective diffusion coefficient of gas in water-saturated coal. *Fuel* **2021**, *284*, No. 118887.
- (290) Renner, T. Measurement and correlation of diffusion coefficients for CO<sub>2</sub> and rich-gas applications. *SPE Reservoir Engineering* **1988**, *3*, 517–523.
- (291) Seyyedi, M.; Rostami, B.; Pasdar, M.; Pazhoohan, J. Experimental and numerical study of the effects of formation brine salinity and reservoir temperature on convection mechanism during CO<sub>2</sub> storage in saline aquifers. *Journal of Natural Gas Science and Engineering* **2016**, *36*, 950–962.
- (292) Li, Z.; Yuan, L.; Sun, G.; Lv, J.; Zhang, Y. Experimental determination of CO<sub>2</sub> diffusion coefficient in a brine-saturated core simulating reservoir condition. *Energies* **2021**, *14*, 540.
- (293) Moghaddam, R. N.; Rostami, B.; Pourafshary, P. A method for dissolution rate quantification of convection-diffusion mechanism during CO<sub>2</sub> storage in saline aquifers. *Spec. Top. Rev. Porous Media* **2013**, *4*, 13.
- (294) de Almeida Martins, J. P.; Topgaard, D. Two-Dimensional Correlation of Isotropic and Directional Diffusion Using NMR. *Phys. Rev. Lett.* **2016**, *116*, No. 087601.
- (295) Ramsahye, N. A.; Gao, J.; Jobic, H.; Llewellyn, P. L.; Yang, Q.; Wiersum, A. D.; Koza, M. M.; Guillerm, V.; Serre, C.; Zhong, C. L.; Maurin, G. Adsorption and Diffusion of Light Hydrocarbons in UiO-66(Zr): A Combination of Experimental and Modeling Tools. *J. Phys. Chem. C* **2014**, *118*, 27470–27482.
- (296) Valiullin, R. *Diffusion NMR of Confined Systems: Fluid Transport in Porous Solids and Heterogeneous Materials*; Royal Society of Chemistry: Cambridge, U.K., 2017.
- (297) Mercier Franco, L. F.; Castier, M.; Economou, I. G. Diffusion in Homogeneous and in Inhomogeneous Media: A New Unified Approach. *J. Chem. Theory Comput.* **2016**, *12*, 5247–5255.
- (298) Falk, K.; Coasne, B.; Pellenq, R.; Ulm, F.-J.; Bocquet, L. Subcontinuum mass transport of condensed hydrocarbons in nanoporous media. *Nat. Commun.* **2015**, *6*, 6949.
- (299) Botan, A.; Rotenberg, B.; Marry, V.; Turq, P.; Noetinger, B. Carbon Dioxide in Montmorillonite Clay Hydrates: Thermodynamics, Structure, and Transport from Molecular Simulation. *J. Phys. Chem. C* **2010**, *114*, 14962–14969.
- (300) Yang, Y.; Narayanan Nair, A. K.; Sun, S. Adsorption and Diffusion of Carbon Dioxide, Methane, and Their Mixture in Carbon Nanotubes in the Presence of Water. *J. Phys. Chem. C* **2020**, *124*, 16478–16487.
- (301) Kadoura, A.; Narayanan Nair, A. K.; Sun, S. Molecular Simulation Study of Montmorillonite in Contact with Variably Wet Supercritical Carbon Dioxide. *J. Phys. Chem. C* **2017**, *121*, 6199–6208.
- (302) Makaremi, M.; Jordan, K. D.; Guthrie, G. D.; Myshakin, E. M. Multiphase Monte Carlo and Molecular Dynamics Simulations of Water and CO<sub>2</sub> Intercalation in Montmorillonite and Beidellite. *J. Phys. Chem. C* **2015**, *119*, 15112–15124.
- (303) Berghe, G.; Kline, S.; Burket, S.; Bivens, L.; Johnson, D.; Singh, R. Effect of CO<sub>2</sub> and H<sub>2</sub>O on the behavior of shale gas confined inside calcite [104] slit-like nanopore: a molecular dynamics simulation study. *J. Mol. Model.* **2019**, *25*, 293–11.
- (304) Yan, F.; Guo, Y.; Wang, Z.; Zhao, L.; Zhang, X. Efficient separation of CO<sub>2</sub>/CH<sub>4</sub> by ionic liquids confined in graphene oxide: A molecular dynamics simulation. *Sep. Purif. Technol.* **2022**, *289*, No. 120736.
- (305) Zhou, W.; Zhu, J.; Wang, H.; Kong, D. Transport Diffusion Behaviors and Mechanisms of CO<sub>2</sub>/CH<sub>4</sub> in Shale Nanopores: Insights from Molecular Dynamics Simulations. *Energy Fuels* **2022**, *36*, 11903–11912.
- (306) Guang, W.; Zhang, Z.; Zhang, L.; Ranjith, P.; Hao, S.; Liu, X. Confinement effect on transport diffusivity of adsorbed CO<sub>2</sub>–CH<sub>4</sub> mixture in coal nanopores for CO<sub>2</sub> sequestration and enhanced CH<sub>4</sub> recovery. *Energy* **2023**, *278*, No. 127929.
- (307) Badmos, S. B.; Bui, T.; Striolo, A.; Cole, D. R. Factors Governing the Enhancement of Hydrocarbon Recovery via H<sub>2</sub>S and/or CO<sub>2</sub> Injection: Insights from a Molecular Dynamics Study in Dry Nanopores. *J. Phys. Chem. C* **2019**, *123*, 23907–23918.
- (308) Feng, Q.; Xing, X.; Wang, S.; Liu, G.; Qin, Y.; Zhang, J. CO<sub>2</sub> diffusion in shale oil based on molecular simulation and pore network model. *Fuel* **2024**, *359*, No. 130332.
- (309) Le, T.; Ogbe, S.; Striolo, A.; Cole, D. R. N-octane diffusivity enhancement via carbon dioxide in silica slit-shaped nanopores – a molecular dynamics simulation. *Mol. Simul.* **2016**, *42*, 745–752.

- (310) Tang, Z.; Lu, L.; Dai, Z.; Xie, W.; Shi, L.; Lu, X. CO<sub>2</sub> Absorption in the Ionic Liquids Immobilized on Solid Surface by Molecular Dynamics Simulation. *Langmuir* **2017**, *33*, 11658–11669.
- (311) Liu, Y.-F.; Xu, Q.-Q.; Wang, Y.-Q.; Yin, J.-Z. Molecular dynamics simulations of CO<sub>2</sub> permeation through ionic liquids confined in – alumina nanopores. *Chem. Eng. Commun.* **2019**, *206*, 301–317.
- (312) Krishna, R.; van Baten, J. M. Investigating the potential of MgMOF-74 membranes for CO<sub>2</sub> capture. *J. Membr. Sci.* **2011**, *377*, 249–260.
- (313) Dhiman, I.; Berg, M.; Cole, D. R.; Gautam, S. Correlation between structure and dynamics of CO<sub>2</sub> confined in Mg-MOF-74 and the role of inter-crystalline space: A molecular dynamics simulation study. *Appl. Surf. Sci.* **2023**, *612*, No. 155909.
- (314) Babarao, R.; Jiang, J. Diffusion and Separation of CO<sub>2</sub> and CH<sub>4</sub> in Silicalite, C<sub>168</sub> Schwarzite, and IRMOF-1: A Comparative Study from Molecular Dynamics Simulation. *Langmuir* **2008**, *24*, 5474–5484.
- (315) Fuentes-Azcatl, R.; Domínguez, H. Carbon Dioxide Confined between Two Charged Single Layers of Graphene: Molecular Dynamics Studies. *J. Phys. Chem. C* **2019**, *123*, 23705–23710.
- (316) Newsome, D.; Coppens, M.-O. Molecular dynamics as a tool to study heterogeneity in zeolites – Effect of Na<sup>+</sup> cations on diffusion of CO<sub>2</sub> and N<sub>2</sub> in Na-ZSM-5. *Chem. Eng. Sci.* **2015**, *121*, 300–312.
- (317) Franco, L. F. M.; Castier, M.; Economou, I. Anisotropic parallel self-diffusion coefficients near the calcite surface: A molecular dynamics study. *J. Chem. Phys.* **2016**, *145*, No. 084702.
- (318) Spera, M. B.; Braga, F. N.; Bartolomeu, R. A.; Economou, I. G.; Franco, L. F. Diffusion of fluids confined in carbonate minerals: A molecular dynamics simulation study for carbon dioxide and methane–ethane mixture within calcite. *Fuel* **2022**, *325*, No. 124800.
- (319) Gautam, S.; Liu, T.; Cole, D. Sorption, Structure and Dynamics of CO<sub>2</sub> and Ethane in Silicalite at High Pressure: A Combined Monte Carlo and Molecular Dynamics Simulation Study. *Molecules* **2019**, *24*, 99.
- (320) Yang, X.; Zhang, C. Structure and diffusion behavior of dense carbon dioxide fluid in clay-like slit pores by molecular dynamics simulation. *Chem. Phys. Lett.* **2005**, *407*, 427–432.
- (321) Cygan, R. T.; Romanov, V. N.; Myshakin, E. M. Molecular Simulation of Carbon Dioxide Capture by Montmorillonite Using an Accurate and Flexible Force Field. *J. Phys. Chem. C* **2012**, *116*, 13079–13091.
- (322) Khorshidi, Z. N.; Khalkhal, M.; Zhang, H.; Choi, P. Molecular Dynamics Study of the Role of Water in the Carbon Dioxide Intercalation in Chloride Ions Bearing Hydrotalcite. *J. Phys. Chem. C* **2018**, *122*, 9507–9514.
- (323) Myshakin, E. M.; Saidi, W. A.; Romanov, V. N.; Cygan, R. T.; Jordan, K. D. Molecular Dynamics Simulations of Carbon Dioxide Intercalation in Hydrated Na-Montmorillonite. *J. Phys. Chem. C* **2013**, *117*, 11028–11039.
- (324) Rahromostaqim, M.; Sahimi, M. Molecular Dynamics Simulation of Hydration and Swelling of Mixed-Layer Clays in the Presence of Carbon Dioxide. *J. Phys. Chem. C* **2019**, *123*, 4243–4255.
- (325) Sena, M. M.; Morrow, C. P.; Kirkpatrick, R. J.; Krishnan, M. Supercritical Carbon Dioxide at Smectite Mineral–Water Interfaces: Molecular Dynamics and Adaptive Biasing Force Investigation of CO<sub>2</sub>/H<sub>2</sub>O Mixtures Nanoconfined in Na-Montmorillonite. *Chem. Mater.* **2015**, *27*, 6946–6959.
- (326) Yazaydin, A. O.; Bowers, G. M.; Kirkpatrick, R. J. Molecular dynamics modeling of carbon dioxide, water and natural organic matter in Na-hectorite. *Phys. Chem. Chem. Phys.* **2015**, *17*, 23356–23367.
- (327) Zhang, W.; Hu, H.; Li, X.; Fang, Z. Interplay of Montmorillonite–H<sub>2</sub>O–sc CO<sub>2</sub> System between Mechanical Behavior and Adsorption: Molecular Dynamics. *J. Phys. Chem. C* **2015**, *119*, 21959–21968.
- (328) Muniz-Miranda, F.; Lodesani, F.; Tavanti, F.; Presti, D.; Malferrari, D.; Pedone, A. Supercritical CO<sub>2</sub> Confined in Palygorskite and Sepiolite Minerals: A Classical Molecular Dynamics Investigation. *J. Phys. Chem. C* **2016**, *120*, 26945–26954.
- (329) Cygan, R. T.; Liang, J.-J.; Kalinichev, A. G. Molecular models of hydroxide, oxyhydroxide, and clay phases and the development of a general force field. *J. Phys. Chem. B* **2004**, *108*, 1255–1266.
- (330) Loganathan, N.; Yazaydin, A. O.; Bowers, G. M.; Kalinichev, A. G.; Kirkpatrick, R. J. Molecular Dynamics Study of CO<sub>2</sub> and H<sub>2</sub>O Intercalation in Smectite Clays: Effect of Temperature and Pressure on Interlayer Structure and Dynamics in Hectorite. *J. Phys. Chem. C* **2017**, *121*, 24527–24540.
- (331) Kerisit, S.; Weare, J. H.; Felmy, A. R. Structure and dynamics of forsterite–sc CO<sub>2</sub>/H<sub>2</sub>O interfaces as a function of water content. *Geochim. Cosmochim. Acta* **2012**, *84*, 137–151.
- (332) Sui, H.; Zhang, F.; Wang, Z.; Wang, D.; Wang, Y. Effect of Kerogen Maturity, Water Content for Carbon Dioxide, Methane, and Their Mixture Adsorption and Diffusion in Kerogen: A Computational Investigation. *Langmuir* **2020**, *36*, 9756–9769.
- (333) Mohammed, S.; Gadikota, G. The Effect of Hydration on the Structure and Transport Properties of Confined Carbon Dioxide and Methane in Calcite Nanopores. *Frontiers in Energy Research* **2018**, *6*, 86.
- (334) Santos, M. S.; Hamza, M.; Franco, L. F. M.; Castier, M.; Economou, I. G. Molecular Understanding of Enhanced Hydrocarbon Recovery Processes: Role of Local Self-Diffusion Coefficients of Complex Mixtures. *Energy Fuels* **2022**, *36*, 8301–8310.
- (335) Xiao, S.; Edwards, S. A.; Gräter, F. A New Transferable Forcefield for Simulating the Mechanics of CaCO<sub>3</sub> Crystals. *J. Phys. Chem. C* **2011**, *115*, 20067–20075.
- (336) Svoboda, M.; Brennan, J. K.; Lísal, M. Molecular dynamics simulation of carbon dioxide in single-walled carbon nanotubes in the presence of water: structure and diffusion studies. *Mol. Phys.* **2015**, *113*, 1124–1136.
- (337) Steele, W. A. The interaction of rare gas atoms with graphitized carbon black. *J. Phys. Chem.* **1978**, *82*, 817–821.
- (338) Dauber-Osguthorpe, P.; Roberts, V. A.; Osguthorpe, D. J.; Wolff, J.; Genest, M.; Hagler, A. T. Structure and energetics of ligand binding to proteins: Escherichia coli dihydrofolate reductase-trimethoprim, a drug-receptor system. *Proteins* **1988**, *4*, 31–47.
- (339) Zhao, B.; Zhou, R.; Sun, C.; Bai, B. PVT properties and diffusion characteristics of H<sub>2</sub>O/H<sub>2</sub>/CO<sub>2</sub> mixtures in graphite nanoslit. *Chem. Phys. Lett.* **2022**, *795*, No. 139502.
- (340) Sizova, A. A.; Sizov, V. V.; Brodskaya, E. N. Diffusion of CO<sub>2</sub>/CH<sub>4</sub> mixture in wet SBA-15 and CMK-5. *Colloids Surf., A* **2017**, *524*, 87–95.
- (341) Jorgensen, W. L.; Maxwell, D. S.; Tirado-Rives, J. Development and testing of the OPLS all-atom force field on conformational energetics and properties of organic liquids. *J. Am. Chem. Soc.* **1996**, *118*, 11225–11236.
- (342) Mayo, S. L.; Olafson, B. D.; Goddard, W. A. DREIDING: a generic force field for molecular simulations. *J. Phys. Chem.* **1990**, *94*, 8897–8909.
- (343) Rappe, A. K.; Casewit, C. J.; Colwell, K. S.; Goddard, W. A. I.; Skiff, W. M. UFF, a full periodic table force field for molecular mechanics and molecular dynamics simulations. *J. Am. Chem. Soc.* **1992**, *114*, 10024–10035.
- (344) Bendt, S.; Dong, Y.; Keil, F. J. Diffusion of Water and Carbon Dioxide and Mixtures Thereof in Mg-MOF-74. *J. Phys. Chem. C* **2019**, *123*, 8212–8220.
- (345) Magnin, Y.; Dirand, E.; Orsikowsky, A.; Plainchault, M.; Pugnet, V.; Cordier, P.; Llewellyn, P. L. A Step in Carbon Capture from Wet Gases: Understanding the Effect of Water on CO<sub>2</sub> Adsorption and Diffusion in UiO-66. *J. Phys. Chem. C* **2022**, *126*, 3211–3220.
- (346) Magnin, Y.; Dirand, E.; Maurin, G.; Llewellyn, P. L. Abnormal CO<sub>2</sub> and H<sub>2</sub>O Diffusion in CALF-20(Zn) Metal–Organic Framework: Fundamental Understanding of CO<sub>2</sub> Capture. *ACS Applied Nano Materials* **2023**, *6*, 19963–19971.
- (347) Mera, H. A.; Gomez-Ballesteros, J. L.; Balbuena, P. B. Structure and Dynamics of Carbon Dioxide, Nitrogen, Water, and Their Mixtures in Metal Organic Frameworks. *Journal of Chemical & Engineering Data* **2014**, *59*, 2973–2981.

- (348) Rudenko, A. N.; Bendt, S.; Keil, F. J. Multiscale Modeling of Water in Mg-MOF-74: From Electronic Structure Calculations to Adsorption Isotherms. *J. Phys. Chem. C* **2014**, *118*, 16218–16227.
- (349) Liu, P.; Harder, E.; Berne, B. J. On the Calculation of Diffusion Coefficients in Confined Fluids and Interfaces with an Application to the Liquid-Vapor Interface of Water. *J. Phys. Chem. B* **2004**, *108*, 6595–6602.
- (350) Spera, M. B.; Franco, L. F. Surface and confinement effects on the self-diffusion coefficients for methane-ethane mixtures within calcite nanopores. *Fluid Phase Equilib.* **2020**, *522*, No. 112740.
- (351) Mittal, J.; Truskett, T. M.; Errington, J. R.; Hummer, G. Layering and Position-Dependent diffusive dynamics of confined fluids. *Phys. Rev. Lett.* **2008**, *100*, No. 145901.
- (352) von Hansen, Y.; Gekle, S.; Netz, R. R. Anomalous anisotropic diffusion dynamics of hydration water at lipid membranes. *Phys. Rev. Lett.* **2013**, *111*, No. 118103.
- (353) Carmer, J.; van Swol, F.; Truskett, T. M. Position-dependent and pair diffusivity profiles from steady-state solutions of color reaction-counterdiffusion problems. *J. Chem. Phys.* **2014**, *141*, No. 046101.
- (354) Chialvo, A. A.; Vlcek, L.; Cole, D. R. Aqueous CO<sub>2</sub> Solutions at Silica Surfaces and within Nanopore Environments. Insights from Isobaric–Isothermal Molecular Dynamics. *J. Phys. Chem. C* **2012**, *116*, 13904–13916.
- (355) Frentrup, H.; Avendaño, C.; Horsch, M.; Salih, A.; Müller, E. A. Transport diffusivities of fluids in nanopores by non-equilibrium molecular dynamics simulation. *Mol. Simul.* **2012**, *38*, 540–553.
- (356) Maginn, E. J.; Bell, A. T.; Theodorou, D. N. Transport diffusivity of methane in silicalite from equilibrium and nonequilibrium simulations. *J. Phys. Chem.* **1993**, *97*, 4173–4181.
- (357) Heffelfinger, G. S.; van Swol, F. Diffusion in Lennard-Jones fluids using dual control volume grand canonical molecular dynamics simulation (DCV-GCMD). *J. Chem. Phys.* **1994**, *100*, 7548–7552.
- (358) Asai, P.; Jin, J.; Deo, M.; Miller, J. D.; Butt, D. Non-equilibrium molecular dynamics simulation to evaluate the effect of confinement on fluid flow in silica nanopores. *Fuel* **2022**, *317*, No. 123373.
- (359) Simonnin, P.; Noetinger, B.; Nieto-Draghi, C.; Marry, V.; Rotenberg, B. Diffusion under Confinement: Hydrodynamic Finite-Size Effects in Simulation. *J. Chem. Theory Comput.* **2017**, *13*, 2881–2889.
- (360) Giestring, P.; Guggenheim, S.; Koster van Groos, A. F.; Busch, A. Interaction of carbon dioxide with Na-exchanged montmorillonite at pressures to 640bars: Implications for CO<sub>2</sub> sequestration. *International Journal of Greenhouse Gas Control* **2012**, *8*, 73–81.
- (361) Lee, M.-S.; McGrail, B. P.; Glezakou, V.-A. Microstructural Response of Variably Hydrated Ca-rich Montmorillonite to Supercritical CO<sub>2</sub>. *Environ. Sci. Technol.* **2014**, *48*, 8612–8619.
- (362) Li, Y.; Narayanan Nair, A. K.; Kadoura, A.; Yang, Y.; Sun, S. Molecular Simulation Study of Montmorillonite in Contact with Water. *Ind. Eng. Chem. Res.* **2019**, *58*, 1396–1403.
- (363) Simonnin, P.; Marry, V.; Noetinger, B.; Nieto-Draghi, C.; Rotenberg, B. Mineral- and Ion-Specific Effects at Clay–Water Interfaces: Structure, Diffusion, and Hydrodynamics. *J. Phys. Chem. C* **2018**, *122*, 18484–18492.
- (364) Wang, Y.; Jiang, X.; Yang, X.; Wang, S.; Qiu, X.; Liu, L.; Gao, S.; Li, Z.; Zhang, C. Molecular Simulation of Adsorption Separation of CO<sub>2</sub> from Combustion Exhaust Mixture of Commercial Zeolites. *Processes* **2023**, *11*, 2987.
- (365) Halgren, T. A.; Damm, W. Polarizable force fields. *Curr. Opin. Struct. Biol.* **2001**, *11*, 236–242.
- (366) Warshel, A.; Kato, M.; Pisliakov, A. V. Polarizable force fields: History, test cases, and prospects. *J. Chem. Theory Comput.* **2007**, *3*, 2034–2045.
- (367) Stirling, A. HCO<sub>3</sub>-Formation from CO<sub>2</sub> at High pH: *Ab Initio* Molecular Dynamics Study. *J. Phys. Chem. B* **2011**, *115*, 14683–14687.
- (368) Leung, K.; Nielsen, I. M. B.; Kurtz, I. Ab initio Molecular Dynamics Study of Carbon Dioxide and Bicarbonate Hydration and the Nucleophilic Attack of Hydroxide on CO<sub>2</sub>. *J. Phys. Chem. B* **2007**, *111*, 4453–4459.
- (369) Guido, C. A.; Pietrucci, F.; Gallet, G. A.; Andreoni, W. The Fate of a Zwitterion in Water from ab Initio Molecular Dynamics: Monoethanolamine (MEA)-CO<sub>2</sub>. *J. Chem. Theory Comput.* **2013**, *9*, 28–32.
- (370) Lee, M.-S.; McGrail, B. P.; Rousseau, R.; Glezakou, V.-A. Structure, dynamics and stability of water/scCO<sub>2</sub>/mineral interfaces from ab initio molecular dynamics simulations. *Sci. Rep.* **2015**, *5*, No. 14857.
- (371) Liu, Y.; Zhao, J.; Xu, J. Dissociation mechanism of carbon dioxide hydrate by molecular dynamic simulation and ab initio calculation. *Computational and Theoretical Chemistry* **2012**, *991*, 165–173.
- (372) Glezakou, V.-A.; Rousseau, R.; Dang, L. X.; McGrail, B. P. Structure, dynamics and vibrational spectrum of supercritical CO<sub>2</sub>/H<sub>2</sub>O mixtures from ab initio molecular dynamics as a function of water cluster formation. *Phys. Chem. Chem. Phys.* **2010**, *12*, 8759.
- (373) Li, Y.; Li, H.; Pickard, F. C.; Narayanan, B.; Sen, F. G.; Chan, M. K. Y.; Sankaranarayanan, S. K. R. S.; Brooks, B. R.; Roux, B. Machine Learning Force Field Parameters from Ab Initio Data. *J. Chem. Theory Comput.* **2017**, *13*, 4492–4503.